Identification and Characterisation of Novel Mechanisms Regulating TNF-Induced Cell Death

Inaugural Dissertation
zur Erlangung des

Doktorgrades
der Mathematisch-Naturwissenschaftlichen Fakultät

der
Universität zu Köln

Vorgelegt von
Deniz Pinar Savcigil
aus
Konak, Izmir

Köln, Februar 2024

Berichterstatter: Dr. Alessandro Annibaldi

Prof. Dr. Kay Hofmann

Prof. Dr. Andrea Morandi

Tag der mündlichen Prüfung: 30.04.2024

TABLE OF CONTENT

I. ABSTRACT

Cell death is a fundamental biological process for tissue homeostasis and tissue remodelling during development and for the defence against a vast range of stressors. However, uncontrolled cell death can impair these programs causing severe pathological consequences. Thus, the regulation of cell death is a critical step to trigger proper immune responses and healing processes following stress conditions. Tumour necrosis factor (TNF), a proinflammatory cytokine secreted during different stress conditions, can determine cell fate, either cell survival and proliferation or cell death, the latter via the formation of a cytosolic, cell death-inducing complex, called complex II. Checkpoints are specific mechanisms in TNF signalling that control the decisison between cell survival and death and, within the latter, control the amplitude of cell death. Therefore, these checkpoints have a high pathophysiological relevance. Hence, our goal is to gain a deeper molecular understanding of how these mechanisms regulate the cytotoxic potential of TNF. Cellular FLICE inhibitory protein (cFLIP) is a crucial regulator of TNF-induced cell death. cFLIP is cleaved at D377 by Caspase-8. Yet, the physiological role of cFLIP cleavage in the regulation of TNF-mediated cell death outcomes remains elusive. Here, we discovered that cFLIP cleavage counterbalances complex II assembly and cytotoxicity. Consequently, abrogation of cFLIP cleavage by the D377A mutation sensitizes cells to TNF-induced cell death by favouring complex II formation. The cell death sensitizing effect of D377A mutation depends on the C-terminal residues of the caspase-like domain on cFLIP, in particular the Q469 resiude. To address the physiological funtions of cFLIP cleavage, we generated a novel mouse line bearing a non-cleavable version of cFLIP (*Cflip*$^{D377A/D377A}$). These mice exhibited increased tissue damage caused by *Sharpin* deficiency, impaired skin wound healing and increased lethality upon SARS CoV-1 infection. These results reveal a previously unknown and unexpected role for cFLIP cleavage in the modulation of cell death amplitude during tissue stress, to ensure the execution of repair programs. Furthermore, we successfully generated and validated a novel genetic tool to study the composition of complex II using an immunoprecipitation-based mass spectrometry-coupled, unbiased approach. As an interesting candidate, we identified protein phosphatase 2 scaffold subunit A alpha (PPP2R1A), a constant regulatory subunit of protein phosphatase 2 (PP2A). The first biochemical and functional investigations indicated the involvement of PPP2R1A in the regulation of TNF-induced cell death. To conclude, we unravelled new layers of regulatior machinery that safeguards TNF-induced complex II-mediated cell death. Our findings therefore provide a better understanding of the role of cell death in health and disease.

II. ZUSAMMENFASSUNG

Der Zelltod ist ein biologischer Prozess der Gewebehomöostase während der Entwicklung und in den Abwehrreaktionen. Unkontrollierter Zelltod stört jedoch die Reparaturprogramme und hat schwerwiegende pathologische Folgen. Daher ist die Regulierung des Zelltodes entscheidend, um angemessene Immunreaktionen auszulösen und die Homöostase aufrechtzuerhalten. Der Tumornekrosefaktor (TNF) ist ein wichtiges Zytokin, das bei verschiedenen Stresssituationen freigesetzt wird. Es steuert das überlebenswichtige Zellgeschehen. Es kann zwischen das Überleben und Prolifereation oder Zelltod, für letzteres durch die Bildung eines zytosolischen, Zelltod induzierenden Komplexes, gennant Komplex II. Daher regulieren sogenannte „Checkpoints“ der TNF Signalweg, ob eine Zelle überlebt oder stirbt und im Letzterem kontrollieren sie das Ausmaß des Zelltodes. Daher haben diese Checkpoints eine hohe pathophysiologische Relevanz. Unser Ziel ist ist es daher, ein tieferes molekulares Verständnis dafür zu erlangen, wie diese Mechanismen das zytotoxische Potenzial von TNF regulieren. Zelluläre FLICE inhibitorische Protein (cFLIP) ist ein entscheidender Regulator des TNF-induzierten Zelltodes. Darüber hinaus spaltet Caspase-8 cFLIP an D377. Jedoch ist die physiologische Rolle dieser Spaltung unklar. Hier zeigte es sich, dass die cFLIP Spaltung Komplex II Bildung und dessen Zytotoxizität. Folglich sensibilisiert die genetische Blockade der cFLIP Spaltung die Zellen für die TNF-induzierten Zelltod, indem sie die Bildung von Komplex II begünstigt. Dies hängt von den C-terminalen Aminosäuren des cFLIPs, insbesondere Q469, ab. Um physiologische Rolle der cFLIP Spaltung zu untersuchen, wurde eine neue Mauslinie mit der nicht spaltbaren cFLIP (*Cflip*$^{D377A/D377A}$) generiert. Diese Mäuse zeigten erhöhte Gewebeschaden durch Defizit an *Sharpin*, gestörte Wundheilung und erhöhte Letalität bei der SARS CoV-1 Infektion. Diese Ergebnisse liefern neue Einblicke in die Funktion von cFLIP bei der präzisen Kontrolle der Amplitude von Zelltod, um die Reparaturprogrammen zu gewährleisten. Zusätzlich dazu wurde ein neues genetisches Model zur Untersuchung von Komplex II entwickelt. Diese Immunpräzipitation und Massenspektrometrie basierten Ansatz weist auf einen interessanten Kandidatprotein hin: die Proteinphosphatase 2 Scaffold Subunit A Alpha (PPP2R1A), die konstante regulatorische Untereinheit der Proteinphosphatase 2 (PP2a). Erste Untersuchungen deuteten auf die Beteiligung von PPP2R1A an der Regulierung des TNF-induzierten Zelltods hin. Schließlich haben wir neue Ebenen der Regulationsmaschinerie aufgedeckt, die den TNF-induzierten Zelltod bei verschiedenen Stimuli absichern. Diese ergebnisse tragen zu einem besseren Verständnis der Rolle des Zelltods bei Gesundheit und Krankheit bei.

III. LIST OF ABREVATIONS

Abbrevation	Name
ABC	Ammonium bicarbonate
ACN	Acetonitrile
AIM2	Absent in melanoma 2
AP-1	Activator protein 1
APS	Ammonium persulfate
ASC	Apoptosis-associated speck-like protein containing a caspase recruitment domain
ATG9A	Autophagy-related 9A
B	Birinapant
BMDMs	Bone marrow derived macrophages
BSA	Bovine serum albumin
C	Cycloheximide
CAA	Chloroacetamide
CAD	Caspase-activated DNase
CARD	Caspase recruitment domain
Cas9	CRISPR-associated endonuclease 9
CD	Cluster of differentiation
cDNA	complementary DNA
Cflar	Capsase-8 and FADD-like apoptosis regulator
cFLIP	cellular FLICE-like inhibitory protein
Cflip^{D377A}	*Cflip$^{D377A/D377A}$*
Cflip^{D377A}Sharpin^{cpdm}	*Cflip$^{D377A/D377A}$Sharpin$^{cpdm/cpdm}$*
Cflip^{D377A}Sharpin^{WT}	*Cflip$^{D377A/D377A}$Sharpin$^{WT/WT}$*
Cflip^{WT}	*Cflip$^{WT/WT}$*
Cflip^{WT}Sahrpin^{cpdm}	*Cflip$^{WT/WT}$Sharpin$^{cpdm/cpdm}$*
Cflip^{WT}Sahrpin^{WT}	*Cflip$^{WT/WT}$Sharpin$^{WT/WT}$*
cIAP1/2	cellular Inhibitor of apoptosis protein 1/2
cpdm	chronic proliferative dermatitis
CRISPR	Clustered regularly interspaced short palindromic repeats
CrmA	Cytokine response modifier A
CYLD	Cylindromatosis
DAMPs	Danger-associated molecular patterns
DMEM	Dulbecco's modified Eagle medium
DNA	Deoxyribonucleic acid
DR	Death receptor
DTT	1, 4-Dithiothreitol
E	Emricasan
EDTA	Ethylenediaminetetraacetic acid
ERK1/2	Extracellular-signal-regulated kinase 1/2
FADD	Fas-associated protein with death domain
FAS-L	FAS ligand
FBS	Fetal bovine serum
FIP200	200kD FAK family kinase-interacting protein
fl	floxed
GFP	Green fluorescence protein
GSDMD	Gasdermin D
H&E	Hematoxylin and Eosin

HEK 293 T cells	Human embryonic kidney 293 T cells
HEPES	(4-(2-hydroxyethyl)-1-piperazineethanesulfonic acid)
HOIL-1	Heme-oxidized IRP2 ubiquitin ligase
HOIP	HOIL-1-interacting protein
IAV	Influenza A virus
ICAD	Inhibitor of CAD
IFN	Interferon
IFN-R	Interferon receptor
IKK	Inhibitor of Nuclear factor kappa B
IL	Interleukin
IPTG	Isopropyl-β-D-1-thiogalactopyranoside
IRP2	Iron regulated protein 2
ISGs	IFN-stimulated genes
JNK	Jun N-terminal kinase
K6	Keratin 6
LB	Lysogeny broth
LC3	Light chain 3A
LDH	Lactate dehydrogenase
LECs	Lung endothelial cells
LFs	Lung fibroblasts
LPS	Lipopolysaccharide
LTA	Large T antigen
LUBAC	Linear ubiquitin chain assembly complex
LysC	Lysyl endopeptidase
MAPK	Mitogen-activated protein kinase
MDFs	Mouse dermal fibroblasts
MEFs	Mouse embryonic fibroblasts
MLKL	Mixed Lineage Kinase Domain Like Pseudokinase
MOI	Multiplicity of infection
N4BP1	Nedd4-binding partner 1
NF-κB	Nuclear factor kappa light chain enhancer of activated B cells
NINJ-1	Ninjurin-1
NLRP	Nucleotide-binding oligomerisation domain (NOD)-like receptor protein
NOD	Nucleotide-binding oligomerisation domain
OCT compound	Optimal cutting temperature compund
OD_{600}	Optical density at 600 nm
PAMPs	Pattern-associated molecular patterns
PARP-1	Poly ADP-ribose polymerase-1
PBS	Phosphate-buffered saline
PCR	Polymerase chain reaction
PFA	Paraformaldehyde
PP2A	Protein phosphatase 2
PPP2R1A	Protein phosphatase 2 scaffold subunit A alpha
PVDF	Polyvinylidene difluorde
PYD	Pyrin domain
RH domain	Rubicon homology domain
RHIM	RIP homotypic interaction motif
RIPK1/3	Receptor-interacting serine threonine kinase-1/-3
RNA	Ribonucleic acid
RT	Room temperature
RT-qPCR	Quantitative reverse transcription PCR
Rubicon	Run domain Beclin-1-interacting and cysteine-rich domain-containing protein

S	AZD5582
SARS-CoV 1	Severe acute respiratory syndrome coronavirus 1
SDS-PAGE	Sodium dodecyl sulphate polyacrylamide gel electrophoresis
Serpin	Serine protease inhibitor
sgRNA	single guide Ribonucleic acid
SH3	SRC Homology 3
SHANK	SH3 and multiple ankyrin repeat domains 3
SHARPIN	SHANK Associated RH Domain Interactor
Sharpin^{cpdm}	*Sharpin$^{cpdm/cpdm}$*
Sharpin^{WT}	*Sharpin$^{WT/WT}$*
SMA	Smooth muscle actin
SRC	Proto-oncogene tyrosine-protein kinase Src (short for sarcoma)
SV40	Simian Virus 40
T	TNF
TAB1/2/3	TAK1 binding protein 1/2/3
TAE Buffer	Tris acetate EDTA buffer
TAK1	Transforming growth factor β activated kinase 1
TANK	TRAF family member associated NF-κB Activator
TAX1BP1	TAX1 binding protein 1
TBK1	TANK-binding kinase 1
$TCID_{50}$	50% tissue culture infectious dose
TEMED	N,N,N′,N′-Tetramethylethylenediamine
TFA	Trifluoroacetic acid
TLR	Toll-like receptor
TNF	Tumour necrosis factor
TNF-R	Tumour necrosis factor receptor
TRADD	TNF-R1 associated death domain protein
TRAF2	TNF-R associated factor 2
TRAIL	TNF-related apoptosis-inducing ligand
TRAIL-R1/2	TNF-related apoptosis-inducing ligandreceptor 1/2
TRIF	TIR-domain-containing adapter-inducing interferon-β
UV	Ultraviolett
v/v	volume/volume
vFLIP	viral FLICE-inhibitory proteins
w/v	weight/volume
WT	Wild-type
ZBP1	Z-DNA binding protein 1

IV. LIST OF UNITS

Abbrevation	Unit
h	hour(s)
°C	degree Celcisus
%	percentage
g	gram
l	liter
min	minute(s)
sec	second(s)
G	Gauge
m	meter
rpm	rounds per minute
rcf (×g)	Relative centrifugal force (×g force)
M	molar
m/z	mass-to-charge ratio
×	times
U	Units
v/v	volume-to-volume
w/v	weight-to-volume
kDa	kilo Dalton
V	Volt

V. LIST OF DIMENSIONS

Dimensions	Abbreavation
nano	n
micro	µ
centi	c
milli	m

VI. INDEX OF FIGURES

VII. INDEX OF TABLES

1 INTRODUCTION

1.1 Cell Death

Tissue homeostasis is a dynamic equilibrium between the survival of functional cells and the death of dysfunctional or obsolete cells. This balance relies on the controlled execution of cell death programs that occur constantly under physiological conditions.[1,2] Apart from controlling tissue homeostasis, cell death has the function to trigger inflammatory responses that are essential for the ability of an organism to cope with threats such as injury or infection. However, deregulated cell death can cause aberrant inflammation leading to severe tissue damage and organ failure. Consequently, both abrogation and exacerbation of cell death can impair the ability of an organism to develop, maintain homeostatic conditions, modulate immune responses and activate tissue regeneration following damage.[3,4] It is therefore of the highest importance to understand the molecular mechanisms regulating the different cell death programs.

To date, various types of programmed cell death have been discovered.[4,5] These are divided into two main categories according to their morphologic features: non-lytic and lytic cell death forms. The so far only known form of non-lytic cell death is apoptosis, which is characterised by plasma membrane blebbing, cell shrinkage, chromatin condensation, nuclear fragmentation and the formation of apoptotic bodies. [5,6] The lytic cell death forms, the most studied ones being necroptosis and pyroptosis, are characterised by cellular swelling, permeabilization of the plasma membrane and the consequent release of intracellular contents (Figure 1).[7] The various cell death types have a different potential to induce inflammation and activate the immune system. While apoptosis is considered immunologically silent, necroptosis and pyroptosis are highly inflammatory.[5] It is therefore believed that the different types of cell death provide a powerful defence mechanism to protect the organisms against a vast range of pathogens that threaten homeostasis through diverse mechanisms.[8] In addition, cell death is also known to participate to inflammatory processes triggered by other types of insult, such as tissue injury, where dying cells are instrumental in activating repair programs.

Tumour necrosis factor (TNF) is a proinflammatory cytokine secreted upon a variety of stressors, including viral infection and tissue injury. It contributes to mount the immune responses and repair processes by both inducing the expression of proinflammatory genes and triggering cell death in the form of apoptosis, necroptosis or pyroptosis. The precise coordination of these functional outcomes, esspecially cell death, is essential to protect organisms from aberrant inflammation and its detrimental consequences. Consequently, dissecting the mechanisms regulating the type and

extent of TNF-induced cell death is crucial to gain a better understanding of how cell death controls the ability of organisms to overcome stress conditions.

1.1.1 Apoptosis

Apoptosis is the first described form of programmed cell death that strictly depends on the proteolytic activity of caspases.[9] It is subdivided into two distinct, but interconnected pathways according to their trigger: the intrinsic and extrinsic pathway. Various types of intracellular stress, such as absence of certain growth factors, DNA damage or endoplasmic reticulum stress, activate intrinsic apoptosis. Extrinsic apoptosis is driven by receptors at the plasma membrane sensing the perturbations in the microenviroment. Particularly, extracellular ligands able to activate a class of surface receptors, called death receptors (DRs), trigger apoptosis. The most commonly studied DR-ligand systems are TNF/ TNF-receptor 1 (TNF/TNF-R1), FAS-ligand/FAS (FAS-L/FAS) and TNF-related apoptosis-inducing ligand/receptor (TRAIL/TRAIL-R1/2).

The execution of both intrinsic and extrinsic apoptosis relies on the activation of initiator caspases (Caspase-9[10] in intrinsic and -8[11] in extrinsic apoptosis), that cleave and activate downstream executioner caspases (Caspase-3 and -7)[12]. Caspases are cysteine proteases that are synthesized as inactive zymogens. Once apoptosis is triggered, caspases are converted into their active forms. They form homodimers and cleave their target protein to execute the biochemical modifications associated with apoptosis[13] (Figure 1). Caspase-activated DNase (CAD) is a crucial enzyme in downstream events of apoptosis. Under normal conditions, CAD is inactive due to its interaction with the Inhibitor of CAD (ICAD). During apoptosis, caspase-3 cleaves ICAD. This releases the activated CAD, which, in turn, degrades chromosomal DNA within the nuclei and induces chromatin condensation.[14,15] Additionally, poly ADP-ribose polymerase-1 (PARP-1), an enzyme that plays a central role in DNA repair, is a substrate of Caspase-3 during apoptosis. The cleavage of PARP-1 produces specific proteolytic cleavage fragments, which are recognized biomarkers for apoptosis.[16,17] Furthermore, Capsase-3 cleaves gelsolin, an actin-binding protein. The cleaved fragments of gelsolin, in turn, cleave actin filaments, leading to the disruption of the cytoskeleton and intracellular transport leading to the disintegration of the cell into apoptotic bodies.[18,19] Phagocytes rapidly remove the apoptotic bodies recognized by the appearance of phosphatidylserine on their surface, preventing the release of cellular content. Therefore, apoptosis is widely accepted to be an immunologically silent cell death type. However, this widely accepted notion is currently under debate. It is now becoming evident that also apoptosis, in certain settings, can induce an immune response in dependence of several factors such as the dying cell type, the cause of death, its microenvironment or the levels of cell death.[20]

1.1.2 Necroptosis

Necroptosis is a lytic cell death type that is independent of caspases and strictly dependent on the activity of a class of kinases, the receptor-interacting serine-threonine kinases (RIPKs), in particular RIPK1 and RIPK3. Signal-induced RIPK1 autophosphorylation is followed by its binding to RIPK3, via a common structural motif, termed the RIP homotypic interaction motif (RHIM) domain. Their interaction is then followed by oligomerisation and autophosphorylation of RIPK3. These events lead to the recruitment and RIPK3-driven phosphorylation of mixed-lineage kinase domain-like pseudokinase (MLKL).[21,22] Subsequently, active MLKL undergoes a conformational change, promoting its ubiquitination, oligomerisation and translocation to the plasma membrane. Here, MLKL oligomers form cation channels that initiate plasma membrane rupture. This cause the release of intracellular content, a characteristic feature of lytic cell death (Figure 1).[23,24] Necroptosis can be initiated by different types of signals and cellular context. Different immune receptors, such as DRs including TNF-R1 or Toll-like receptors (TLRs), including TLR3 and 4), upon binding to their respective ligands have the potential to activate the RIP1/RIPK3/MLKL axis to induce necroptosis. For necroptosis to occur, the absence of Caspase-8 or inhibition of Caspase-8 catalytic activity, either genetic or pharmacologic, is prerequisite[25–31] since Caspase-8 would otherwise block necroptosis by cleaving of RIPK1[32,33]. In addition, an intracellular sensor, Z-DNA-binding protein 1 (ZBP1)[34], which recognises left-handed double-helix Z-nucleic acids of viral origin particularly, can interact with RIPK1 and RIPK3 via RHIM domains and activate necroptosis.[35–37]

1.1.3 Pyroptosis

Pyroptosis is another type of lytic cell death, mediated by caspases, that was first discovered in immune cells.[38] It can be triggered in response to pathogenic, stress-derived and environmental factors, each of which is recognised by its respective sensor. The most common sensors are nucleotide-binding oligomerisation domain (NOD)-like receptor proteins (NLRPs)[39] and absent in melanoma 2 (AIM2)[40]. Once bound to ta damage- or pathogen-associated molecular patterns (DAMPs and PAMPs), these sensors undergo a conformational change that promotes their binding to Apoptosis-associated Speck-like protein containing a caspase recruitment domain (ASC) through homotypic pyrin domain (PYD) interactions. ASC then recruits Caspase-1 via the caspase recruitment domain (CARD). These proteins form a large cytosolic multimeric protein complex, known as the canonical inflammasome, which ultimately promotes the activation of Caspase-1.[41] This occurs by proximity-driven intermolecular activation of pro-Caspase-1, followed by intramolecular auto-proteolytic cleavage releasing fully active Caspase-1 into cytosol (Figure 1).[42] Here, Caspase-1 cleaves Gasdermin D (GSDMD), the effector molecule for the plasma membrane rupture.[43] It also cleaves pro-inflammatory cytokines, such as interleukin (IL)-1β and IL-18, to their

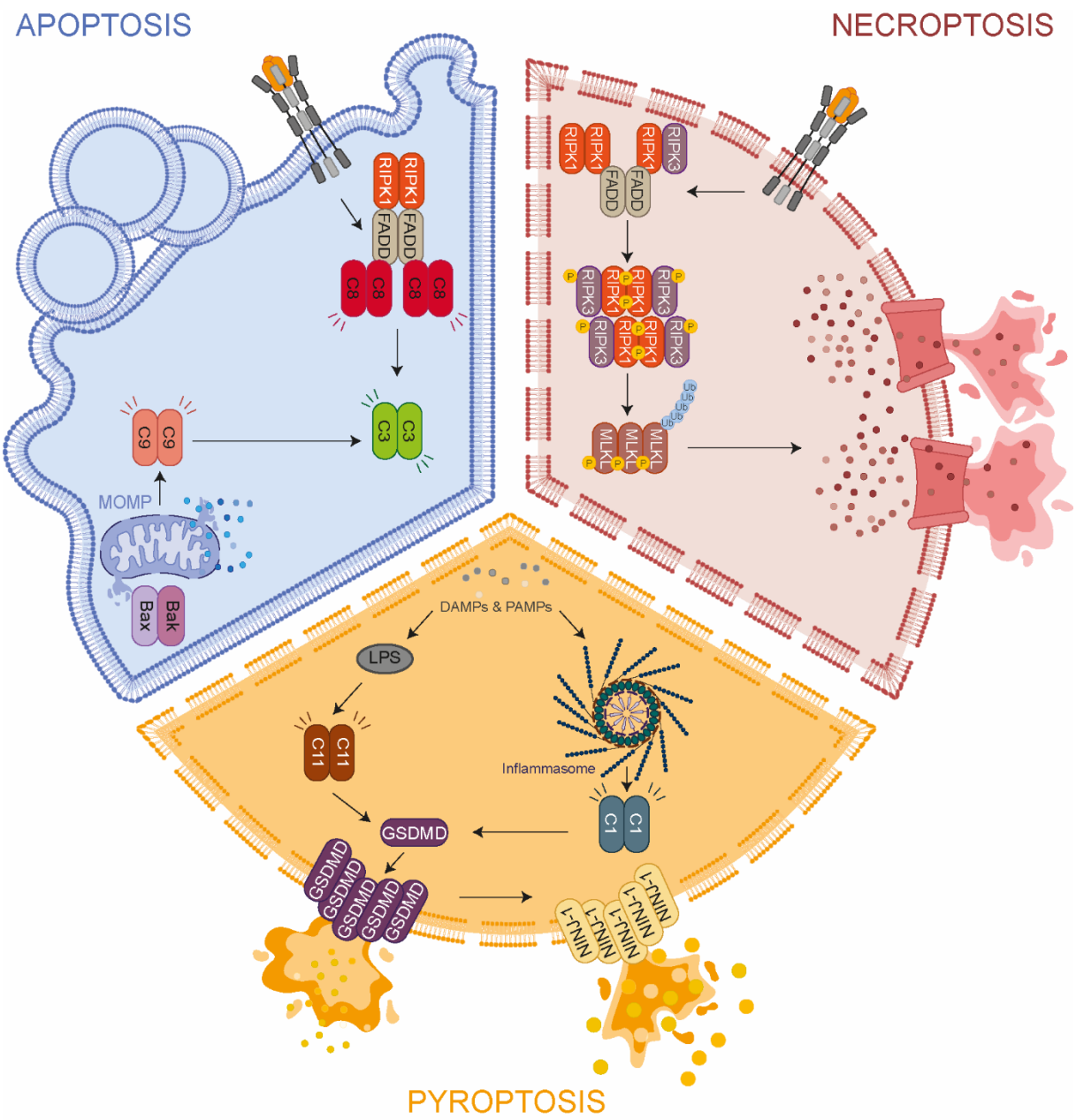

Figure 1. Overview of different forms of programmed cell death. Cells undergo various programmed cell death pathways that differ in their execution and outcomes. Apoptosis can be triggered by either the extrinsic (death receptor-induced) or the intrinsic (mitochondrial) pathways. The extrinsic pathway is activated by death receptors at the plasma membrane and leads to the formation of a Caspase-8 activating complex. The intrinsic pathway can be induced intracellularly by various stress stimuli that cause mitochondrial outer membrane permeabilization (MOMP) and activation of the initiator Caspase-9. After the initiator caspases are activated, both apoptotic pathways converge to the proteolytic activation of the executioner Caspase-3 and -7. They promote DNA fragmentation, membrane blebbing, formation of apoptotic bodies and exposure of phosphatidylserine on the outer layer of the cell membrane of a dying cell. Necroptosis is initiated upon activation of the receptor-interacting serine-threonine kinases RIPK1 and RIPK3. RIPK3 phosphorylates pseudo-kinase mixed-lineage kinase domain-like (MLKL), which undergoes conformational modifications causing its ubiquitination and translocation to the cell membrane. At the cell membrane, MLKL induces membrane rupture. This leads to swelling of the cell, disruption of membrane potential, and eventually cell lysis. Pyroptosis is another type of lytic cell death, triggered by damage- or pathogen-associated molecular patterns (DAMPs and PAMPs). These activate a cascade of events leading to the formation of a cytosolic protein complex, called the inflammasome, which promotes the activation of Caspase-1. Activation of Caspase-1 leads to cleavage of Gasdermin D (GSDMD), an effector molecule for plasma membrane rupture. The N-terminal fragment of GSDMD induces the formation of small plasma membrane pores that facilitate the release of mature proinflammatory cytokines. Downstream of GSDMD pore formation, Ninjurin-1 (NINJ-1) further mediates plasma membrane rupture leading to the release of larger cell contents such as lactate dehydrogenase (LDH), which cannot pass through the GSDMD pores.

mature form[44]. The N-terminal GSDMD fragment then translocates to plasma membrane, where it forms initial small plasma membrane pores facilitating the release of mature proinflammatory cytokines[45,46]. Downstream of GSDMD pore formation, Ninjurin-1 (NINJ-1) mediates plasma membrane rupture by forming NINJ1 oligomers and membrane blebs. This results in the release of cellular content, such as lactate dehydrogenase (LDH), which are too large to pass through GSDMD pores (Figure 1).[47,48] The release of these factors promotes recruitment and activation of immune cells to the site of infection or injury. Alternatively, Caspase-4 and 5 in humans (Caspase-11 in mice) are activated by cytoplasmic bacterial lippolysaccharide (LPS) within the non-canonical inflammasome, most likely, by direct interaction.[49] These active caspases cleave GSDMD to its active form that mediates pyroptosis. GSDMD-dependent cellular changes, in turn, trigger the NLRP3 inflammasome activating Caspase-1 for the release of prinflammatory cytokines (Figure 1).[50] This builds a bridge between the canonical and non-canonical inflammasomes and increaes the amplitude of pyroptosis. Recently it was discovered that GSDMD can also be cleavaed by active Caspase-8 during extrinsic apoptosis. However, in this scenario, this GSDMD activating cleavage is counterbalanced by the inactivating cleavage of the N-terminal GSDMD fragment by Caspase-3.[51–54] This observation reveals an important crosstalk between apoptosis and pyroptosis, indicating how layered and intricated are the mechanisms controlling cell death.

1.2 Death Receptor/Ligand Systems

DRs are a subgroup of TNF-R superfamily proteins and are characterised by a cytoplasmic region referred to as death domain. This domain enables the aforementioned receptors to initiate cell death in form of apoptosis and necroptosis upon binding to their corresponding ligands. Despite their name, death receptors not only engage cell death but also the expression of proinflammatory genes (Figure 2).[55] Indeed, it is now clear that they orchestrate inflammatory programs, both by inducing the expression of proinflammatory and prosurivival genes and by activating cell death. These downstream signalling outcomes rely on the formation of spatially and temporally distinct complexes, whose assembly and regulation are unique for different DR/ligand systems (Figure 2).[56] While the TNF/TNFR1 activation initially leads to the formation of a signalling complex, followed by the formation of a cell death-inducing complex, cytotoxic activities are primary outcomes in TRAIL/TRAIL-R1/2 signalling and a secondary complex mediates proinflammatory gene expression.

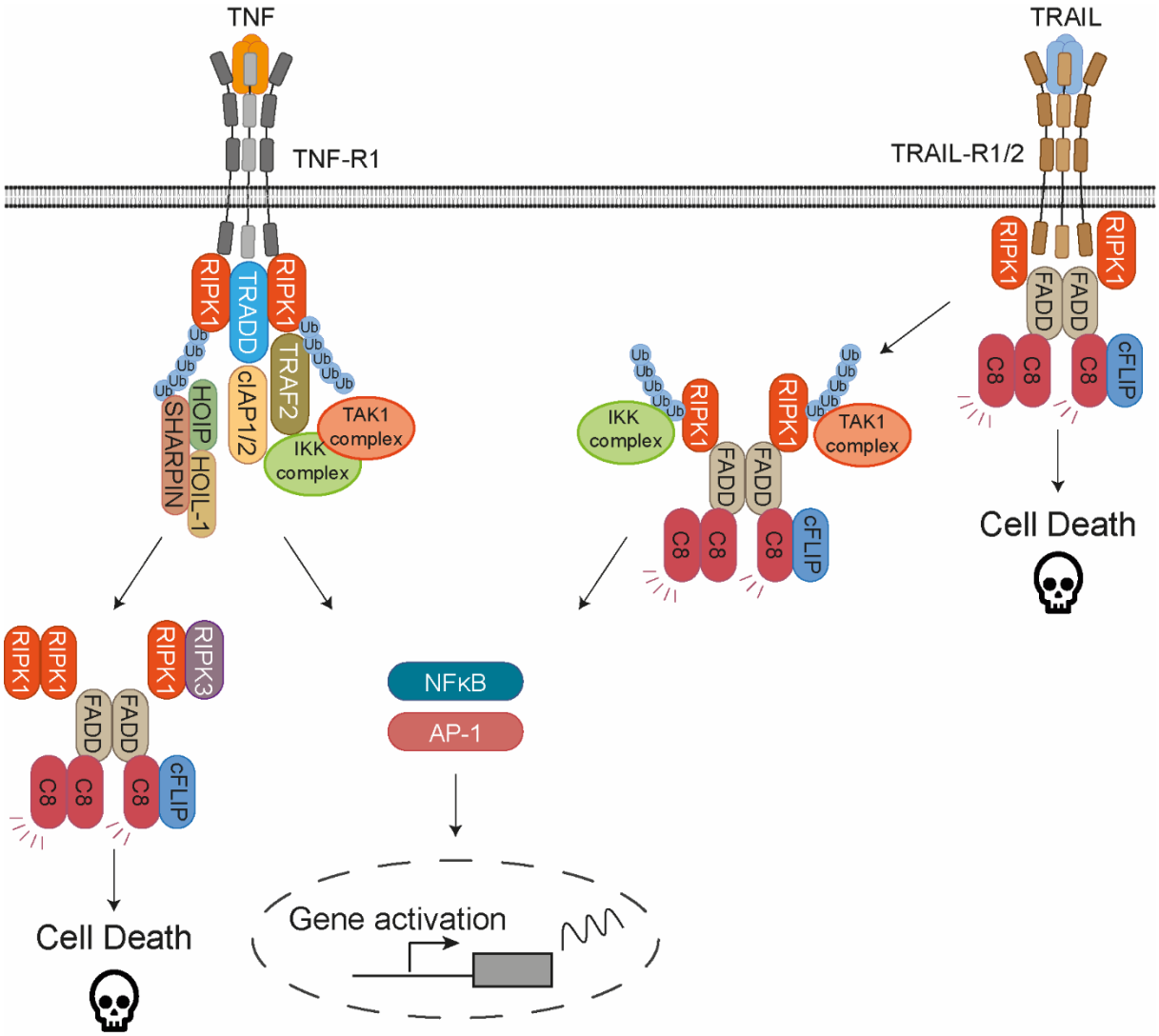

Figure 2. Overview of different death receptor/ligand signalling pathways. Binding of tumour necrosis factor (TNF) to the TNF-receptor 1 (TNF-R1) triggers receptor trimerization and the formation of the membrane-bound complex I. This complex contains adaptor proteins like TNF R1 associated death domain protein (TRADD) and TNF-R associated factor 2 (TRAF2), protein kinases, the most important one being RIPK1 ubiquitin ligases such as cellular inhibitor of apoptosis protein 1/2 (cIAP1/2) and linear ubiquitin chain assembly complex (LUBAC). These proteins decorate complex I with posttranslational modifications including phosphorylation and ubiquitination. These serve as scaffolding to recruit kinase complexes which activate nuclear factor kappa light chain enhancer of activated B cells (NF-κB) and mitogen-activated protein kinase (MAPK) pathways for proinflammatory and prosurvival gene expression. While the primary outcome of TNF signalling is gene expression, TRAIL has the potential to induce cell death through recruitment of FADD, Caspase-8, among others, to the membrane-bound complex as the primary outcome. These two primary complexes dissociate from the respective receptors and incorporate additional proteins to form a secondary cytosolic complex called complex II. In the case of TNF-R1, this complex induces different cell death types. TRAIL-R1/2 complex II triggers gene activation via NF-κB and MAPKs.

1.3 TNF/TNF-R1 Signalling Pathway

TNF transduces signals through two distinct transmembrane receptors: TNF-R1 and TNF-R2. TNF-R1 is one of the most characterised members of the death receptors. In contrast to TNF-R2, TNF-R1 is ubiquitously expressed and recognises both soluble and membrane-bound TNF.[57] Through its death domain, which is absent in TNF-R2, TNF-R1 is able to transduce cytotoxic signals in addition to engaging proinflammatory signalling.[55] Thus, TNF/TNF-R1 signalling pathway is one of the best-studied death receptor ligand systems.[58]

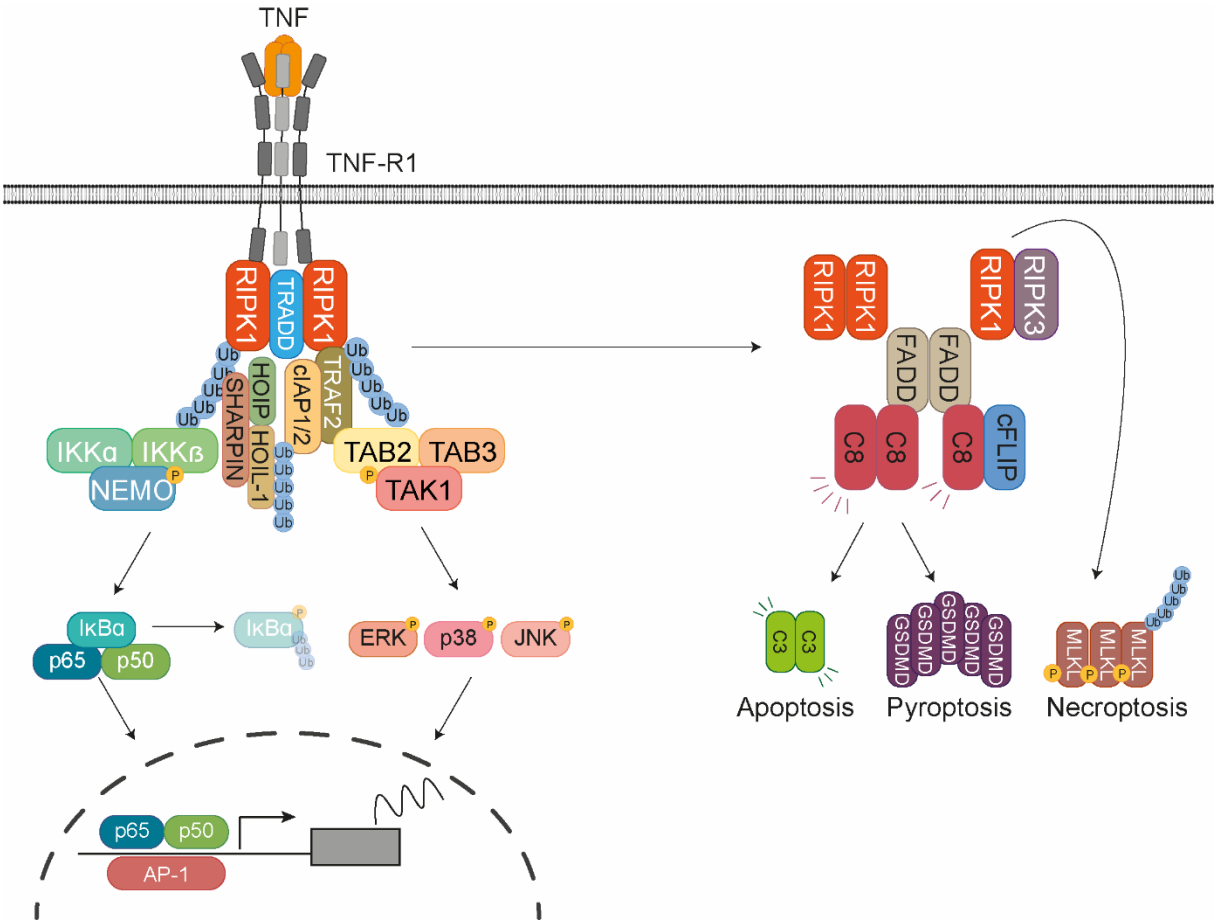

Figure 3. Simplified overview of TNF/TNF-R1 signalling. The binding of tumour necrosis factor (TNF) to the TNF-receptor 1 (TNF-R1) engages the recruitment of several adaptor proteins and enzymes, most importantly kinases and ubiquitin ligases. The phosphorylation and ubiquitination events in complex I serve as an activation platform for two important kinase complexes, that further phosphorylates the target proteins. The kinases in TAK1 complex, that consists of transforming growth factor-β-activated kinase 1 (TAK1), TAK1-binding proteins 2 and 3 (TAK1/TAB2/TAB3) induce activation of mitogen-activated protein kinases (MAPKs) through phosphorylation of extracellular signal-regulated kinase 1/2 (ERK1/2), c-Jun N-terminal kinase (JNK) and p38 that in turn activates transcription factor Activator protein 1 (AP-1). Similarly, IKK complex, including the inhibitor of nuclear factor-κB kinase subunit α and β (IKKα/IKKβ) and NF-κB essential modulator (NEMO) activates p65/p50 dimer of nuclear factor κ light-chain enhancer of activated B cells (NF-κB) through phosphorylation of IκBα. Subsequently, inhibitor of nuclear factor-κB kinase α (IκBα) is targeted for ubiquitylation and proteasomal degradation leading to the release of NF-κB dimers (p50/p65). This enables the translocation of NF-κB dimers to the nucleus, where they mediate gene expression. In addition to this activity, these two kinase complexes act to keep the kinase activity of receptor-interacting protein kinase 1 (RIPK1) in check by inhibiting its release from complex I. Once disassociated, RIPK1 nucleate a secondary cytoplasmic complex, complex II. Complex II consists of are Fas-associated protein with death domain (FADD), Caspase 8, cellular FLICE-like inhibitory protein (cFLIP), RIPK1 and, depending on the cell type, RIPK3. It has the potential to trigger Caspase-8/Caspase-3-mediated apoptosis, RIPK1/RIPK3-mediated necroptosis and in some cells Caspase-8/Gasdermin D (GSDMD)-mediated pyroptosis. FADD brings Caspase-8 to complex II, which, upon proximity-driven activation process, initiates apoptosis. When Caspase-8 activity is completely absent, the RIPK1/RIPK3 axis is unchecked. The autophosphorylations of RIPK1 and RIPK3 stabilise their oligomers, which subsequently phosphorylates mixed lineage kinase domain-like pseudokinase (MLKL) to activate necroptosis. In some cells, Caspase-8 activates GSDMD through proteolysis to initiate pyroptosis.

As one of the major proinflammatory cytokines, TNF contributes to mount immune responses and repair processes by inducing the expression of proinflammatory genes and triggering cell death. Soon after discovery of TNF, it became evident that the primary outcome of TNF/TNF-R1 signalling in many cell types is the rapid expression of proinflammatory genes and, only under certain circumstances, TNF induces cell death (Figure 2).[2,57,58] Accordingly, several mechanisms, called

checkpoints, have been discovered that suppress the cytotoxic potential of TNF.[1,2,20,56,58–62] Since deregulated TNF-mediated cell death is involved in several chronic inflammatory diseases, it is utmost important to elucidate the complex molecular mechanisms regulating the balance between cell death and inflammation downstream of TNF-R1.

1.3.1 TNF-Induced Proinflammatory Signalling

TNF/TNF-R1-induced signalling outcomes are delivered through the formation of two spatially and temporally distinct platforms: a membrane-bound proinflammatory signalling complex, referred to as complex I and a cytosolic death-inducing complex, referred to as complex II (Figure 3).[63] The binding of TNF to TNF-R1 triggers receptor trimerization.[64] This initiates the formation of complex I through homotypic interactions of the death domains on the intracellular portion of TNF-R1 and the adaptor protein TNF-R1 associated death domain protein (TRADD).[62] This event is followed by the recruitment of further adaptor proteins, such as TNF-R associated factor 2 (TRAF2)[63], kinases, the most important one being RIPK1[62,65], ubiquitin ligases such as cellular inhibitor of apoptosis protein 1/2 (cIAP1/2)[66] and linear ubiquitin chain assembly complex (LUBAC)[67] as well as deubiquitinases including cylindromatosis (CYLD)[68] (Figure 3). The E3 ligases decorate different components of complex I, most importantly RIPK1, with ubiquitin chains of different topologies (e.g., K48, K63 and M1). Ultimately, these events lead to the recruitment of kinase complexes, which ensure proper activation of canonical nuclear factor kappa light chain enhancer of activated B cells (NF-κB) and mitogen-activated protein kinase (MAPK) pathways for proinflammatory and prosurvival gene expression (Figure 3).[69] These three kinase complexes are canonical inhibitor of nuclear factor kappa B (IKK) complex, which is composed of kinases IKKα and IKKβ together with regulatory subunit IKKγ/NEMO, the transforming growth factor β activated kinase 1 (TAK1) complex, which is composed of TAK1 together with TAK1 binding protein 1, 2 and 3 (TAB1, TAB2, TAB3) and non-canonical IKK-related kinase complex including TRAF family member associated NF-κB Activator (TANK), IKKε and TANK-binding kinase 1 (TBK1). In the activation cascade of NF-κB signalling, TAK1 phosphorylates and activates IKKβ, which in turn phosphorylates IκBα. Subsequently, IκBα is targeted for ubiquitination and proteasomal degradation leading to the release of NF-κB dimers (p50/p65). This enables the translocation of NF-κB dimers to the nucleus, where they mediate gene expression (Figure 3).[70,71] Similar to the NF-κB pathway, the MAPK pathway relies on the phosphorylation events by TAK1. TAK1-dependent activation of extracellular-signal-regulated kinase 1/2 (ERK1/2), Jun N-terminal kinase (JNK) and p38 results in the translocation of activator protein 1 (AP-1) to the nucleus and the subsequent induction of target genes (Figure 3).[70,72] Taken together, the binding of TNF to TNF-R1 results in a complex signalling network through the recruitment of several proteins in a post-translational modification-dependent

manner that ultimately induces transcriptional programs promoting prosurvival and proinflammatory cascades.

1.3.2 TNF-Induced Cell Death

Under physiological conditions, TNF stimulation of TNF-R1 rapidly leads to the formation of complex I. The concerted action of phosphorylation and ubiquitination events that occur during complex I assembly serve not only for signal transduction but also as checkpoints that safeguard its correct assembly and stability and as a consequence, its prosurvival functions. Impairment of any of these checkpoints causes a shift from gene expression activation to the induction of different cell death types via the formation of complex II (Figure 3).[60,62,63] Complex II share some components with complex I, while other components are incorporated from the cytoplasm. For example, RIPK1 and TRADD are components of complex I that can nucleate complex II formation under specific circumstances. [73] Together with RIPK1 or TRADD, the core components of complex II are Fas-associated protein with death domain (FADD), Caspase-8, cellular FLICE-like inhibitory protein (cFLIP), RIPK1 and, depending on the cell type, RIPK3 (Figure 3).[63] FADD serves as an adaptor protein by associating with pro-Caspase-8 via its death effector domain and RIPK1 via its death domain. Thereupon, Caspase-8 can either bind to Caspase-8 forming homodimers or to cFLIP, a catalytically inactive homolog of Caspase-8, forming heterodimers (Figure 6B). A proximity-driven activation process via homodimerization of Caspase-8 and two sequential autoproteolytic cleavage events are required to release fully active Caspase-8 (p18 fragments) and the activation of apoptosis through the cleavage of executor caspases, Caspase-3 and -7 (Figure 3). In contrast, the binding of cFLIP to Caspase-8 serves as a brake to the full activation of Caspase-8 and Caspase-8-mediated cell death (Figure 3).[74] Secondly, the binding of FADD to RIPK1 is followed by its autophosphorylation and recruitment of RIPK3 through homotypic RHIM domain interactions that ultimately leads to necroptosis via phosphorylation events (Figure 3), in conditions whereby Caspase-8 is absent or its catalytic activity in inhibited. While RIPK1 and potentially RIPK3[75] also contribute to Caspase-8 mediated apoptosis, Caspase-8 cleaves RIPK1 preventing further initiation of necroptosis. Accordingly, the genetic ablation of FADD or Caspase-8 or inhibition of Caspase-8 activity shifts TNF-mediated cell death from apoptosis to necroptosis.[7] Recent findings showed that Caspase-8 can activate GSDMD-mediated pyroptosis, a further lytic cell death type with the active release of proinflammatory cytokines, in certain cell types (Figure 3).[52,54,76,77] Through the ability to control functionally distinct cell death types such as RIPK1/Caspase-8/Caspase-3-dependent apoptosis, RIPK1/RIPK3/MLKL-mediated necroptosis and Caspase-8/GSDMD-mediated pyroptosis (Figure 3), complex II, represents a key node controlling TNF-induced cell death and the pathophysiological outcome thereof.[2,59] However, the

molecular mechanisms behind the transition from complex I to II and the regulation of the multifaceted functions of complex II in controlling TNF-induced cell death remain elusive.

Over the years, it has been shown that multiprotein complexes play a crucial role not only in TNF-induced signalling outcomes but also in various other different immune receptor signalling e.g.,

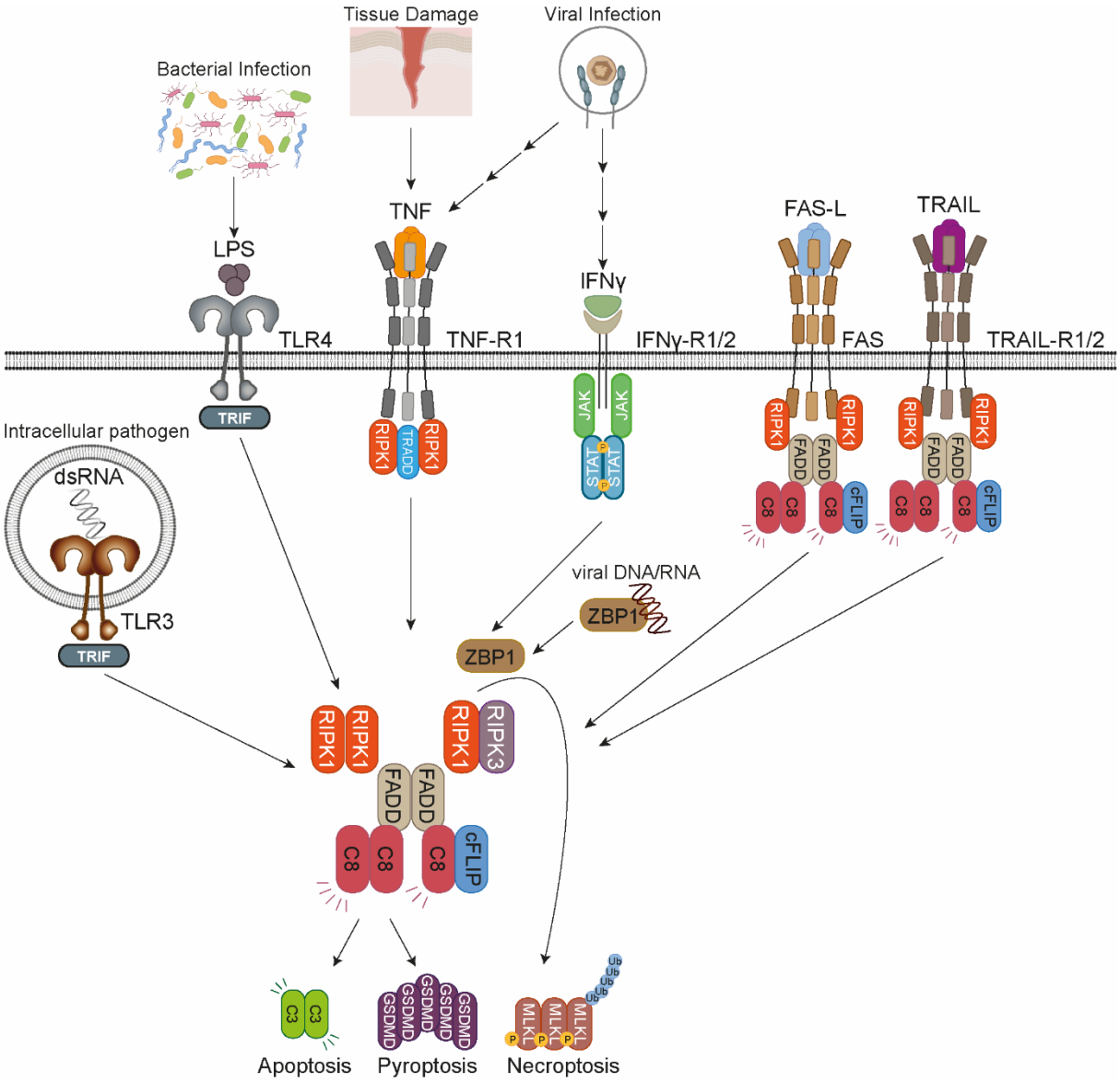

Figure 4. Overview of upstream stimuli that activate complex II. Various direct and indirect stimuli have been shown to activate complex II-like cell death-inducing platforms. These signalling pathways are closely associated with various pathologies. Tumour necrosis factor (TNF), as a proinflammatory cytokine that is secreted under many stress conditions, like viral infection and tissue damage, induces the formation of complex II. Once one or more checkpoints in TNF signalling fails, complex II induces molecularly and functionally distinct cell death outcomes. During viral infection, infected cells secrete an array of cytokines, including interferon γ (IFNγ), that leads to the expression of anti-viral response genes, i.e. Z-DNA-binding protein 1 (ZBP1). Expression and activation of ZBP1 through viral genetic material trigger the formation of a Caspase-8/RIPK1/RIPK3-containing cell death-inducing complex to induce necroptosis and potentially apoptosis. Beisde the indirect activation of cell death programs through cytokines, different immune sensors like Toll-like receptors 3/4 (TLR3/4) can be activated directly by specific molecules derived from pathogens such as double-stranded RNA or lipopolysaccharides (LPS). Through RIP homotypic interaction motif domain interactions, activation of TLR3/4 can induce the formation of a complex II-like death inducing platform to trigger cell death. Additionally, other death receptor/ligand systems like FAS-ligand/FAS (FAS-L/FAS) and TNF-related apoptosis-inducing ligand/receptor (TRAIL/TRAIL-R1/2) can initiate both membrane-bound or cytosolic complex II-like platforms with distinct cellular outcomes.

TLRs and type I and II interferon receptor (IFN-R), as well as other death receptor ligand systems, FAS-L/FAS and TRAIL/TRAIL-R1/2. Recent findings suggest that various immune receptor signalling pathways, other than TNF, have the potential to induce the assembly of a complex II-like death-inducing platform, which is reminiscent of TNF-induced complex II (Figure 4).[27,35,78–81] These complex II-like death-inducing platforms share the same molecular and regulatory components. Similar to the TNF-induced complex II, these platforms initiate cell death via the assembly of a Caspase-8/RIPK1/RIPK3-containing complex. For example, TLR3/4 signalling relies on the RHIM domain-mediated interaction between TRIF and RIPK1/RIPK3 to initiate the assembly of complex II-like death-inducing platform (Figure 4) and trigger necroptosis in a kinase activity-dependent manner. Similarly, ZBP1, a gene upregulated upon IFN-R signalling, can facilitate the assembly of complex II-like death-inducing platform through RHIM-domain interactions with RIPK1/RIPK3, independent of TNF singalling.[35] This, in turn, activates IFN-induced RIPK3/MLKL-mediated necroptosis[35,82] as well as, in certain instances, Caspase-8-mediated apoptosis and pyroptosis[81,83,84]. The biological relevance of these complexes and their regulation becomes even more relevant since they are activated by various pathogens like bacteria and viruses and defects in these mechanisms are associated with severe inflammatory consequences (Figure 4). Hence, it is of the highest biological relevance to decipher the regulatory mechanisms of complex II-mediated cytotoxicity.

1.4 Checkpoints of TNF-Induced Cell Death

The balance between cell survival and death upon TNF signalling relies on a number of checkpoints actively suppressing TNF-induced cell death to ensure the proper activation of gene expression and to protect the organism from the detrimental consequences of aberrantly regulated TNF-induced cell death. Failure of any of these checkpoints leads to the formation and the stabilisation of complex II and thus promotes its cytotoxic activity. More importantly, defects in these checkpoints are closely associated with severe inflammatory pathologies and embryonic lethality in both mice and humans.[69] Therefore, there is an arising interest in the molecular mechanisms fulfilling checkpoint functions downstream of TNF signalling. These checkpoints can be grouped into five categories (Figure 5): NF-κB-driven transcription-dependent, ubiquitination-dependent, phosphorylation-dependent, Caspase-8-dependent and degradation-dependent checkpoints. It is becoming increasingly clear that several checkpoints are interlaced with each other and some of the checkpoints are shared among different death receptor/ligand systems. Indeed, the differential roles of the checkpoints described so far suggest that there is a more complex and layered regulation to prevent aberrant TNF cytotoxicity than initially thought. It is most plausible to think that

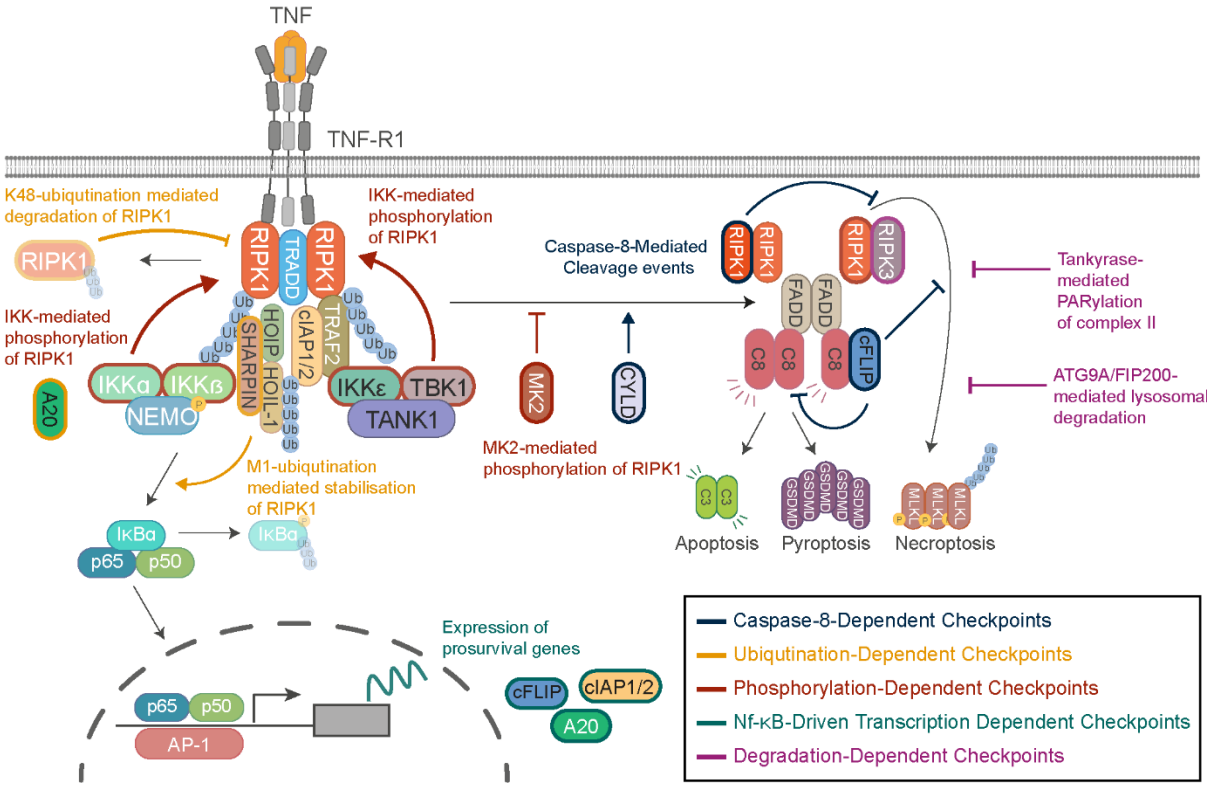

Figure 5. Overview of existing checkpoints that control the formation and cytotoxic activity of complex II. Several checkpoints keep the cytotoxicity of complex II in check through various mechanisms. Here, we divided the known checkpoints into five main categories: NF-κB-driven transcriptional checkpoints (green lines), ubiquitination-dependent checkpoints (yellow lines), phosphorylation-dependent checkpoints (red lines), Caspase-8-dependent checkpoints (blue lines) and degradation dependent checkpoints (purple lines). Activation of NF-κB pathway leads to expression of not only proinflammatory genes but also prosurvival genes that counteract the formation and cytotoxicity of complex II. Decrease in the level of these genes due to impairments in TNF-induced gene expression promotes cell death. Ubiquitination-dependent checkpoints have two important functions. On the one hand, ubiquitinated proteins serve as a scaffold to promote the formation and stability of complex I and II. On the other hand, ubiquitination signals for proteasomal degradation of key proteins in TNF signalling. Phosphorylation-dependent checkpoints in complex I are important for its stabilisation and to inhibit the formation of complex II. Caspase-8-dependent checkpoints are predominantly cleavage events that target proteins promoting complex II formation and cytotoxicity. Thus, the outcome of ubiquitination events is highly dependent on the cellular context. Furthermore, the degradation of cell death components, most importantly complex II, is a pivotal intoxication mechanism to prevent complex II-mediated cell death. Nevertheless, many of these individual checkpoints are related to more than one category depending on their core constituents and components of TNF signalling due to the hierarchical order and interdependency of these processes.

more checkpoints are yet unknown. Therefore, studies on both the regulatory function of known components and novel regulators of TNF-induced complex II-mediated cell death are of the highest biological relevance.

1.4.1 NF-κB-Driven Transcription-Dependent Checkpoints

The first identified checkpoint in TNF signalling is the NF-κB-dependent upregulation of prosurvival proteins.[58] The existence of this checkpoint is evident from the wide *in vitro* use of the protein translation inhibitor cycloheximide that together with TNF induces cell death[85,86]. TNF, in combination with cycloheximide, induce Caspase-8-dependent RIPK1-independent apoptosis due to the absence of the *de novo* protein synthesis important to counteract TNF cytotoxicity, including A20[87], cIAP2[88] and cFLIP[89,90]. As an important NF-κB responsive gene, the cFLIP is rapidly induced

upon TNF stimulation to prevent Caspase-8-mediated cell death. The decrease in cFLIP levels resulting from defects in the gene expression or protein synthesis induces Caspase-8-mediated apoptosis.[74] Therefore, controlling cFLIP levels transcriptionally is an important mechanism to regulate the sensitivity to Caspase-8 mediated cell death.

1.4.2 Ubiquitination-Dependent Checkpoints

Ubiquitination is an E3 ligase-mediated post-translational modification, in which a small protein called ubiquitin is covalently attached to one or more lysine residues of a substrate protein. This process can result in mono- or poly-ubiquitination. In mono-ubiquitination, only one ubiquitin is bound to a lysine on the target protein. In poly-ubiquitination, multiple ubiquitin molecules are bound to different lysine residues on the substrate (poly-monoubiquitination) or multiple ubiquitin molecules are linked to one another forming a chain structure attached to one lysine residue on the substrate (polyubiquitination). The ubiquitination of several complex I components has an essential role in the assembly of TNF-R1 induced complex I.[91,92]

RIPK1 ubiquitination is one of the most studied ubiquitination events in TNF signalling pathway. The ubiquitin chains on RIPK1 not only represent a platform for further recruitment of complex I components but they also prevent the nucleation of complex II via inhibiting the release of enzymatically active RIPK1 to cytosol (Figure 3).[62] Once this occurs, RIPK1 promotes the assembly of complex II, in a kinase dependent manner, that ultimately results in cell death. Consistently with this notion, the impairement of RIPK1 ubiquitination by Smac mimetics[93–95], which are small molecule compounds depleting the E3 ligases cIAP1/2, or its abrogation, via genetic deletion of cIAP1/2[85], unleash the cytotoxic potential of TNF by favouring complex II formation. Equally, the genetic deletion of LUBAC, the only E3 ligase capable of generating M1-ubiquitin chains, causes an impairment of RIPK1 ubiquitination and causes a cell death upon TNF stimulation. LUBAC consists of Heme-oxidized IRP2 ubiquitin ligase 1 (HOIL-1), HOIL-1-interacting protein (HOIP)[96] and Shank-associated RH domain-interacting protein (SHARPIN)[97,98] (Figure 5). As a critical subunit of LUBAC, earlier studies identified *Sharpin* as the gene mutated in chronic proliferative dermatitis mice (cpdm). *Sharpin*$^{cpdm/cpdm-}$ mice developed spontaneously severe chronic multi-organ inflammation, including in skin, gut, liver, spleen and lung.[97] These mice develop a systemic sterile inflammatory condition that becomes evident through severe dermatitis between 15 to 20 weeks and splenomegaly. In addition, these mice exhibit loss of marginal zones in the spleen and Peyer's patches in the small intestine. This phenotype is driven by TNF-mediated RIPK1-kinase activity-dependent cell death, since *Sharpin*$^{cpdm/cpdm}$*Tnf*$^{-/-}$ [97], *Sharpin*$^{cpdm/cpdm}$*Ripk1*$^{K45A/K45A}$ [99] (the K45A mutation inactivates RIPK1 kinase) and

Sharpin$^{cpdm/cpdm}$*Fadd*$^{E\text{-}KO}$*Ripk3*$^{-/-}$ [100] mice did not develop signs of inflammation in skin and liver. The cpdm model was instrumental to understand that RIPK1 ubiquitination is essential to prevent killing potential of TNF and that exacerbated TNF-induced cell death can cause inflammatory diseases.

Ubiquitinated RIPK1 is required, at least in some cell types, activate gene expression, whereas deubiquitination of RIPK1 stimulates cell death. However, the ubiquitination-mediated regulation of RIPK1 is more complicated than initially thought since the topology of the ubiquitin chains determines its unique functions in complex I and II.[101] In this regard, K48-polyubiquitination mainly marks RIPK1 for proteasomal degradation[102], whereas K11-[103], K63-[104] and M1-polyubiquitin chains[97] serve as important scaffolds of proinflammatory signalling.[1,62,91,101] cIAP1/2 conjugate K48- and K63-linked ubiquitin chains to RIPK1, while LUBAC decorates RIPK1 with M1-linear ubiquitin chains (Figure 3). This dynamic process of K63- and M1-ubiquitination is counterbalanced by the activity of deubiquitinase enzymes that hydrolyse the ubiquitin chains and thus induce disassembly of complex I.[62,92] Among these, CYLD removes K63- and M1-ubiquitin chains in complex I promoting cell death and reducing proinflammatory gene activation.[105] In contrast, A20 replaces K63- from RIPK1 with K48-ubiquitin chains[106], leading to its proteasomal degradation and thus inhibition of both RIPK1-mediated proinflammatory signalling and cell death. Moreover, A20 protects M1-ubiquitin chains from CYLD-mediated degradation (Figure 5).[105] Hence, the interplay between RIPK1 and various E3 ligases/deubiquitinases downstream is extremely important for the outcome of TNF-R1 activation.[62,68,91,101] To sum up, the activation of TNF signalling induces multiple ubiquitination events of several target proteins and the complex ubiquitination status of complex I and II has a pivotal role in determining the TNF signalling outcomes.

1.4.3 Phosphorylation-Dependent Checkpoints

The integration of RIPK1 into different signalling complexes and its kinase activity are tightly controlled by phosphorylation.[2,107] In TNF-induced complex I, RIPK1 is not only ubiquitinated but also phosphorylated by the canonical and non-canonical IKK complex[108,109]. It is believed that IKKα/β phosphorylate predominantly ubiquitinated RIPK1 in complex I to suppress RIPK1 autoactivation and its recruitment to complex II (Figure 5). The inhibitory functions of IKK-mediated phosphorylation on RIPK1 are non-redundant, as its inactivation is sufficient to switch the TNF response from survival to RIPK1 kinase-dependent apoptosis. The physiological importance of this checkpoint is underlined by the fact that genetic deletion of *Ikk1/2* in mice results in early lethality due to aberrant cell death in several organs.[108,110–112] Similar to canonical IKK complex, non-canonical IKK complex, consisting of TBK1 and IKKε, directly phosphorylates RIPK1 at multiple sites to prevent TNF-induced cell death. This checkpoint is functionally independently of

canonical IKK complex, while is requires M1-ubiquitination for the recruitment of its components to complex I (Figure 5).[109] Equal to the *Ikk1/2*$^{-/-}$ mice, *Tbk1* deficiency leads to embryonic lethality due to aberrant TNF-induced cell death as a consequence of unleashed RIPK1 activity. Patients with *Tbk1* deficiency suffer from TNF-induced cell death driven chronic inflammation.[113] In the recent literature, MK2-mediated phosphorylation-dependent regulation of RIPK1 has also emerged as a checkpoint of TNF-induced cell death (Figure 5). This phosphorylation event inhibits the autophosphorylation of RIPK1, which is required for its kinase activity. However, differently from phosphorylation events mediated by canonical and non-canonical IKK complexes, MK2-mediated phosphorylation seems to be a secondary checkpoint that limits the cytotoxic potential of RIPK1only in conditions, where a primary checkpoint, e.g. RIPK1 ubiquitination, has been disabled. Accordingly, genetic and pharmacological inhibition of MK2 increased the sensitivity to cell death induced by TNF in combination with Smac mimetics or IKK inhibiton.[73,114] Collectively, these facts suggest that phosphorylation of RIPK1 at multiple sites regulates the activation status and the interaction of RIPK1 with downstream effectors and the activation of cell death. Once activated and recruited to complex II, RIPK1 promotes the autophosphorylation and activation of RIPK3, which in turn phosphorylates MLKL, leading to necroptosis. Thus, phosphorylation events have emerged as central regulators downstream of different death-inducing stimuli that contribute to the pathogenesis of inflammatory diseases. While the phosphorylation events that control TNF/TNF-R1 signalling and the responsible kinases are well characterised, the presence and role of of phosphotases, as a counteracting mechanism, are almost completely unknown.

1.4.4 Caspase-8-Dependent Checkpoints

Caspase-8 represents an important checkpoint that is based on its catalytic activity and is critical to prevent TNF-induced cell death upon various stimuli.[115] Caspase-8 is a cysteinyl aspartate-specific protease that consists of a death effector domain and a catalytic domain with a small and a large subunit containing the catalytic site at C360 in human (C362 in mouse) (Figure 6A).[11] Upon its recruitment to death-inducing platforms such as TNF-induced complex II, its zymogen form, pro-Caspase-8, undergoes a proximity-driven autoproteolytic cleavage between the small and large subunits (Figure 6A-B). Furthermore, homodimerisation and intermolecular cleavage event between the death effector domain and the large subunit of Caspase-8 molecules are required for complete activation and release of Caspase-8 into the cytosol. Here, it induces apoptosis by cleaving further downstream molecules. Moreover, the catalytic activity of Caspase-8 is necessary to prevent necroptosis by cleaving RIPK1.[7] Consequently, *Caspase-8* full-body deficiency results in embryonic lethality in mice due to deregulated necroptosis[31], which can be rescued by co-deleting either *Ripk3*[116] or *Mlkl*[76]. Similarly, conditional deletion of *Caspase-8* in

skin[28] and intestines[26,27,30] results in aberrant activation of RIPK1/RIPK3/MLKL-mediated necroptosis, causing premature death in mice.[117] Furthermore, aberrant activation of Caspase-8 mediated apoptosis is embryonically lethal.[75] In parallel, FADD, as the only known adaptor and activator of Caspase-8, is essential to control Caspase-8 activity to mediate apoptosis and suppress RIPK1/RIPK3/MLKL-mediated necroptosis.[118] Deletion of *Fadd* inhibits Caspase-8-mediated apoptosis, but promotes RIPK1/RIPK3/MLKL-mediated necroptosis due to the lack of Caspase-8-mediated suppression. Therefore, *Fadd*$^{-/-}$ mice, similar to *Caspase-8*$^{-/-}$ mice, are embryonically lethal[119,120] and tissue-specific deletion of *Fadd* is associated with severe inflammation[30,121,122]. In fact, these phenotypes are driven by aberrant RIPK1/RIPK3/MLKL-mediated necroptosis and thereby are rescued by the concomitant deletion of RIPK3. Collectively, the proximity-driven regulation of Caspase-8 activity through its recruitment to complex II is critical to protect the cells from aberrant cell death.

1.4.4.1 cFLIP as the main regulator of Caspase-8

cFLIP is the most direct and non-redundant regulator of Caspase-8 and its catalytic activity. The current model suggests that the prosurvival functions of cFLIP are isoform- and concentration-dependent as well as tissue-specific.[74,78,123–126] cFLIP has distinct isoforms generated through alternative splicing at the mRNA level, of which three major isoforms predominate, $cFLIP_L$, $cFLIP_S$, and $cFLIP_R$. The predominant cFLIP isoform at the protein level is $cFLIP_L$ (hereafter referred to as cFLIP). As a catalytically inactive Caspase-8 homolog, the protein structure of cFLIP and Caspase-8 is highly similar (Figure 6C). cFLIP is composed of a death effector domain followed by a caspase-like domain with large and small subunits. However, cFLIP lacks proteolytic activity due to several amino acid substitutions, particularly the crucial cysteine residue in the catalytic domain (Figure 6A). Similar to Caspase-8, cFLIP is recruited to complex II through interactions with its death effector domain in a Caspase-8 dependent manner (Figure 6B-D).[74] cFLIP has been reported as either an activator or inhibitor of Caspase-8 activity. Later structural studies explained this dual function of cFLIP with a cooperative and hierarchical binding model[74], in which Caspase-has more affinity for cFLIP than for Caspase-8, itself. This binding induces a rearrangement of the Caspase-8 catalytic site. Thereby, cFLIP facilitates the autoproteolytic processing of pro-Caspase-8 and modulates its prosurvival activity as well as substrate specificity.[74,124,125] Binding of cFLIP confers on Caspase-8 spatially restricted proteolytic activity, which is required to block RIPK1/RIPK3/MLKL-mediated necroptosis[29], and blocks the second Caspase-8 cleavage event required for the full activation of Caspase-8 and thus apoptosis[120] (Figure 5). Consistent with its critical impact on Caspase-8-mediated cell death outcomes, the *Cflip*$^{-/-}$ mice are embryonically lethal at E10.5 due to the concomitant activation of apoptosis and necroptosis.[117,127] Accordingly,

Cflip$^{-/-}$ mice, in contrast to *Caspase-8*$^{-/-}$ and *Fadd*$^{-/-}$mice, can only be rescued by co-deletion of RIPK3 and FADD. Furthermore, the tissue-specific loss of cFLIP leads to severe cell death-dependent inflammation in the skin and intestine.[117,128–130] In other words, the regulation of Caspase-8 through its interaction with cFLIP is a critical checkpoint in determining Caspase-8-mediated signalling outcomes. However, the underlying mechanisms remain poorly understood.

1.4.4.2 Caspase-8 mediated cleavage of cFLIP

cFLIP has been long reported as a substrate of Caspase-8. Comparably to the first autoproteolytic cleavage event of Caspase-8, Caspase-8 cleaves cFLIP between the large and small subunits (Figure 6A). In the current literature, it is widely accepted that Caspase-8 targets D376 in human (D377 in mouse) residue on cFLIP for cleavage.[74,124,131,132] However, the potential role of other aspartic acid residues in this cleavage, e.g. D369 in human (D371 in mouse), has never been

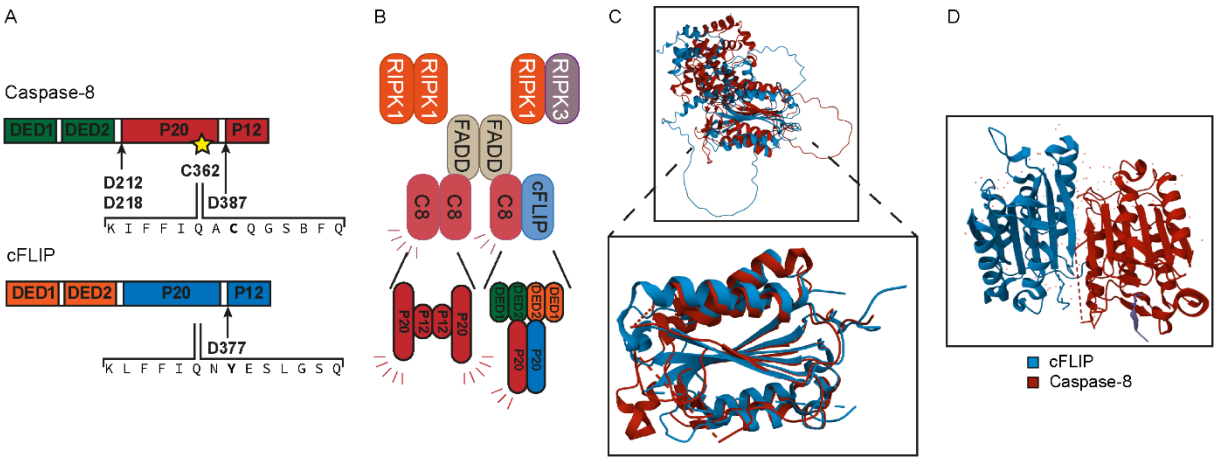

Figure 6. Structural and functional comparison of Caspase-8 and cFLIP. A. Domain compostiton of Caspase-8 and cFLIP. Caspase-8 is a cysteinyl aspartate-specific protease that consists of one death effector domain and a catalytic domain with a small and large subunit containing the catalytic site at C362. A proximity-driven activation process via dimerization and two sequential autoproteolytic cleavage events is required to unleash the full Caspase-8 enzymatic activity, that drives apoptosis and prevents necroptosis. The first cleavage occurs at D387 residue between small and large subunits and governs Caspase-8 a spatially restricted enzymatic activity targeting proteins in close proximity. Homodimerization and a second intermolecular cleavage event between the death effector domain and large subunit, at D212/218 residues, are required for complete activation and release of Caspase-8 into the cytosol. Cellular FLICE-like inhibitory protein (cFLIP) is a catalytically inactive Caspase-8 homolog that critically lacks proteolytic activity due to several amino acid substitutions, particularly the substitution of the crucial C362 in the catalytic domain of Caspase-8 with Y362 in the small subunit of cFLIP. **B. Differential control of Caspase-8 activity in complex II through its homo- and heterodimerisation**. Once TNF-mediated complex II assembles, Caspase-8 can form either homodimers that, once fully activated, are released to the cytosol or an enzymatically active heterodimer with cFLIP to block aberrant activation of apoptosis and necroptosis. The proximity-driven regulation of Caspase-8 activity through its recruitment to complex II and its interaction with cFLIP is critical to prevent aberrant cell death under homeostatic conditions. **C. Structural alignment of Caspase-8 and cFLIP.** The predicted structures of Caspase-8 and cFLIP are very close with 74 % equivalent residues. (upper panel) Besides, empirically determined structures of their death effector domains exhibit 33 % identity with a root mean square root of 2,24 Å (PDB ID 3H11, lower panel). **D. Interaction of death effector domains of Caspase-8 and cFLIP.** Caspase-8 and cFLIP are recruited to death-inducing platforms through their death effector domain interaction. First, Caspase-8 is recruited to complex II, which in turn interacts preferentially with cFLIP and recruits it to complex II. This interaction modulates the prosurvival functions of Caspase-8. (PDB ID 3H11)

addressed to identify the exact cleavage site(s) of cFLIP by Caspase-8 and the plasticity between these residues. Of note, in a previous study, a mutant mouse expressing non-cleavable cFLIP was generated, where both D371 and D377 residues were mutated. These mice were viable without any overt phenotype, indicating that cFLIP cleavage is not essential for embryonic development and homeostasis.[33] Nevertheless, the physiological role of cFLIP cleavage by Caspase-8, particularly under stress conditions, and how this event mechanistically modulates Caspase-8 activity remains to be elucidated.

1.4.5 Degradation-Dependent Checkpoints

In the last decade, several novel checkpoints were found to safeguard the proper functioning of TNF signalling pathway via regulating the stability and dynamics of complex I and II. Very recently, an autophagy-related "detoxification" mechanism was identified. This mechanism promotes the degradation of complex II through an autophagy-related 9A (ATG9A)- and 200kD FAK family kinase-interacting protein (FIP200)-mediated lysosomal targeting process (Figure 5). It relies on the recognition of M1-ubiquitinated RIPK1 in complex II by TAX1 binding protein 1 (TAX1BP1). TAXBP1 then recruits FIP200 and the upstream autophagy machinery to initiate its encapsulation. Encapsulation and the subsequent lysosomal degradation mediated by alternative light chain 3A (LC3)-independent autophagy blocks the cytotoxic activity of complex II. Accordingly, defects in the lysosomal degradation of complex II cause excessive apoptosis due to the accumulation of complex II and active Caspase-8, ultimately leading to embryonic lethality.[133] Another degradation-dependent checkpoint is the tankyrase-1-mediated PARylation of complex II (Figure 5). This post-translational modification promotes K48-ubiquitination and thus proteasomal degradation. It has been shown that a number of virulence factors that interfere with this checkpoint to ensure microbial persistence render infected cells to TNF-induced cell death.[134] These pieces of evidence validate the physiological relevance of the degradation-dependent checkpoints. This strengthens the notion that the degradation-dependent checkpoints of the TNF pathway are vital sensors not only for eliminating the pathogens but also for facilitating a well-coordinated immune response and to resolve the inflammation for a proper tissue repair.

1.5 Pathophysiological Implications of TNF-Induced Cell Death

The ability of tissues to overcome stress-induced damage lies in their capacity to tightly control the amplitude of TNF-induced cell death responses. Indeed, in the absence of cell death, tissue repair programs cannot be initiated. However, excessive cell death can lead to hyperinflammatory responses causing organ failure. The checkpoints studied so far are increasingly recognised as

essential components of homeostasis since they prevent embryonic lethality or severe inflammatory pathology due to aberrant cell death in mice. Furthermore, current evidence emphasizes that these checkpoints can also be considered as sensors of pathogens, since, once manipulated, they activate cell death to ensure a proper immune response aimed to eliminate the pathogens (Figure 4). Taken together with other previously mentioned checkpoints of TNF signalling, it is currently believed that there are multiple layers of regulation to limit the TNF cytotoxicity. It is becoming increasingly clear that different checkpoints collectively contribute to this regulation and that the severity of the stress condition might determine which checkpoint(s) is/are inactivated, impacting the extent of TNF-induced cell death.[1,2,55,56,62,91] However, it remains poorly understood, how the different checkpoints are interconnected to regulate TNF signalling outcomes in health and disease. Therefore, a detailed understanding of the biology of TNF-induced complex II, its composition and the related checkpoints might provide novel insights into the pathophysiological relevance TNF-induced cell death responses.

1.5.1 TNF-Induced Cell Death in Skin Wound Healing

Wound healing is a highly dynamic process based on the cooperation of different cell types in the wound microenvironment[135], the most important ones being macrophages[136], endothelial cells and myofibroblasts. The healing process is initiated by local inflammation triggered by tissue injury. This is followed by the formation of granulation tissue filling the wound with new tissue and vasculature. Finally, the resolution of inflammation and the regeneration of tissue and extracellular matrix lead to wound closure. The process of wound healing is divided into three phases: early-stage inflammation, intermediate proliferation and late-stage resolution.[137] During these phases, immune cells, such as macrophages, and stromal cells, such as endothelial cells and myofibroblasts, orchestrate the wound healing and tissue repair through timely and spatially coordinated cell death and proliferation of distinct cell types in the granulation tissue. Accordingly, increased numbers of wound macrophages and their uncontrolled activity in granulation tissue are the main causes of impaired tissue repair.[138] Recent studies have profiled the macrophages in the wound microenvironment at transcriptional and functional levels, indicating the dual role of TNF signalling in the dynamics of wound healing.[138,139] On the one hand, TNF-induced gene expression contributes to the activation and polarisation of early-stage wound macrophages and proliferation of the stromal cells.[140] On the other hand, TNF-dependent FADD/Caspase-8-mediated cell death of wound macrophages contributes to the resolution of inflammation and tissue repair in the later stages (Figure 4).[138] Thus, excessive Nf-κB-mediated proinflammatory signalling and impaired TNF-induced cell death play a key role in wound healing failure.[138,141] However, it remains enigmatic how different checkpoints of TNF signalling contribute to the timely activation of

macrophage cell death. Ultimately, the characterisation of these checkpoints and their contribution to the wound healing process deepen our mechanistic understanding of the complex role of TNF in tissue inflammation, repair and homeostasis.

1.5.2 TNF-Induced Cell Death in Viral Infection

Different forms of cell death play a crucial role in the defence against viruses. However, viruses often disrupt these cell death pathways to promote their survival. Caspase inhibitors have evolved as a major viral strategy to interfere particularly with cell death pathways and to prolong the host cell survival. This ensures viral replication and prevents the release of inflammatory cytokines, thus avoiding the activation of an immune response against the pathogen.[142,143] The inhibition of caspases is achieved either by interacting with the catalytically active site or by inhibiting the processes required for caspase activation. Several herpes- and poxviruses encode for viral FLICE-inhibitory proteins (vFLIPs)[144], which are structurally related to their cellular homolog $cFLIP_S$, to block apoptosis to ensure a replication niche for virus propagation. Similar to $cFLIP_S$, the vFLIPs bind to Caspase-8 through homotypic DED interactions and inhibit its recruitment, processing and activity.[74,78,145–147] In addition to inhibitors regulating the dynamics of Caspase-8, there are also inhibitors directly targeting the catalytic active site of caspases. One such inhibitor is cytokine response modifier A (CrmA). CrmA encoded by the cowpox virus is a unique member of the serine protease inhibitor (serpin) superfamily.[148,149] It is originally identified as an inhibitor of Caspase-1. However, it became quickly clear that it can inhibit a wide range of caspases including Caspase-8, -10, -3 and -7, which explains its protective properties against extrinsic and intrinsic apoptosis. The inactivation of caspases occurs through a conformational trapping mechanism, in which caspases are inactivated as its active site becomes conformationally distorted and trapped in an irreversibly stable complex.[143] Overall, Caspase-8 has both cell death promoting the activity by inducing apoptosis and prosurvival function by supressing necroptosis. The dual function of Caspase-8 is modulated by viral and cellular factors. [115] This determines the sensitivity to cell death to safeguard against viral infection and influences the disease progression. Therefore, the biological significance of Caspase-8 regulators is becoming increasingly profound.

During the viral infection, a variety of cytokines, IFNγ and TNF among the most important ones, are secreted. Acting in a paracrine and autocrine manner, IFNγ triggers a signal transduction cascade leading to the transcription of downstream genes, so called IFN-stimulated genes (ISGs), regulating immune response, cell survival and death. ZBP1 has emerged as an important ISG and mediator of IFN-induced proinflammatory signalling[37] and cell death[83]. Several studies have reported that ZBP1 can trigger the formation of a Caspase-8:RIPK1:RIPK3-containing complex II-like

death-inducing platform, independently of TNF signalling (Figure 4). This, in turn, can lead to a mixed cell death phenotype.[35,81–84] However, the mechanisms that control the type of cell death and the extent to which cells die during viral infection and whether cell death pathways can compensate for each other remain unclear.

Recent evidence points out that strict control of cell death levels is required for an optimal anti-viral response and viral clearance. Indeed, the abrogation of cell death was shown to prevent viral clearance.[150] In contrast, excessive levels of cell death trigger a hyperinflammatory state due to the overactivation of the immune system. This causes exaggerated secretion of cytokines, the so-called cytokine storm, which can have detrimental effect on tissue integrity and can cause organ failure. This phenomenon is observed in various respiratory viral infections, including influenza A (IAV) and severe acute respiratory syndrome coronavirus (SARS-CoV), which can lead to detrimental tissue damage and organ failure due to excessive cytokine-induced cell death.[151–153] In this regard, it is an important aspect to investigate, to which extent checkpoints of TNF signalling affect the cytokine production and release upon TNF-induced cell death during viral infections.

2 SPECIFIC AIMS

The following thesis is focused on the identification of novel mechanisms regulating the formation and cytotoxic activity of TNF-induced complex II using both hypothesis-driven and unbiased approaches.

AIM 1: Elucidating the role of cFLIP cleavage by Caspase-8 in the regulation of TNF-induced cell death

Downstream of the TNF/TNF-R1 signalling pathway, the formation of the Caspase-8/cFLIP heterodimer is essential to control the signalling outcomes. Apart from being a regulator of Caspase-8, cFLIP is also a substrate of Caspase-8 and is cleaved at D377 residue. However, the cell death regulatory potential of this cleavage event has never been addressed. Here, we aim to investigate the physiological role of Caspase-8-mediated cFLIP cleavage in the regulation of TNF-induced complex II formation and cytotoxicity. On the one hand, we seek to determine the molecular requirements for cFLIP cleavage and molecular mechanims behing its regulatory function. On the other hand, our goal is to decipher the biological relevance of cFLIP cleavage under TNF-mediated pathological challenges, including *Sharpin* deficiency-mediated sterile inflammation, excisional skin injury and viral infection.

AIM 2: Identification of novel regulators of TNF-induced complex II-mediated cell death

The regulation of TNF-induced cell death is essential in decision of cell fate between life and death. This precise regulation is highly complex and multi-layered for a proper response to a variety of insults. Therefore, beyond the known components, there are potentially more regulators to be identified and characterised. Here, we aim to unravel potential novel regulators of complex II and to gain insight into their impact on dynamics of complex II assembly and cytotoxicity. Further biochemical validation and functional characterisation of the selected candidate aim to characterise its role in the regulation of TNF-induced cell death outcomes.

3 RESULTS

3.1 cFLIP cleavage by Caspase-8 restrains TNF-induced cell death during viral infection and tissue damage.

3.1.1 Activation of TNF/TNF-R1 induces cFLIP cleavage by Caspase-8 at D377 residue, to counteract TNF cytotoxicity.

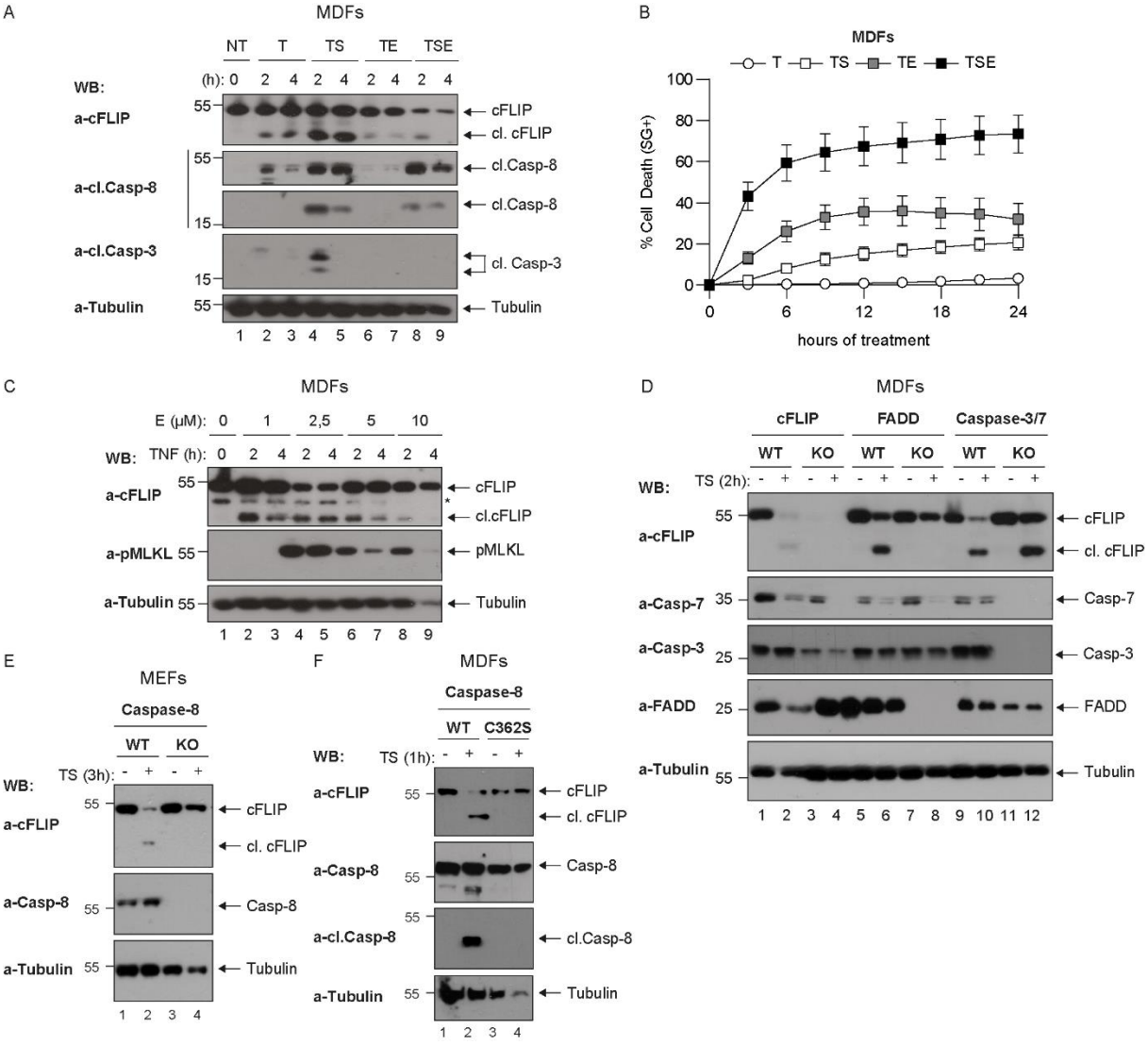

Figure 7. cFLIP is cleaved upon activation of TNF/TNF-R1 signalling. A. *Cflip*^{WT} mouse dermal fibroblasts (MDFs) were treated with TNF (100 ng/ml), Smac mimetic (250 nM) and Emricasan (1 μM) as indicated at the defined time points. Cell lysates were analysed by immunoblotting using the indicated specific antibodies (n=2). **B.** The cell death response of *Cflip*^{WT} MDFs, treated as in **(A)**, was measured over time by quantifying Sytox Green-positive cells. (n=3, mean±SD) **C.** *Cflip*^{WT} MDFs were treated with TNF (100 ng/ml) and increasing concentration of Emricasan (1 to 10 μM) for the indicated time points. Cell lysates were analysed by immunoblotting using the indicated specific antibodies (n=3). The asterisk (*) indicates a non-specific band. **D-F.** MDFs, mouse embryonic fibroblasts (MEFs) and bone marrow-derived macrophages (BMDMs) with genetic deletion **(D-E)** or alterations **(F)** of target proteins and their respective wild-type controls were treated with TNF (10 ng/ml) and Smac mimetics (250 nM) for the indicated time points. Cell lysates were analysed by immunoblotting using indicated specific antibodies (n=2).

Firstly, we characterised the dynamics and molecular requirements for cFLIP processing upon TNF/TNF-R1 signalling activation *in vitro.* For this purpose, we treated mouse dermal fibroblasts (MDFs) with TNF alone (T) or in combination with Smac mimetic AZD5582 (S) and/or Emricasan (also known as IDN-6556, E). The activation of the TNF pathway, even without the induction of cell death and full Caspase-8 activation, was sufficient for cFLIP cleavage, as shown by the presence of the p43 fragment (Figure 7A-B). Of note, inhibition of Caspase-8 activity using a pan-caspase inhibitor E, even at high doses, could not prevent cFLIP cleavage (Figure 7C). This indicates that cFLIP cleavage occurs even under conditions, in which the activation of Caspase-8 is inhibited by blocking its second cleavage event (Figure 7A-C). To mechanistically understand which molecules are responsible for cFLIP cleavage, we employed cell lines with genetic deletion or inhibition of cell death-mediating proteins (Supplementary Figure 1A-E). cFLIP cleavage was absent in *Fadd*$^{-/-}$, *Caspase-8*$^{-/-}$ and *Caspase-8*$^{-/C362S}$ cells (Figure 7D-F). This indicates that the presence of FADD (adaptor protein) and an enzymatically active Caspase-8 (initiator caspase) is an essential for cFLIP cleavage, while Caspase-3/7 (executioner caspases) are dispensable (Figure 7D-F).

A previous study[33] described two aspartic acid residues in close proximity on cFLIP, D371 and D377, that can potentially undergo Caspase-8-mediated cleavage (Figure 8A). To identify the exact

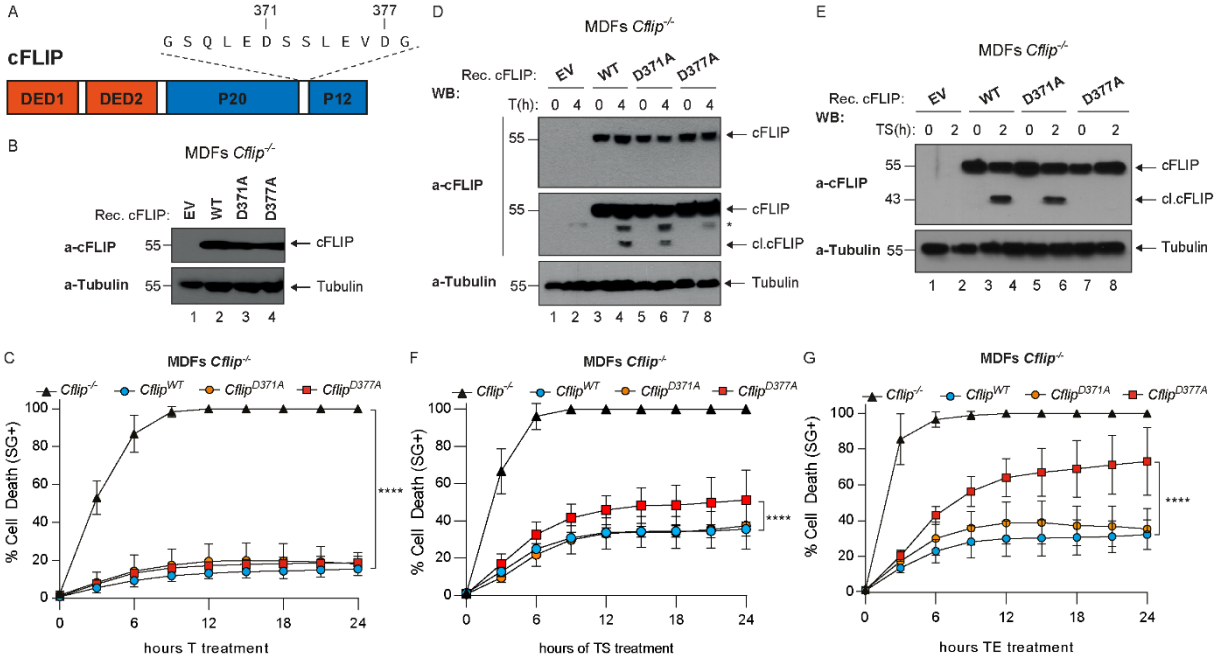

Figure 8. cFLIP cleavage by Caspase-8 occurs at D377 position. A. Cartoon depicting cFLIP domain composition and the location of aspartic acid residues D371 and D377. **B.** Reconstitution of cFLIP expression in *Cflip*$^{-/-}$ mouse dermal fibroblasts (MDFs) together with respective empty vector controls were analysed by immunoblotting using indicated specific antibodies (n=3). **C.** The cell death response of reconstituted cells from **(B)** to TNF (100 ng/ml) was measured over time by quantifying Sytox Green-positive cells (n=3, mean±SD). **D-E.** Reconstituted cells from (B) treated with TNF (100 ng/ml) alone **(D)** or in combination with Smac mimetics (250 nM) **(E)** as indicated. Cell lysates were analysed by immunoblotting with the indicated specific antibodies (n=2). **F-G.** The cell death response of reconstituted cells from **(B)** to TNF (10 ng/ml) in combination with either Smac mimetics (250 nM) and Emricasan (1 µM) was measured over time by quantifying Sytox Green-positive cells (n=3, mean±SD). **** p≤0,0001

cleavage site of cFLIP by Caspase-8 and to exclude redundancy between these two residues, we reconstituted *Cflip*$^{-/-}$ MDFs with WT cFLIP or mutant cFLIP bearing alanine substitutions at D371 or D377 (Figure 8B). Re-expression of cFLIP constructs restored cFLIP-mediated protection against cell death induced by TNF treatment alone in *Cflip*$^{-/-}$ MDFs, demostrating the prosurvival functionality of all cFLIP variants (Figure 8C). More interestingly, the D377A, but not the D371A mutation, abolished cFLIP cleavage as shown by the absence of the p43 fragment (Figure 8D-E). Intriguingly, cells bearing the non-cleavable cFLIP, the D377A variant, were sensitised to TS- and TE-induced apoptosis and necroptosis (Figure 8F-G). Collectively, our results strengthen the notion that, upon TNF stimulation, cFLIP is cleaved by Caspase-8 at residue D377 ensuring some prosurvival function.

3.1.2 The *cFLIP*^{D377A} mice are indistinguishable from their *cFLIP*^{WT} littermates.

To address the biological relevance of Caspase-8-mediated cFLIP cleavage, we generated a genetically modified mouse model bearing a non-cleavable version of cFLIP, the *Cflip*$^{D377A/D377A}$, hereafter referred to as the *Cflip*^{D377A} mouse (Figure 9A). Consistent with the results from the reconstitution system, the cleavage of cFLIP was absent in MDFs isolated from *Cflip*^{D377A} mice upon activation of the TNF signalling, whereas MDFs from *Cflip*^{WT} littermates clearly showed the cleavage product. Comparable levels of cFLIP expression were observed in both genotypes (Figure 9B). The *Cflip*^{D377A} mice were weaned at the expected Mendelian ratio and did not exhibit any overt phenotype (Figure 9C-E). Indeed, they aged and gained weight in the same manner as their *Cflip*^{WT} counterparts (Figure 9D-E). Furthermore, we analysed defined immune cell populations in different immune organs of the *Cflip*^{D377A} mice since genetic alterations of various complex II components are associated with changes in the immune compartment.[116,118–120,154–157] These mice had an overtly normal immune system with comparable levels of both immune cell progenitors in the bone marrow (Figure 9F) and resident immune cells in the spleen compared to *Cflip*^{WT} mice (Figure 9G-J). Overall, *Cflip*^{D377A} mice were indistinguishable from their *Cflip*^{WT} littermates. These results suggest that cleavage of cFLIP does not affect the capability of the Caspase-8/cFLIP heterodimer to suppress complex II cytotoxicity during embryonic and adult development and does not affect the immune cell populations.

3.1.3 cFLIP cleavage limits TNF cytotoxicity by controlling complex II assembly, independently of gene expression.

To elucidate the role of cFLIP cleavage in the regulation of TNF-induced signalling outcomes, we isolated different cell types, including MDFs, lung fibroblasts (LFs), lung endothelial cells (LECs),

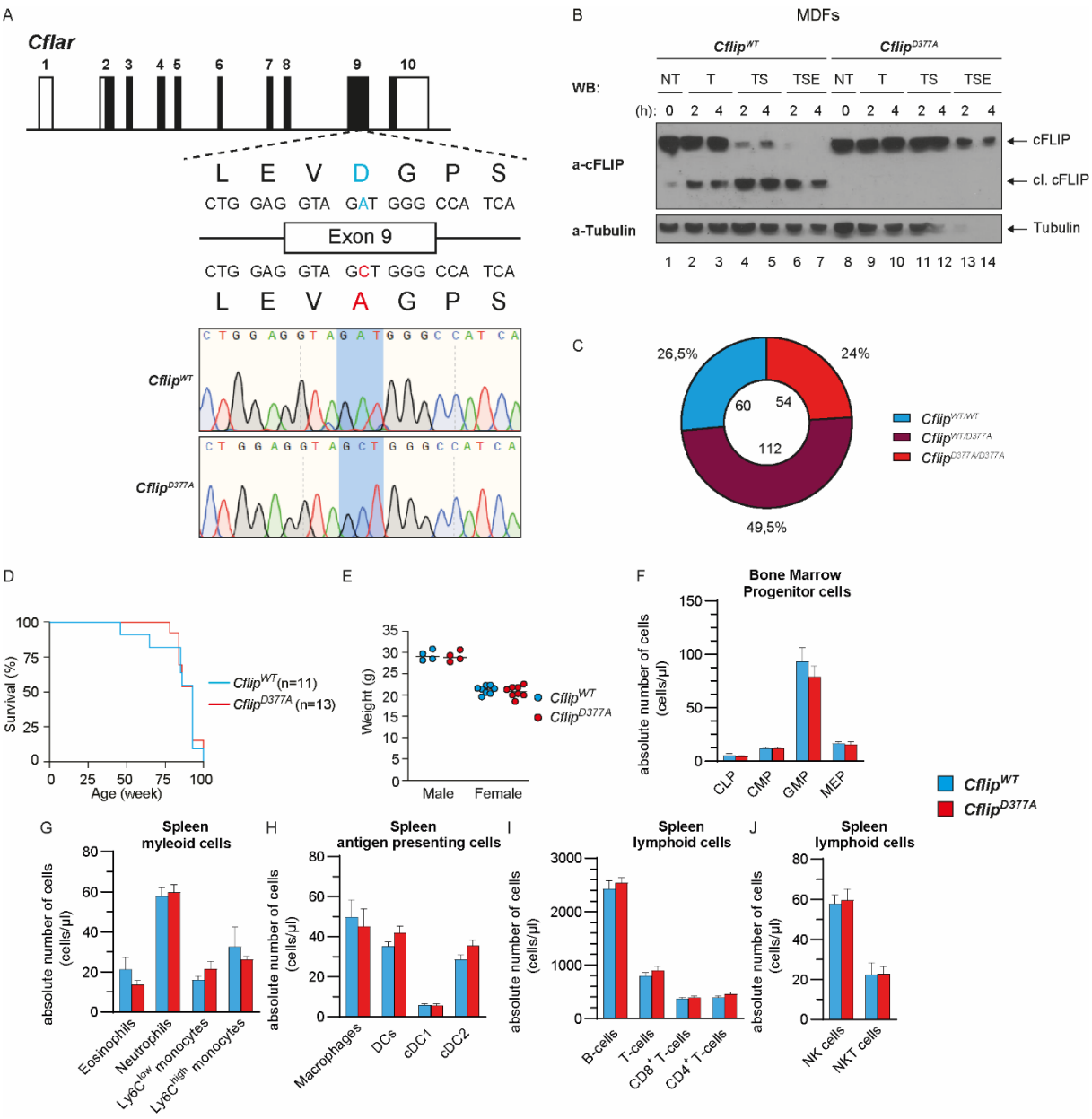

Figure 9. *Cflip*^{D377A} mice were indistinguishable from their *Cflip*^{WT} counterparts. A. Cartoon depicting the *Cflar* exons (upper part). DNA and protein sequence of the region in exon 9 bearing the A>C mutation causing the substitution of aspartic acid (D) with alanine (A) at 377 position (middle part). DNA sequence alignment of the region of interest in the genome of *Cflip*^{WT} and *Cflip*^{D377A} mice (lower part). **B.** *Cflip*^{WT} and *Cflip*^{D377A} mouse dermal fibroblasts (MDFs) were treated as indicated (TNF100 ng/ml, Emricasan 1 µM and Smac mimetics 250 nM) and cell lysates were analyzed by immunoblotting using the indicated specific antibodies (n=2). **C.** Observed absolute numbers and mendelian ratios of mice born from the breeding of heterozygous parental mice depicted in a pie chart. D. The survival of *Cflip*^{WT} and *Cflip*^{D377A} mice was assessed by ageing curves mice in a long-term cohort over 100 weeks. E. The weight of *Cflip*^{WT} and *Cflip*^{D377A} mice was assessed at the age of 10-12 weeks. **F-J.** Different immune cell populations in the bone marrow and spleen from 10-12-week-old mice, including immune cell progenitors **(F)** in the bone marrow as well as myeloid cells **(G)**, antigen-presenting cells (H) and cells with lymphoid origin **(I-J)** in the spleen, were analysed by flow cytometry (n=4).

and bone marrow-deried macrophages (BMDMs). First, we assessed whether the D377A mutation affects the ability of TNF to induce cell death. Therefore, we treated different cell types with TNF in combination with the Smac mimetic Birinapant (TB) to deplete the cIAPs and induce Caspase-8-mediated RIPK1-dependent apoptosis. Strikingly, MDFs (Figure 10A), LFs (Figure 10B) and LECs (Figure 10C) isolated from *Cflip*^{D377A} mice were significantly more sensitive to

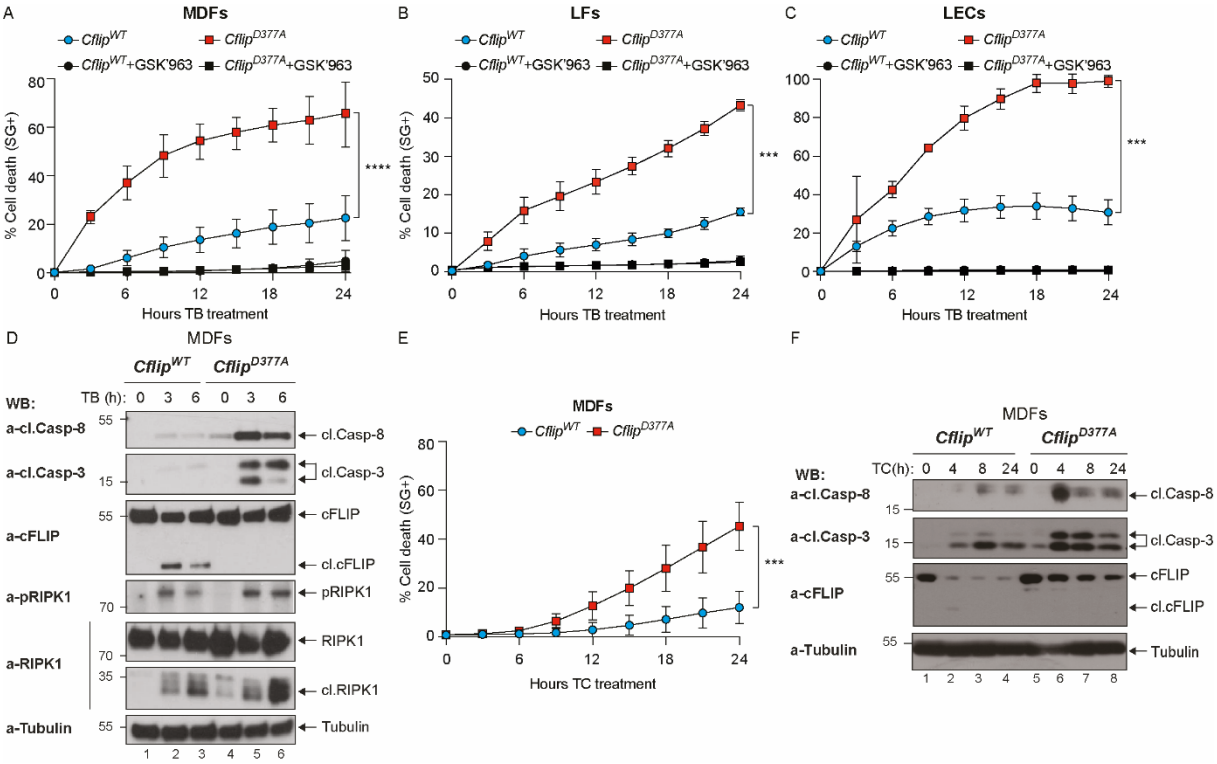

Figure 10. cFLIP cleavage restrains TNF-induced apoptosis. A-C. Various cell types isolated from *Cflip*^{WT} and *Cflip*^{D377A} mice, including mouse dermal fibroblasts (MDFs, **A**), lung fibroblasts (LFs, **B**) and lung endothelial cells (LECs, **C**), were treated with TNF (10 ng/ml) and Birinapant (250 nM) in the presence or absence of the RIPK1 specific inhibitor GSK'963 (100 nM) and cell death was measured over time by calculating the percentage of Sytox Green-positive cells (n=4, mean±SD). **D.** *Cflip*^{WT} and *Cflip*^{D377A} MDFs were treated with TNF (10 ng/ml) and Birinapant (250 nM) for the indicated time points. Cell lysates were analysed by immunoblotting using the indicated specific antibodies (n=3). **E.** *Cflip*^{WT} and *Cflip*^{D377A} MDFs were treated as indicated (TNF10 ng/ml, Cycloheximide 10 µg/ml) and cell death was measured over time by calculating the percentage of Sytox Green-positive cells (n=3, mean±SD). **F.** *Cflip*^{WT} and *Cflip*^{D377A} MDFs were treated as in **(E)** and cell lysates were analysed by immunoblotting using the indicated specific antibodies (n=2). *** p≤0,001, **** p≤0,0001

TB-induced apoptosis. This type of cell death relies on RIPK1 kinase activity-dependent activation of Caspase-8, which in turn cleaves and activates the executioner Caspase-3. Consistently with this and as observed in Figure 10A-C, the RIPK1 inhibitor GSK'963 was able to abrogate TS-induced cell death in both genotypes. Importantly, the increased sensitivity of *Cflip*^{D377A} cells to apoptosis correlates with increased Caspase-8 and -3 cleavage together with increased RIPK1 phosphorylation and cleavage in the *Cflip*^{D377A} MDFs compared to *Cflip*^{WT} MDFs (Figure 10D). Next, we treated *Cflip*^{WT} and *Cflip*^{D377A} MDFs with TNF in combination with cycloheximide (TC) to induce RIPK1-independent apoptosis by blocking the protein synthesis and therefore the expression of anti-apoptotic proteins. *Cflip*^{D377A} MDFs were also significantly more sensitive to TC-induced apoptosis (Figure 10E). Consistently with these data, we observed substantially increased proteolytic processing of Caspase-8 and -3 (Figure 10F). These results support the notion that cFLIP cleavage is crucial to restrain TNF-induced apoptosis. Moreover, we tested whether the sensitising effect of the D377A mutation is specific to TNF-induced apoptosis. For this purpose, we utilized genotoxic drugs, Gemcitabine, Paclitaxel, Doxorubicin and Cisplatin, to activate intrinsic

apoptosis. Interestingly, *Cflip*^{WT} and *Cflip*^{D377A} MDFs died to the same extent upon genotoxin treatments (Supplementary Figure 2A-D). This indicates that cFLIP cleavage plays no role in genotoxin-induced cell death. Secondly, we assessed the role of cFLIP cleavage in TNF-induced necroptosis. For this purpose, we treated MDFs (Figure 11A), LFs (Figure 11C), LECs (Figure 11F) with TNF in combination with Emricasan (TE) and BMDMs (Figure 11D) with TNF, Birinapant and Emricasan (TBE) to induce RIPK1/RIPK3/MLKL-mediated necroptosis. Strikingly, all *Cflip*^{D377A} cell types were significantly more sensitive to TE/TBE-induced necroptosis than their respective *Cflip*^{WT} counterparts. TNF-induced necroptosis is driven by the formation of the complex II in a RIPK1-dependent manner. Accordingly, selective inhibition of RIPK1 could abolish TNF-induced

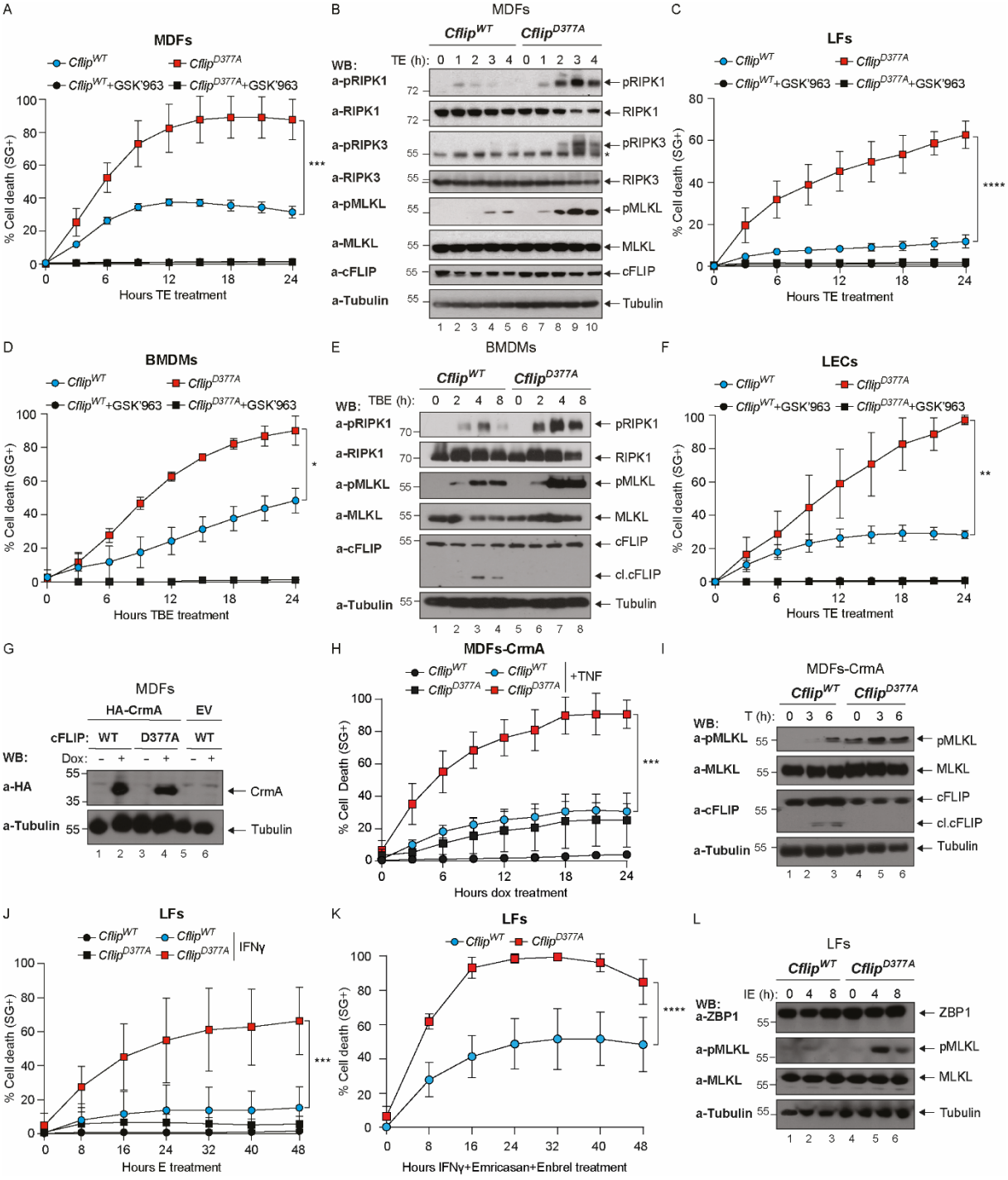

Figure 11. cFLIP cleavage limits TNF-induced as well as TNF-independent, IFN-induced ZBP1-mediated necroptosis. A. *Cflip*^{WT} and *Cflip*^{D377A} mouse dermal fibroblasts (MDFs) were treated with TNF (1 ng/ml) and Emricasan (1 µM) in the presence or absence of the RIPK1-specific inhibitor GSK'963 (100 nM) and cell death was measured over time by calculating the percentage of Sytox Green-positive cells. (n=3, mean±SD) **B.** *Cflip*^{WT} and *Cflip*^{D377A} MDFs were treated with TNF (1 ng/ml) and Emricasan (1 µM) for the indicated time points. Cell lysates were immunoblotted using the indicated specific antibodies. (n=3) **C.** *Cflip*^{WT} and *Cflip*^{D377A} lung fibroblasts (LFs) were treated with TNF (10 ng/ml) and Emricasan (1 µM) in the presence or absence of the RIPK1 specific inhibitor GSK'963 (100 nM) and cell death was measured over time by calculating the percentage of Sytox Green-positive cells. (n=4, mean±SD) **D.** *Cflip*^{WT} and *Cflip*^{D377A} bone marrow-derived macrophages (BMDMs) were treated with TNF (10 ng/ml), Birinapant (250 nM) and Emricasan (1 µM) in the presence or absence of the RIPK1 specific inhibitor GSK'963 (100 nM) and cell death was measured over time by calculating the percentage of Sytox Green-positive cells. (n=5, mean±SD) **E.** *Cflip*^{WT} and *Cflip*^{D377A} BMDMs were treated with TNF (10 ng/ml), Birinapant (250 nM) and Emricasan (1 µM) for the indicated time points. Cell lysates were immunoblotted using the indicated specific antibodies. (n=3) **F.** *Cflip*^{WT} and *Cflip*^{D377A} lung endothelial cells (LECs) were treated with TNF (10 ng/ml), Birinapant (250 nM) and Emricasan (1 µM) in the presence or absence of the RIPK1 specific inhibitor GSK'963 (100 nM) and cell death was measured over time by calculating the percentage of Sytox Green-positive cells. (n=3, mean±SD) **G.** MDFs stably expressing either empty vector (EV) or HA-tagged CrmA were generated in *Cflip*^{WT} and *Cflip*^{D377A} background using a doxycycline-inducible system. CrmA^{+} *Cflip*^{WT} and *Cflip*^{D377A} MDFs were treated with doxycycline (100 ng/ml) for 72 h prior to the protein extraction. Cell lysates were immunoblotted using the indicated specific antibodies (n=1). **H.** CrmA^{+} *Cflip*^{WT} and *Cflip*^{D377A} MDFs were treated as in (G) in the presence or absence of the TNF (100 ng/ml) and cell death was measured over time by calculating the percentage of Sytox Green-positive cells (n=3, mean±SD). **I.** CrmA^{+} *Cflip*^{WT} and *Cflip*^{D377A} MDFs were treated as in (H) for the indicated time points. Cell lysates were immunoblotted using the indicated specific antibodies (n=3). **J-K.** *Cflip*^{WT} and *Cflip*^{D377A} LFs were primed with IFN (100 ng/ml) and treated with Emricasan (1 µM) in the presence or absence of the TNF-neutralizing antibody Enbrel (50 µg/ml) and cell death was measured over time by calculating the percentage of Sytox Green-positive cells. (n=3, mean±SD) **L.** *Cflip*^{WT} and *Cflip*^{D377A} LFs were primed with IFN (100 ng/ml) and treated with Emricasan (1 µM) for the indicated time points. Cell lysates were immunoblotted using the indicated specific antibodies. (n=2) * P ≤ 0,05, ** P ≤ 0,01, *** P ≤ 0,001 and **** P ≤ 0,0001

necroptosis in these cells (Figure 11A-C-D-F). In line with *Cflip*^{D377A} cells being more sensitive to necroptosis, we observed considerably higher levels of phosphorylated RIPK1, RIPK3 and MLKL in *Cflip*^{D377A} MDFs (Figure 11B) and BMDMs (Figure 11E) following TE/TBE-treatment, respectively, than in their *Cflip*^{WT} counterparts. To further prove that cFLIP cleavage limits TNF-induced necroptosis, we utilised a naturally occurring viral caspase inhibitor, CrmA, whose expression together with TNF treatment induces necroptosis. For this purpose, we generated CrmA expressing MDFs in the *Cflip*^{WT} and *Cflip*^{D377A} background (Figure 11G). In this approach, we utilised a doxycycline-inducible system to control the expression levels of CrmA. Surprisingly, expression of CrmA alone could induce necroptosis, although to low levels, in *Cflip*^{D377A} MDFs. Moreover, *Cflip*^{D377A} CrmA expressing MDFs were more sensitive to TNF-induced necroptosis than *Cflip*^{WT} counterparts (Figure 11H). As expected, the increased sensitivity to TNF-induced necroptosis correlates with increased phosphorylation of MLKL (Figure 11I). These results suggest that cFLIP cleavage limits TNF-mediated necroptosis not only upon pharmacologic inhibition of Caspase-8, via Emricasan, but also in the presence of a virus-encoded caspase inhibitor, CrmA. In addition, necroptosis can also be triggered by IFNγ-induced ZBP1 upregulation in combination with Caspase inhibition (IE). *Cflip*^{D377A} LFs showed increased sensitivity to IE-induced cell death compared to *Cflip*^{WT} LFs (Figure 11J). Of note, IE-induced cell death is independent of TNF signalling, since Enbrel, a TNF-neutralising antibody, did not affect the levels of induced cell death

(Figure 11K). As evident from Figure 11L, the subsequent immunoblot analysis indicated higher levels of phosphorylated MLKL in *Cflip*^{D377A} LFs. These results suggest that cFLIP mutation can also limit the TNF-independent, ZBP1-dependent IE-induced necroptosis. Altogether, these data

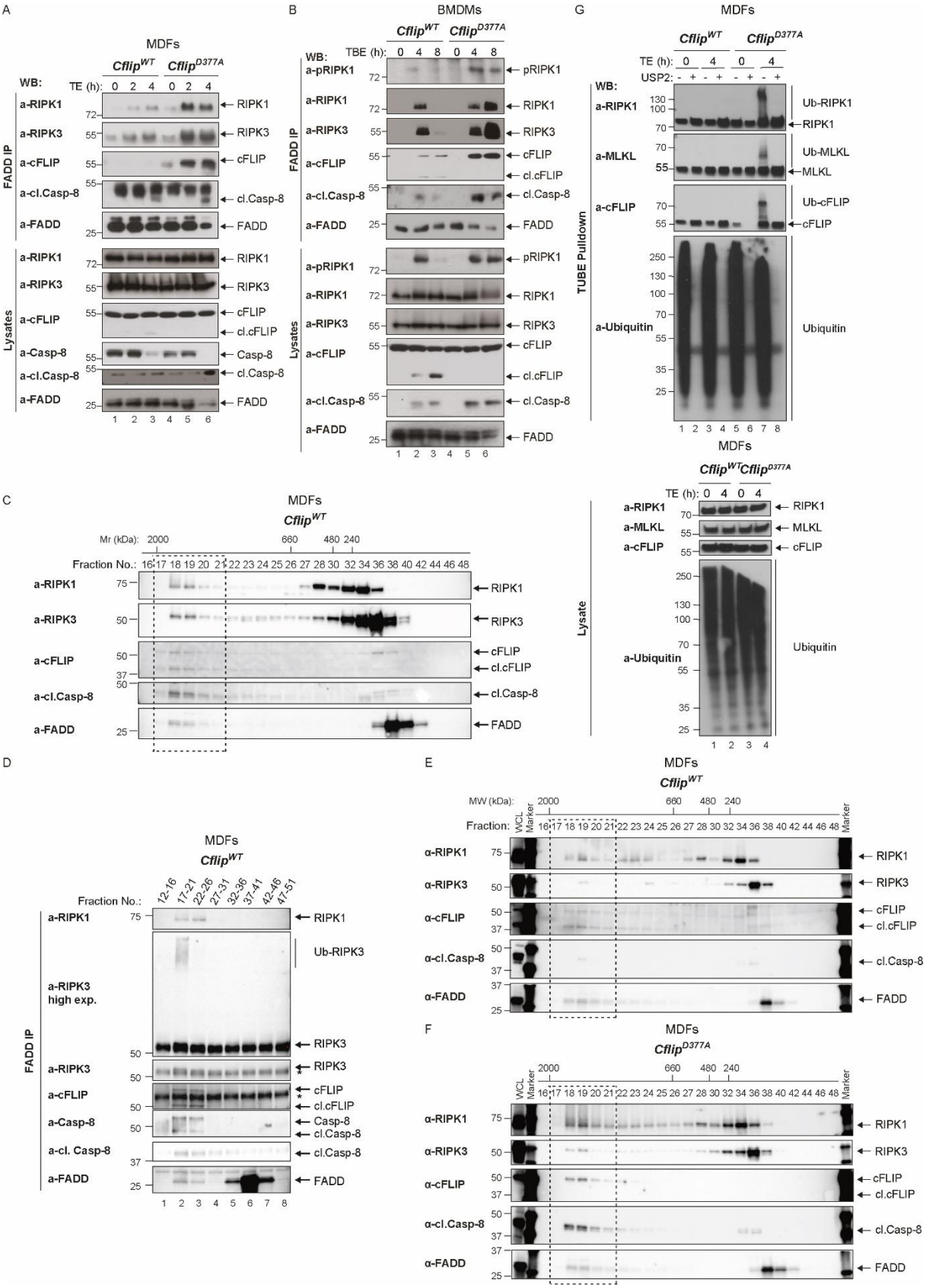

Figure 12. cFLIP cleavage counterbalances complex II formation. A. *Cflip*^{WT} and *Cflip*^{D377A} mouse dermal fibroblasts (MDFs) were treated with TNF (1 ng/ml) and Emricasan (1 µM) for the indicated time points. Cell lysates were subjected to immunoprecipitation using a FADD-specific antibody. Immunocomplexes and cellular lysates were then analysed by immunoblotting using the indicated specific antibodies (n=3). **B**. *Cflip*^{WT} and *Cflip*^{D377A} mouse dermal fibroblasts (MDFs) were treated with TNF (1 ng/ml), Birinapant (250 nM) and Emricasan (1 µM) for the indicated time points. Cell lysates were subjected to immunoprecipitation using a FADD-specific antibody. Immunocomplexes and cellular lysates were then analysed by immunoblotting using the indicated specific antibodies (n=3). **C**. *Cflip*^{WT} MDFs were treated with TNF (10 ng/ml), Birinapant (250 nM) and Emricasan (1 µM) and lysates were separated on a Superose 6 column. Aliquots of each fraction were retained and analysed by immunoblotting with the indicated specific antibodies (n=1). **D.** Pooled fractions retained in **(C)** were subjected to FADD immunoprecipitation. Immunoprecipitates were analysed by immunoblotting using indicated specific antibodies. **E-F.** *Cflip*^{WT} **(E)** and *Cflip*^{D377A} **(F)** MDFs were treated with TNF (10 ng/ml), Birinapant (250 nM) and Emricasan (1 µg/ml) for 4 hours and lysates were separated on a Superose 6 size-exclusion column. Aliquots from each fraction were retained and analysed by immunoblotting with the indicated specific antibodies. **G.** *Cflip*^{WT} and *Cflip*^{D377A} MDFs were treated with TNF (1 ng/ml) and Emricasan (1 µM) for the indicated time points. Cell lysates were subjected to TUBE pulldown in the presence or absence of the USP2 deubiquitinase (2 µM). Immunocomplexes and cellular lysates were then analysed by immunoblotting using the indicated specific antibodies (n=3).

lead to the conclusion that cFLIP cleavage is a unique mechanism to control the extent of complex II-mediated cell death upon various stimuli in multiple cell types.

To gain mechanistic insights, we analysed the dynamics of complex II using immunoprecipitation approaches. For this purpose, we treated *Cflip*^{WT} and *Cflip*^{D377A} MDFs with TE or BMDMs with TBE and immunoprecipitated complex II via FADD at different time points. The subsequent immunoblotting analysis of the immunocomplexes revealed an increased presence and abundance of the known complex II components RIPK1, RIPK3, cFLIP and Caspase-8 in *Cflip*^{D377A} MDFs (Figure 12A) and BMDMs (Figure 12B). These results suggest that cFLIP cleavage limits the extent of complex II. Hence, abrogation of cFLIP cleavage sensitizes cells to TNF-induced cell death by favouring complex II formation. We further investigated complex II architecture using size exclusion chromatography followed by immunoprecipitation upon TSE treatment. Initially, we observed the presence of RIPK1, RIPK3, cFLIP, cleaved Caspase-8 and FADD in fractions (17-21) which contain high molecular weight complexes with an approximate molecular mass of ~2 Mda (Figure 12C). The subsequent immunoprecipitation of FADD from the pooled fractions (17-21) further confirmed the association of these proteins in the same complex corresponding to complex II (Figure 12D). Strikingly, when performed in *Cflip*^{D377A} MDFs, complex II components co-eluted with FADD in the same high molecular weight fractions, although with a higher abundance than in *Cflip*^{WT} MDFs (Figure 12E-F). This indicates that cleavage of cFLIP at D377 residue is a prosurvival mechanism limiting the extent of complex II. Thus, we hypothesise that this cleavage event is involved in a previously unknown regulatory mechanism of TNF-induced complex II assembly.

Ubiquitination is a post-translational modification implicated in the regulation of cell death.[61,62,91,158] Consistent with *Cflip*^{D377A} MDFs being more sensitive to TNF-induced necroptosis, MLKL and RIPK1 underwent dramatically higher levels of ubiquitination in *Cflip*^{D377A} MDFs compared to

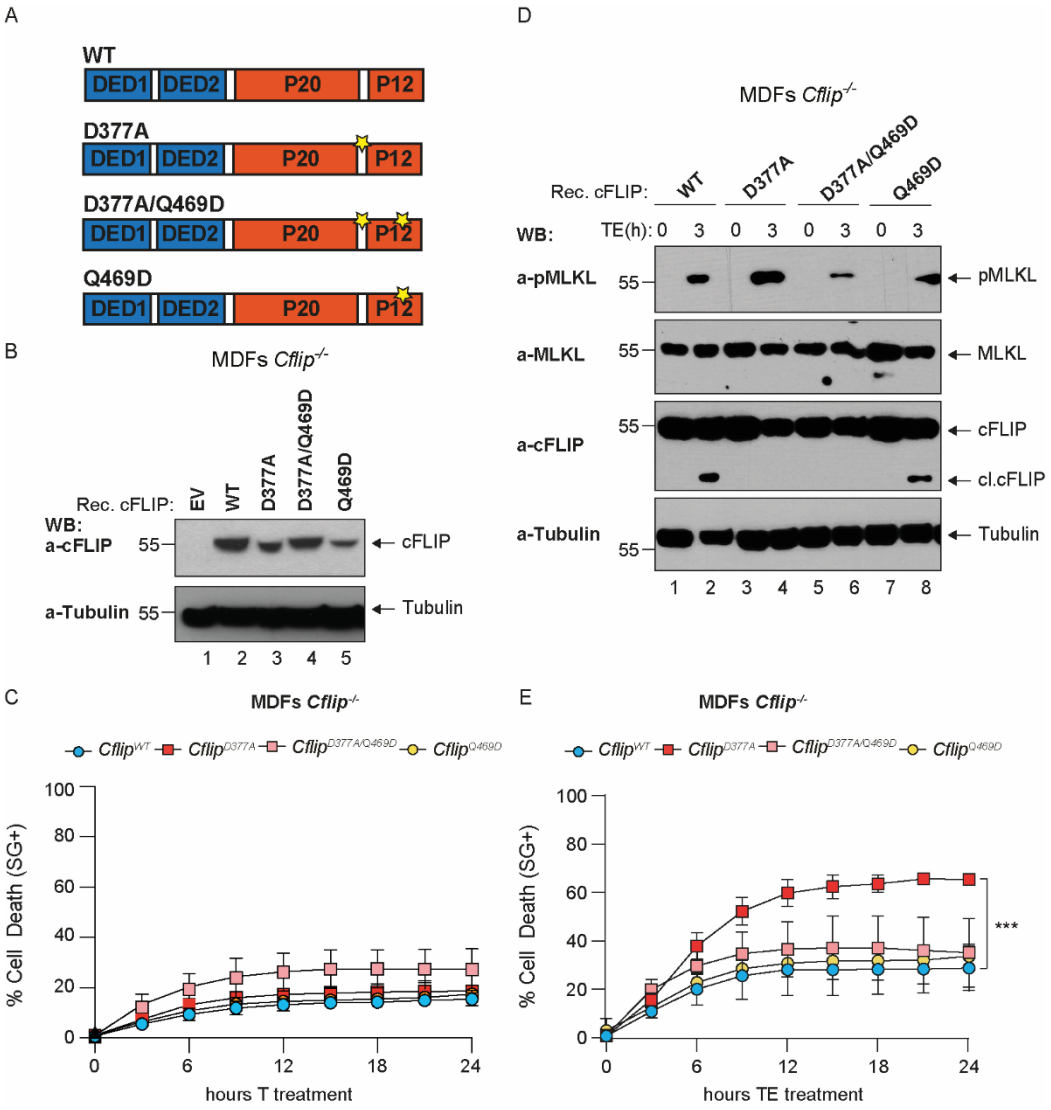

Figure 13. Residues at the C-terminal domain of cFLIP contribute to the assembly and stability of complex II in *Cflip*^{D377A} MDFs. A. Cartoon depicting cFLIP domain composition and position of the D377 and Q469 residues. **B.** Reconstitution of cFLIP expression in *Cflip*$^{-/-}$ mouse dermal fibroblasts (MDFs) together with respective empty vector controls were analysed by immunoblotting using indicated specific antibodies (n=3). **C.** *Cflip*$^{-/-}$ MDFs reconstituted as in (B) were treated with TNF (100 ng/ml) and cell death response was measured over time by calculating the percentage of Sytox Green-positive cells (n=3, mean±SD). **D.** *Cflip*$^{-/-}$ MDFs reconstituted as in **(B)** were treated with TNF (1 ng/ml) and Emricasan (1 µM) for 3 h and cell lysates were analysed by immunoblotting using the indicated specific antibodies. (n=3) **E.** *Cflip*$^{-/-}$ MDFs reconstituted as in **(B)** were treated with TNF (1 ng/ml) and Emricasan (1 µM). Cell death response was measured over time by calculating the percentage of Sytox Green-positive cells (n=3, mean±SD). *** p≤0,001

Cflip^{WT} MDFs upon TE-treatment. Furthermore, we observed significantly enhanced ubiquitination of cFLIP (Figure 12G). Taken together, these data indicate that abrogation of cFLIP cleavage enhances ubiquitination events promoting killing potential during necroptosis.

Based on the reported structure of the cFLIP/Caspase-8 heterodimer[74,78,79], we hypothesise that the C-terminal residues of the caspase-like domain on the cFLIP, which are located after the D377 cleavage site, might impact the assembly and stability of complex II in *Cflip*^{D377A} cells. Of particular interest was the glutamine residue at position 469 (Q469), known to contribute to cFLIP/Caspase-8 heterodimerisation[74]. Therefore, we next investigated the involvement of the Q469 residue in the

D377A-mediated enhancement of TNF cytotoxicity. For this purpose, we reconstituted *Cflip*$^{-/-}$ MDFs with either WT or mutant versions of cFLIP, as indicated in Figure 13A. All cFLIP mutant variants, similar to WT, could protect the cells from the lethal effects of TNF alone (Figure 13B-C). Interestingly, the Q469D mutation could revert the sensitizing effect of the D377A mutation following TE treatment, while the Q469D alone phenocopied WT cFLIP in terms of cell death levels. These results were consistent with the levels of phosphorylated MLKL observed in these reconstituted cells following TE treatment (Figure 13D-E). These data suggest that the Q469D mutation could abrogate the sensitization to TNF-induced cell death caused by the D377A mutation. Importantly, the Q469 residue alone is dispensable for the ability of the cFLIP/Caspase-8 heterodimer to control TNF-induced cell death. Altogether, our results show that cFLIP cleavage is a prosurvival checkpoint that limits the extent of complex II formation via the removal of the C-terminal domain. Abrogation of cFLIP cleavage therefore enhances the assembly and stability of complex II, most probably by stabilizing the cFLIP/Caspase-8 heterodimer, which in turn exacerbates TNF-induced cell death responses.

The default outcome of TNF stimulation is it the induction of NF-κB and MAPK pathways for the activation of prosurvival and proinflammatory genes. To determine whether cFLIP cleavage affects gene expression in TNF signalling, we treated *Cflip*^{WT} and *Cflip*^{D377A} cells with TNF alone and assessed the activation patterns of NF-κB and MAPK pathways. As expected, TNF alone did not affect the viability of both *Cflip*^{WT} and *Cflip*^{D377A} cells (Figure 14A-C). Moreover, as shown in Figure 14B-D, we observed no differences between *Cflip*^{WT} and *Cflip*^{D377A} cells in the activation pattern of NF-κB and MAPK pathways. This indicates that cFLIP cleavage by Caspase-8 has no significant impact on the activation of NF-κB and MAPK pathways in TNF signalling. Moreover, recent studies reported on the transcriptional role of Caspase-8 downstream of inflammasome[118], TLR[159] and TRAIL[160] signalling. Most recent findings indicate that cFLIP regulates not only Caspase-8-mediated cell death outcomes but also Caspase-8-mediated cytokine production under certain signalling pathways.[161,162] For example, upon TLR signalling, Caspase-8 can cleave and inactivate Nedd4-binding partner 1 (N4BP1) to allow the expression of proinflammatory cytokines.[159] Therefore, we set up to understand whether cFLIP cleavage impacts Caspase-8-mediated cytokine production. Western blot analysis of *Cflip*^{WT} and *Cflip*^{D377A} BMDMs treated with LPS, to stimulate TLR4, or Poly I:C, to stimulate TLR3, revealed a highly similar N4BP1 cleavage pattern without inducing cell death (Figure 14E-F). The following RT-qPCR analysis of mRNA expression levels for TNF and CCL2 were comparable between *Cflip*^{WT} and *Cflip*^{D377A} cells (Figure 14G-J). Altogether, our data indicate that cFLIP cleavage represents a novel checkpoint to

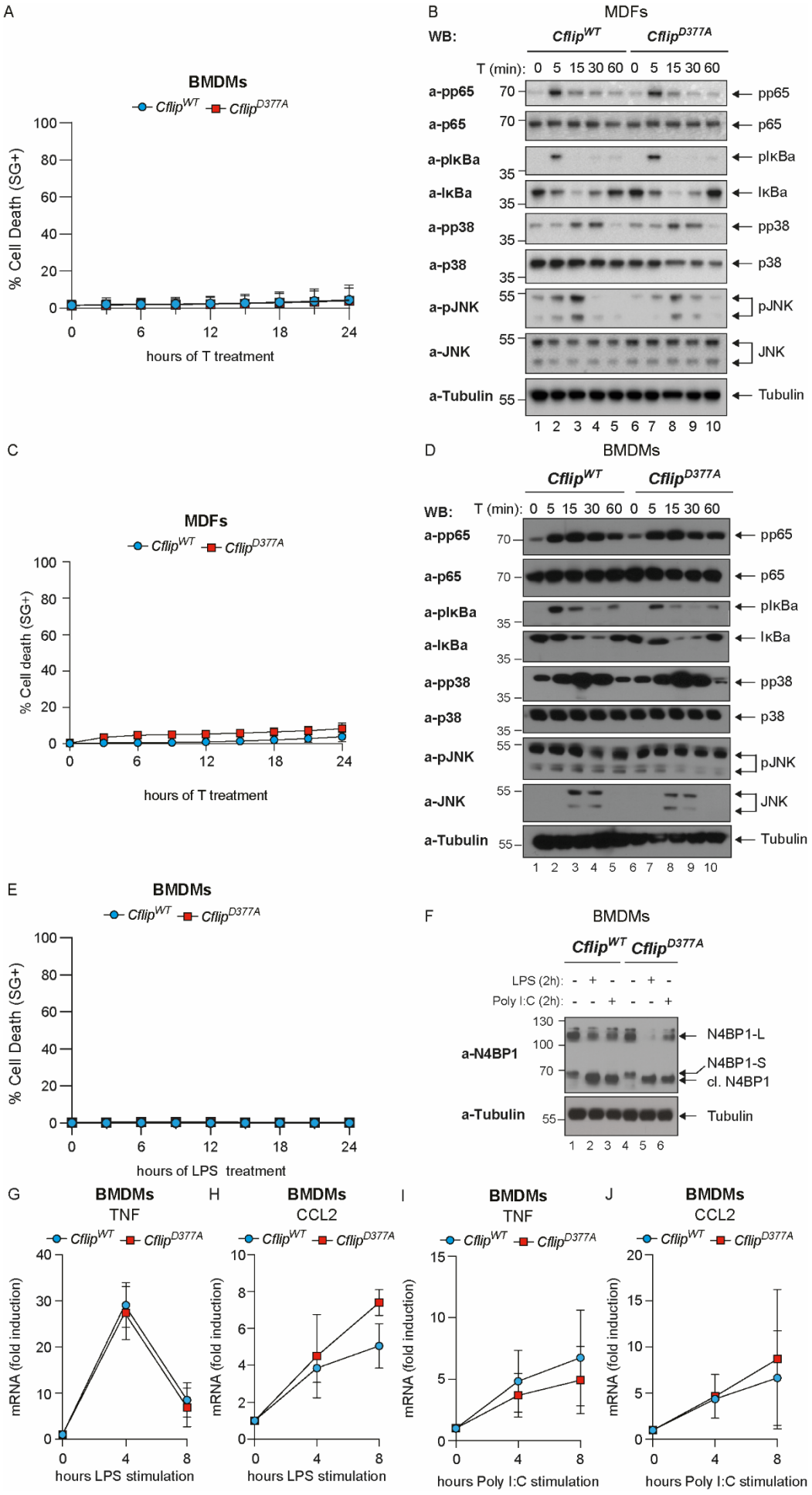
A
BMDMs
CflipWT CflipD377A
% Cell Death (SG+)
hours of T treatment
B
MDFs
WB:
CflipWT CflipD377A
T (min): 0 5 15 30 60 0 5 15 30 60
a-pp65
a-p65
a-pIκBa
a-IκBa
a-pp38
a-p38
a-pJNK
a-JNK
a-Tubulin
pp65
p65
pIκBa
IκBa
pp38
p38
pJNK
JNK
Tubulin
1 2 3 4 5 6 7 8 9 10
C
MDFs
% Cell death (SG+)
hours of T treatment
D
BMDMs
E
BMDMs
hours of LPS treatment
F
BMDMs
LPS (2h):
Poly I:C (2h):
a-N4BP1
N4BP1-L
N4BP1-S
cl. N4BP1
1 2 3 4 5 6
G
BMDMs
TNF
mRNA (fold induction)
hours LPS stimulation
H
BMDMs
CCL2
I
BMDMs
TNF
hours Poly I:C stimulation
J
BMDMs
CCL2

Figure 14. cFLIP cleavage does not affect TNF-R1 and TLR-mediated proinflammatory gene expression. **A.** *Cflip*^{WT} and *Cflip*^{D377A} mouse dermal fibroblasts (MDFs) were treated with TNF (100 ng/ml) and cell death was measured over time by calculating the percentage of Sytox Green-positive cells. (n=3, mean±SD) **B.** *Cflip*^{WT} and *Cflip*^{D377A} MDFs were treated with TNF (100 ng/ml) for the indicated time points. Cell lysates were immunoblotted using the indicated specific antibodies. (n=3) **C.** *Cflip*^{WT} and *Cflip*^{D377A} bone marrow-derived macrophages (BMDMs) were treated with TNF (100 ng/ml) and cell death was measured over time by calculating the percentage of Sytox Green-positive cells. (n=3, mean±SD) **D.** *Cflip*^{WT} and *Cflip*^{D377A} BMDMs were treated with TNF (100 ng/ml) for the indicated time points. Cell lysates were immunoblotted using the indicated specific antibodies. (n=3) **E.** *Cflip*^{WT} and *Cflip*^{D377A} BMDMs were treated with LPS (20 ng/ml) and cell death was measured over time by calculating the percentage of Sytox Green-positive cells. (n=1) **F.** *Cflip*^{WT} and *Cflip*^{D377A} BMDMs were treated with LPS (100 ng/ml) or poly I:C (1 µg/ml) for the indicated time points. Cell lysates were immunoblotted using the indicated specific antibodies. (n=3) **G-J.** *Cflip*^{WT} and *Cflip*^{D377A} BMDMs were treated with LPS (100 ng/ml, **G-H**) or poly I:C (1 µg/ml, **I-J**) for indicated time points. TNF **(G-I)** and CCL2 **(H-J)** mRNA levels were measured by RT-PCR (n=3, mean±SD).

restrain complex II formation and thus TNF-induced cytotoxicity, independently of proinflammatory gene expression.

3.1.4 The phenotype of *Sharpin*^{cpdm} mice worsens in the absence of cFLIP cleavage.

Next, we sought to elucidate the physiological significance of the cFLIP cleavage and its cell death-limiting functions in a genetic model of TNF-induced cell-death-mediated tissue damage using *Sharpin*-mutant mice. *Sharpin*$^{cpdm/cpdm}$ (*Sharpin*^{cpdm}) mice spontaneously develop severe chronic multi-organ inflammation due to exacerbated TNF-induced RIPK1 kinase activity-dependent cell death. These mice exhibit inflammatory lesions together with epidermal hyperplasia in the skin, loss of marginal zones in the spleen and Peyer's patches in the small intestine.[97–100,163] Increased formation of TNF-induced complex II was previously associated with increased cell death in *Sharpin*^{cpdm} mice.[164] To understand whether the D377A mutation could affect the onset and progression of the phenotype observed in *Sharpin*^{cpdm} mice, we next generated *Cflip*$^{D377A/D377A}$*Sharpin*$^{cpdm/cpdm}$ (*Cflip*^{D377A}*Sharpin*^{cpdm}) double mutant mice. Given the sensitising effect of the D377A mutation towards TNF-induced cell death, and that the *Sharpin*-deficiency causes a TNF-induced cell death-mediated pathology, we expected the D377A mutation would worsen the phenotype of the *Sharpin*^{cpdm} mice. Indeed, *Cflip*^{D377A}*Sharpin*^{cpdm} mice were born runted and displayed significantly lower body weight throughout their life span compared to *Sharpin*^{cpdm} and healthy littermates despite being born at the expected Mendelian ratio (Figure 15A-B). Moreover, the overall survival of *Cflip*^{D377A}*Sharpin*^{cpdm} mice was between 10 and 12 weeks after birth due to severe skin lesions compared to *Sharpin*^{cpdm} littermates with a life span of up to 18 weeks, with the first skin lesions being detected around 15 weeks after birth (Figure 15C). A detailed histological and immunofluorescence analysis of skin samples from *Cflip*^{D377A}*Sharpin*^{cpdm} mice confirmed the early onset of epidermal tissue disruptions. Indeed, TUNEL staining of skin sections from 3-weeks-old mice revealed higher levels of cell death in the skin of *Cflip*^{D377A}*Sharpin*^{cpdm} mice compared to *Sharpin*^{cpdm} and healthy littermates at the same age

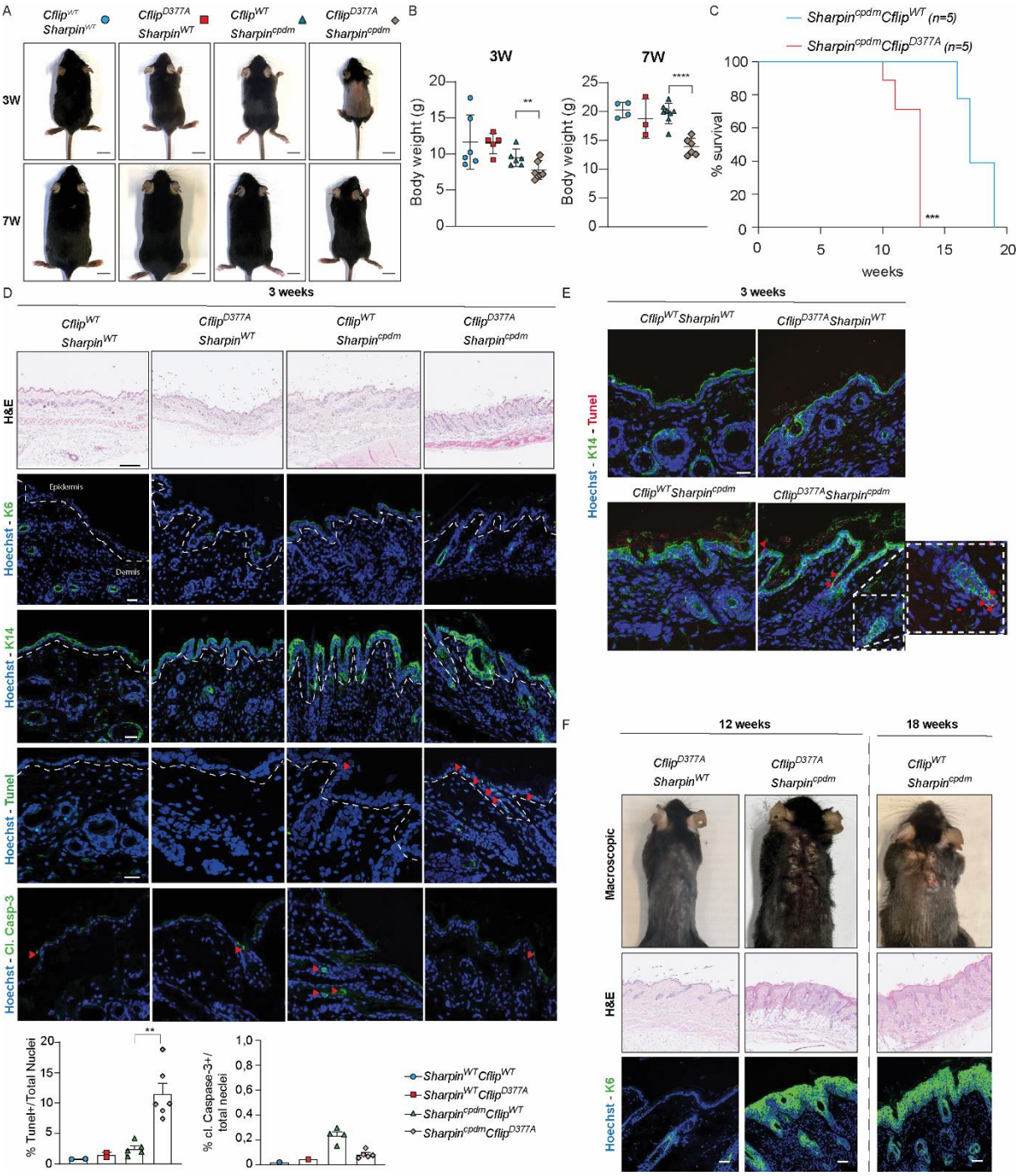

Figure 15. Abrogation of cFLIP cleavage exacerbates systemic and skin phenotype of *Sharpin^{cpdm}*. **A.** Representative pictures of 3 and 7 weeks-old *Cflip^{WT}Sharpin^{WT}*, *Cflip^{D377A}Sharpin^{WT}*, *Cflip^{WT}Sharpin^{cpdm}* and *Cflip^{D377A}Sharpin^{cpdm}* mice. Scale bar 1 cm. **B**. Body weight of *Cflip^{WT}Sharpin^{WT}*, *Cflip^{D377A}Sharpin^{WT}*, *Cflip^{WT}Sharpin^{cpdm}* and *Cflip^{D377A}Sharpin^{cpdm}* mice was measured at the indicated time points. Each symbol corresponds to one mouse. (n=5-6, mean±SD) **C**. Kaplan-Meier survival curve of *Cflip^{WT}Sharpin^{cpdm}* and *Cflip^{D377A}Sharpin^{cpdm}* mice. The mice were sacrificed when the termination criteria, based on the severity of dermatitis, were reached. **D.** Representative skin sections of 3 weeks-old mice of the indicated genotypes stained with H&E, K6, K14, cleaved Caspase-3 and TUNEL. (upper panel) Nuclei were stained with Hoechst. White dashed lines separate the epidermis from the dermis. Red arrowheads indicate TUNEL- and cleaved Caspase-3-positive cells. The graphics represent the percentage of TUNEL-and cleaved Caspase-3-positive cells over the total number of cells (bottom panel, n=4-6 for *Cflip^{WT}Sharpin^{cpdm}*, *Cflip^{D377A}Sharpin^{cpdm}* mice and n=2 for *Cflip^{WT}Sharpin^{WT}*, *Cflip^{D377A}Sharpin^{WT}* mice, mean±SD). Scale bars 20 µm. **E.** Representative skin sections of 3 weeks old mice of the indicated genotypes co-stained with K14 and TUNEL. Nuclei were stained with Hoechst. Red arrowheads indicate TUNEL-positive/K14-positive cells. Scale bars 20 µm. **F.** Representative pictures of mice and skin sections, stained with H&E and K6, of the indicated genotypes and age. Scale bars 20 µm ** P ≤ 0,01, *** P ≤ 0,001 and **** P ≤ 0,0001

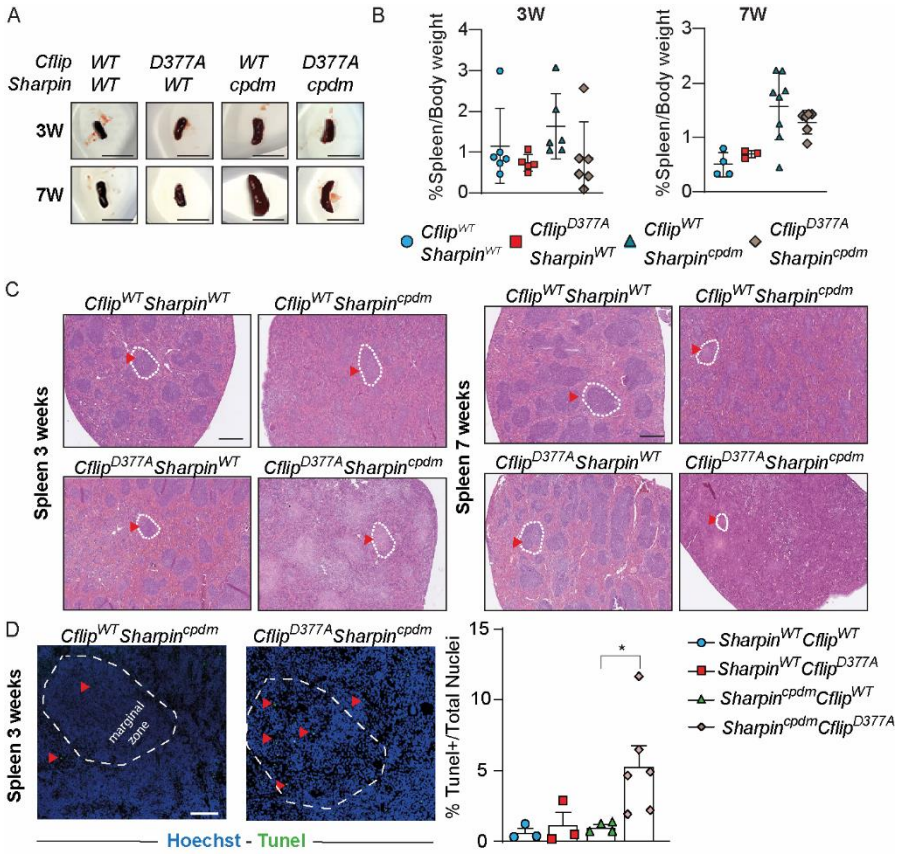

Figure 16. Abrogation of cFLIP cleavage exacerbates tissue damage in spleen caused by *Sharpin* deficiency. A. Representative pictures of spleen from 3 and 7 weeks-old *Cflip*^{WT}*Sharpin*^{WT}, *Cflip*^{D377A}*Sharpin*^{WT}, *Cflip*^{WT}*Sharpin*^{cpdm} and *Cflip*^{D377A}*Sharpin*^{cpdm} mice. Scale bar 2,5 mm. **B.** Spleen weight of *Cflip*^{WT}*Sharpin*^{WT}, *Cflip*^{D377A}*Sharpin*^{WT}, *Cflip*^{WT}*Sharpin*^{cpdm} and *Cflip*^{D377A}*Sharpin*^{cpdm} mice was measured at the indicated time points and expressed as a percentage of total body weight. Each symbol corresponds to one mouse (n=5-6, mean±SD). **C.** Representative images of spleen sections of 3- and 7-weeks-old mice of the indicated genotypes stained with H&E. Dotted with circles and red arrowheads indicate marginal zones. Scale bar 500 µm. **D.** Representative pictures of TUNEL staining of spleen sections of 3 weeks-old mice of the indicted genotypes (left panel) and the relative quantification (right panel) expressed as percentage of TUNEL-positive cells over the total number of cells. Nuclei were stained with Hoechst. Red arrowheads indicate TUNEL-positive cells. Each symbol corresponds to one mouse (n=3 for *Cflip*^{WT}*Sharpin*^{WT}, *Cflip*^{D377A}*Sharpin*^{WT}, n=4 for *Cflip*^{WT}*Sharpin*^{cpdm} and n=6 for *Cflip*^{D377A}*Sharpin*^{cpdm} mice, mean±SD). Scale bar 100 µm. * P ≤ 0,05.

(Figure 15D-E). Of note, despite showing elevetaed levels of cell death, the skin of 3-weeks-old *Cflip*^{D377A}*Sharpin*^{cpdm} mice did not exhibit any sign of inflammation or hyperplasia, consistently with the notion that cell death precedes inflammation. Moreover, TUNEL/K14 double staining showed that the dead cells in the skin of 3-weeks-old *Cflip*^{D377A}*Sharpin*^{cpdm} mice were predominantly keratinocytes (Figure 15E). At the termination point, both *Sharpin*^{cpdm} and *Cflip*^{D377A}*Sharpin*^{cpdm} mice displayed similar levels of epidermal hyperplasia shown by epidermal thickening in H&E staining and increased numbers of Keratin 6-positive (K6-positive) hyperproliferative keratinocytes (Figure 15F). These findings strongly suggest that the abrogation of cFLIP cleavage enhances the cell death-inducing potential of *Sharpin* deletion in keratinocytes and thereby the onset of dermatitis *in vivo*. Another feature of *Sharpin*^{cpdm} mice is splenomegaly and loss of marginal zones. As expected, *Sharpin*^{cpdm} mice displayed enlargement of the spleen size, while the D377A mutation did not exacerbate splenomegaly (Figure 16A-B). However, *Cflip*^{D377A}*Sharpin*^{cpdm} mice exhibited

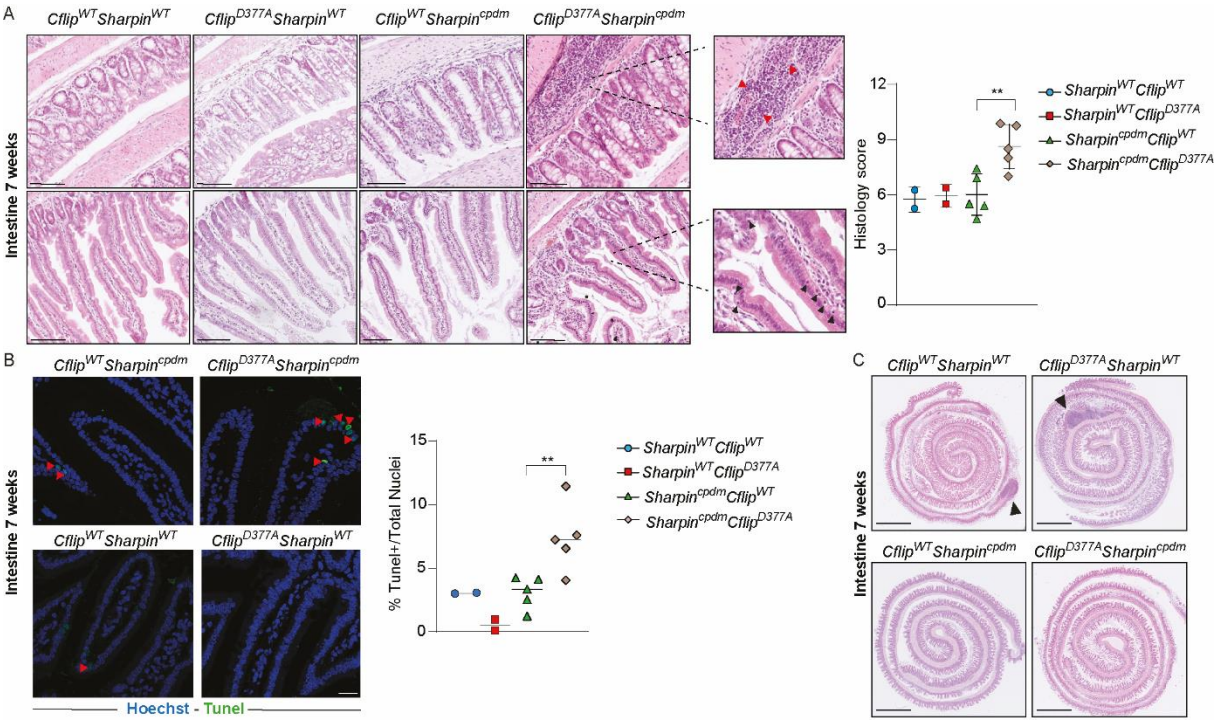

Figure 17. Abrogation of cFLIP cleavage exacerbates intestinal tissue damage and cell death caused by *Sharpin* deficiency. A. Representative images of large (top) and small (bottom) intestinal sections of the indicated genotypes (left panel) at 7 weeks and the relative histology score to the whole intestine (right panel) Red and dark arrowheads indicate areas of inflammation and dead cells, respectively. Each symbol represents one mouse (n=2 for $Cflip^{WT}Sharpin^{WT}$, $Cflip^{D377A}Sharpin^{WT}$, n=5 for $Cflip^{WT}Sharpin^{cpdm}$ and $Cflip^{D377A}Sharpin^{cpdm}$ mice, mean±SD). Scale bar 100 µm. **B**. Representative pictures of TUNEL staining of small intestine sections of 7-weeks-old mice of the indicted genotypes (left panel) and the relative quantification (right panel) expressed as percentage of TUNEL-positive cells over the total number of cells. Nuclei were stained with Hoechst. Red arrowheads indicate TUNEL-positive cells. Red arrowheads indicate TUNEL-positive cells. Each symbol corresponds to one mouse (n=2 for $Cflip^{WT}Sharpin^{WT}$, $Cflip^{D377A}Sharpin^{WT}$, n=5 for $Cflip^{WT}Sharpin^{cpdm}$ and $Cflip^{D377A}Sharpin^{cpdm}$ mice, mean±SD). Scale bar 20 µm. **C.** Representative images of small Intestinal sections of the indicated genotypes at 7 weeks. Dark arrowhead indicates a Peyer's patch. Scale bar 1 mm. ** P ≤ 0,01.

severe loss of marginal zones and therefore severe loss of spleen architecture (Figure 16C). In parallel, already at the age of 3 weeks, $Cflip^{D377A}Sharpin^{cpdm}$ mice displayed increased cell death levels, shown by high levels of TUNEL-positive cells in the marginal zones (Figure 16D). At this age, the spleens of $Sharpin^{cpdm}$ mice only exhibited minor alterations (Figure 16C-D), indicating that the D377A mutation accelerates the loss of spleen structure caused by *Sharpin* deficiency. Moreover, the histological examinations of the intestines of $Sharpin^{cpdm}$ and $Cflip^{D377A}Sharpin^{cpdm}$ mice revealed that the intestines of 7-weeks-old $Sharpin^{cpdm}$ mice were normal and largely comparable to those of control mice, apart from the expected loss of Peyer's patches in the small intestine in *Sharpin*-deficient mice (Figure 17A-C). On the contrary, the intestines of $Cflip^{D377A}Sharpin^{cpdm}$ mice exhibited signs of damage, inflammation and cell death, both in the small and large intestines, as shown by the histology score (Figure 17A). This correlated with a significant increase in the amount of TUNEL-positive cells (Figure 17B). Collectively, these findings indicate that abrogation of cFLIP cleavage enhances multi-organ inflammation due to increased sensitivity to cell death caused by *Sharpin*-deficiency *in vivo*.

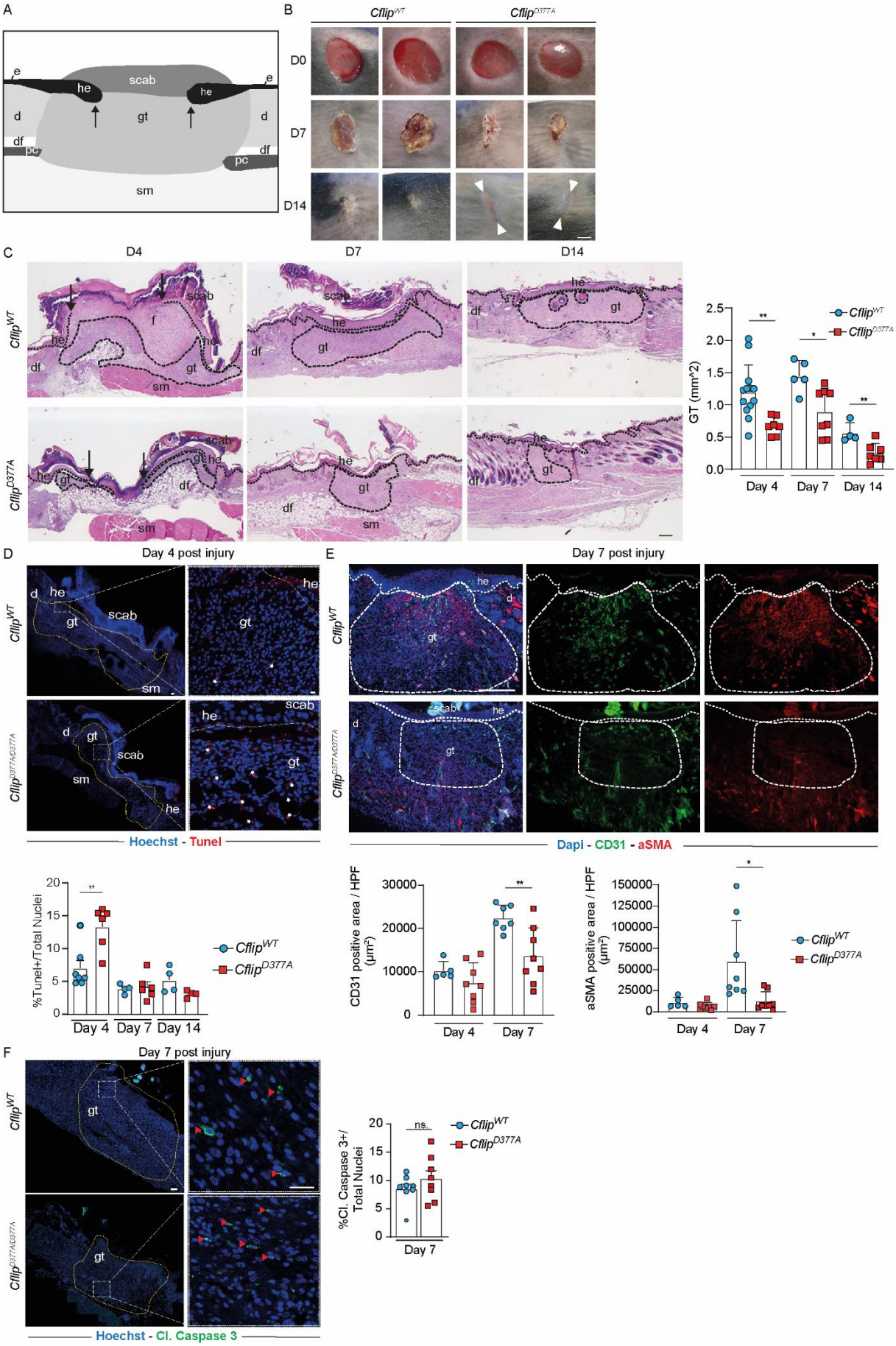
A
B
CflipWT
CflipD377A
D0
D7
D14
e
he
scab
d
gt
df
pc
sm
C
D4
D7
D14
f
GT (mm^2)
Day 4
Day 7
Day 14
D
Day 4 post injury
Hoechst - Tunel
%TuneH+/Total Nuclei
E
Day 7 post injury
Dapi - CD31 - aSMA
CD31 positive area / HPF (µm²)
aSMA positive area / HPF (µm²)
F
Day 7 post injury
Hoechst - Cl. Caspase 3
%Cl. Caspase 3+/ Total Nuclei
ns.

Figure 18. *Cflip*^{D377A} mice exhibit impaired skin wound healing. **A.** Cartoon representing the histology of a skin wound at around 4-days post-injury (dpi), where the following skin areas are marked: d, dermis; df, dermal fat tissue; e, epidermis; gt, granulation tissue; he, hyperproliferative epithelium; pc, panniculus carnosus; sm, skeletal muscle. **B**. Macroscopic pictures of wounds at 0-, 7- and 14-dpi in *Cflip*^{WT} and *Cflip*^{D377A} mice. White arrows indicate scar tissue. Arrows indicate the tips of the epithelial tongues. Scale bar 2 mm. **C.** Representative H&E-stained wound sections of *Cflip*^{WT} and *Cflip*^{D377A} mice at 4-, 7- and 14-dpi (left panel) and the respective quantitative analysis of gt area of skin sections (right panel, n=4-12 total wounds per genotype per dpi, mean±SD). Scale bar 200 µm. **D.** Representative TUNEL-stained wound sections at 4 dpi of *Cflip*^{WT} and *Cflip*^{D377A} mice (top panel). Nuclei were stained with Hoechst. White asterisks indicate TUNEL-positive cells. Relative quantification as a percentage of TUNEL-positive cells over the total number of cells at 4-dpi (bottom panel, n= 4-7 total wounds per genotype per dpi, mean±SD). Scale bars 50 µm in left images and 20 µm in right images. **E**. Representative CD31- and smooth muscle actin (SMA)-immunostainings at day 7 dpi of wound sections of *Cflip*^{WT} and *Cflip*^{D377A} mice (top panel). Nuclei were stained with Hoechst. The respective relative quantification as a percentage of total CD31- and SMA-positive area per high power field (hpf) at 4- and 7-dpi (bottom panel, n=5-8 total wounds per genotype per dpi, mean±SD). Scale Bar 200 µm. **F.** Representative cleaved Caspase-3-stained wound sections at 7-dpi (left panel) Nuclei were stained with Hoechst. Red arrowheads indicate cleaved Caspase-3-positive cells. The respective percentages of cleaved Caspase-3-positive cells over the total number of cells at 7-dpi (right panel, n=4-7 total wounds per genotype per dpi, mean±SD) Scale bars 50 µm in left images and 20 µm in right images. * P ≤ 0,05, ** P ≤ 0,01.

3.1.5 Abrogation of cFLIP cleavage impairs skin wound healing.

Skin excision injury results in formation of a scar tissue that histologically is composed of scab, hyperproliferative epithelium and, most importantly, granulation tissue surrounded by healthy skin (Figure 18A). Different cell types, including macrophages, myofibroblasts and endothelial cells, migrate from the adjacent tissues into the wound microenirorment to regenrate the skin tissue and its vascularisation leading to wound closure. The wound healing process requires spatiotemporally coordinated cell death programs in the wound microenvironment. TNF signalling, in particular TNF-induced cell death, promotes wound healing. Thus, disruption of TNF-induced Caspase-8-mediated death of wound macrophages delays wound closure by impairing the resolution of tissue inflammation.[135,137,138,141] To further validate the contribution of cFLIP cleavage-mediated regulation of Caspase-8-induced cell death outcomes in the context of tissue damage, we utilized a model of mouse full-thickness excisional skin injury. Interestingly, immunohistological analysis showed a significantly delayed wound closure in *Cflip*^{D377A} mice as compared to *Cflip*^{WT} mice. This was evident by reduced scar formation (Figure 18B) and reduced granulation tissue area on days 4, 7 and 14 after injury (Figure 18C). Consistently, *Cflip*^{D377A} mice exhibited significantly higher levels of TUNEL-positive cells (Figure 18D) at day 4 post-injury, reduced wound vascularization (CD31-positive area) and fewer myofibroblasts (smooth muscle actin [SMA]-positive area) at day 7 after injury (Figure 18E). However, no difference in the percentage of cleaved Caspase-3-positive cells was detected (Figure 18F). Thus, abrogation of cFLIP cleavage causes an increased cell death response that interferes with the wound healing process. We therefore conclude that cFLIP cleavage is crucial to control the extent of cell death occurring after wound injury to ensure an optimal healing process.

3.1.6 cFLIP cleavage limits viral-induced cell death and the lethal effects of SARS-CoV 1 infection.

Given our earlier observations that abrogation of cFLIP cleavage sensitises the cells to necroptosis induced by a viral protein, CrmA, and IFNγ, a major cytokine during viral infection, (Figure11G-L), we addressed the relevance of cFLIP cleavage in controlling cell death during viral infection. To mimic anti-viral response, we primed LFs isolated from *Cflip*^{WT} and *Cflip*^{D377A} mice with IFNγ and then treated them with TNF (IT). Interestingly, we found that *Cflip*^{D377A} LFs were significantly more sensitive to IT-induced cell death compared to *Cflip*^{WT} LFs (Figure 19A). Intriguingly, the subsequent analysis of the lysates revealed that, in *Cflip*^{D377A} LFs, both necroptosis, apoptosis and pyroptosis occurred at an increased extent compared to *Cflip*^{WT} LFs. This was shown by the higher levels of phosphorylated MLKL, cleaved caspase-3 and N-terminal fragment of GSDMD, respectively (Figure 19B). These findings seem to suggest that cFLIP cleavage controls cell death occurring following viral infection.

Encouraged by the *in vitro* data, we next investigated the relevance of cFLIP cleavage during viral infection *in vivo*. For this purpose, we employed the SARS-CoV 1 infection model. SARS-CoV1 is a strain of coronavirus that infects epithelial cells in the lung of host organisms.[165] After infection, SARS-CoV 1 tiggers the acute release of proinflammatory cytokines, including IFNγ and TNF. This phenomenon, the so called cytokine storm, can have serious pathological consequences for the host, including lung damage and multi-organ failure. Recent reports showed that SARS-CoV-induced cytokines can trigger cell death in the form of apoptosis, necroptosis and pyroptosis, which, in turn, further enhance the production of cytokines resulting in the hyperactivation of the immune system that causes the lethality in infected organisms.[151,153,166] To test whether cFLIP cleavage contributes to the cytokine-induced cell death observed during the disease progression, we infected *Cflip*^{WT} and *Cflip*^{D377A} mice with sublethal doses of MA15, a mouse-adapted strain of SARS-CoV 1. Remarkably, *Cflip*^{D377A} mice were dramatically more susceptible to SARS-CoV 1 induced mortality than their *Cflip*^{WT} age-matched counterparts even though there was no significant difference in the viral titre between the two genotypes (Figure 19C-D). In addition, the levels of proinflammatory cytokines and chemokines in the lungs tend to be only slightly higher in *Cflip*^{D377A} mice than their *Cflip*^{WT} counterparts (Figure 19E-M). These data strongly suggest that the increased sensitivity of *Cflip*^{D377A} mice to SARS-CoV 1 lethality is not caused by higher viral titre or exaggerated cytokine production. Based on these observations, it was tempting to speculate that cFLIP cleavage is involved in regulating the extent of cell death induced by cytokines following infection. Thus, the increased levels of cell death observed in *Cflip*^{D377A} LFs treated with IFNγ and TNF (Figure 19A) might correlate with the

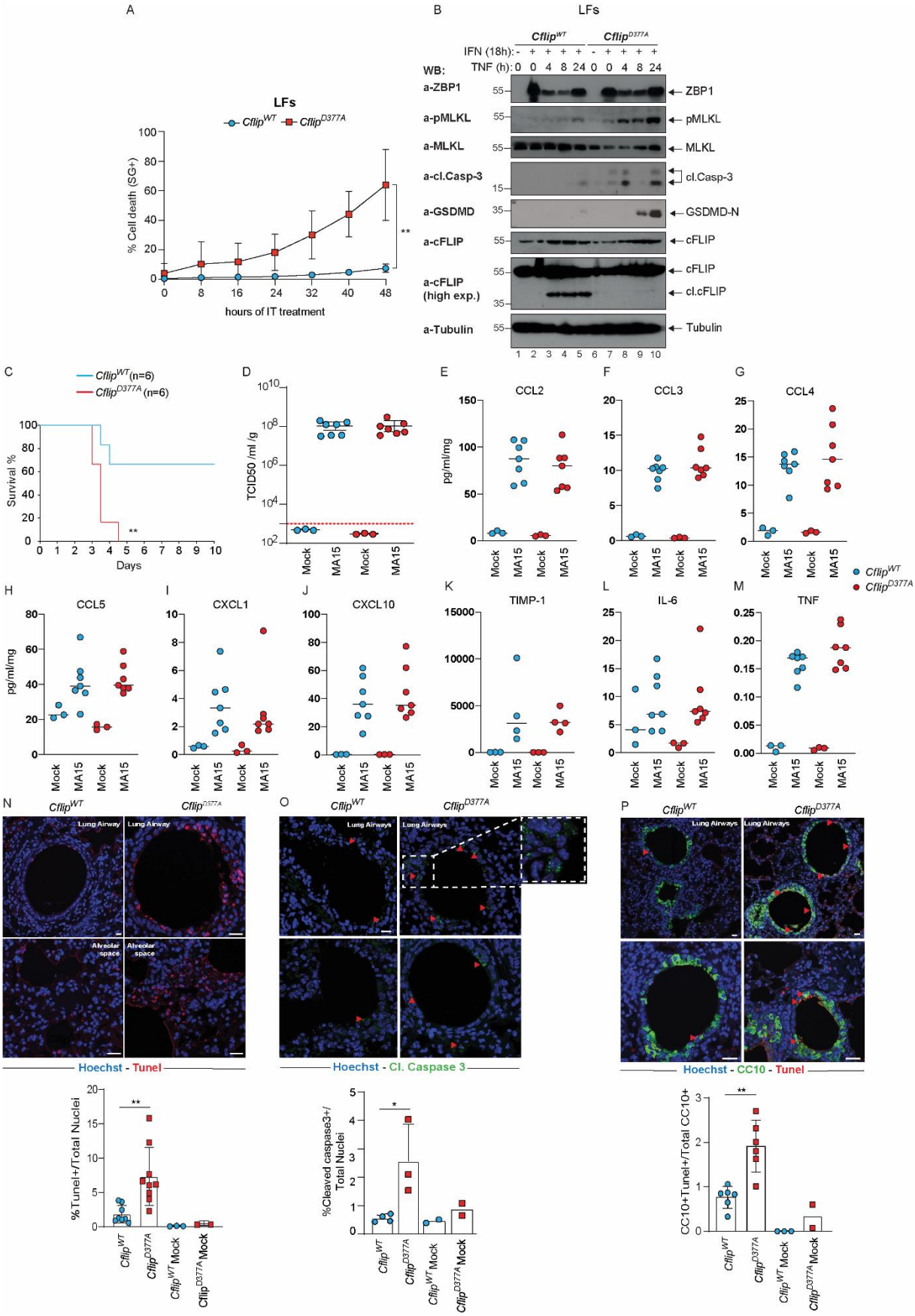
A
LFs
Cflip^WT Cflip^D377A
% Cell death (SG+)
hours of IT treatment
**
B
LFs
Cflip^WT Cflip^D377A
IFN (18h): - + + + + - + + + +
WB: TNF (h): 0 0 4 8 24 0 0 4 8 24
a-ZBP1
a-pMLKL
a-MLKL
a-cl.Casp-3
a-GSDMD
a-cFLIP
a-cFLIP (high exp.)
a-Tubulin
ZBP1
pMLKL
MLKL
cl.Casp-3
GSDMD-N
cFLIP
cFLIP
cl.cFLIP
Tubulin
C
Cflip^WT (n=6)
Cflip^D377A (n=6)
Survival %
Days
D
TCID50 /ml /g
Mock MA15 Mock MA15
E
CCL2
F
CCL3
G
CCL4
pg/ml/mg
H
CCL5
I
CXCL1
J
CXCL10
K
TIMP-1
L
IL-6
M
TNF
N
Cflip^WT Cflip^D377A
Lung Airway
Alveolar space
Hoechst - Tunel
%Tunel+/Total Nuclei
O
Hoechst - Cl. Caspase 3
%Cleaved caspase3+/ Total Nuclei
P
Hoechst - CC10 - Tunel
CC10+Tunel+/Total CC10+

Figure 19. cFLIP cleavage limits the lethal effects of SARS-CoV 1 infection. A. *Cflip*^{WT} and *Cflip*^{D377A} lung fibroblasts (LFs) were primed with IFNγ (100 ng/ml) and treated with TNF (100 ng/ml). Cell death was measured over time by calculating the percentage of Sytox Green-positive cells (n=3, mean±SD) **B.** *Cflip*^{WT} and *Cflip*^{D377A} lung fibroblasts (LFs) were primed with IFNγ (100 ng/ml) and treated with TNF (100 ng/ml) for the indicated time points. Cell lysates were immunoblotted using the indicated specific antibodies. (n=3) **C.** Kaplan-Meier survival curve of *Cflip*^{WT} and *Cflip*^{D377A} mice infected with SARS-CoV 1 MA15 virus (n=6). **D-M.** Viral titer **(D)** and cytokine levels (F-N) from lungs of *Cflip*^{WT} and *Cflip*^{D377A} mice 3 dpi (days-post-infection, n=3 for mock infection and n=7 for *Cflip*^{WT} and *Cflip*^{D377A} infected lungs). **N.** Representative TUNEL-stained lung sections of *Cflip*^{WT} and *Cflip*^{D377A} mice 3-dpi top panel). Nuclei were stained with Hoechst. The respective percentages of TUNEL-positive cells over total number of cells (bottom panel, n=8 for *Cflip*^{WT} infected lungs, n=10 for *Cflip*^{D377A} infected lungs and n=2-3 for mock infection, mean±SD) Scale bars 10 μm for upper left image and 20 μm for upper right and bottom images **O.** Representative cleaved Caspase-3-stained lung sections of *Cflip*^{WT} and *Cflip*^{D377A} mice 3-dpi. Nuclei were stained with Hoechst. Red arrowheads indicate cleaved Caspase-3-positive cells. The respective percentage of cleaved Caspase-3-positive cells at 3-dpi (bottom panel, n=4 for *Cflip*^{WT} infected lungs, n=3 for *Cflip*^{D377A} infected lungs and n=2 for mock infection, mean±SD). Scale bars 10 μm. **P.** Representative lung sections co-stained with CC10 and TUNEL at 3-dpi (top panel). Nuclei were stained with Hoechst. Red arrowheads indicate TUNEL-positive/CC10-positive cells. The respective percentage of CC10-positive/TUNEL-positive cells over the total number of CC10-positive cells at 3-dpi (n=6 for *Cflip*^{WT} and *Cflip*^{D377A} mice and n=2-3 for mock infection, mean±SD) Scale bars 10 μm for upper images and 20 μm for bottom images. * P ≤ 0,05, ** P ≤ 0,01.

increased levels of cytokine-induced cell death, apoptosis and potentially necroptosis, occurring in the lungs of the infected mice. This might, in turn, interfere with the restoration of tissue integrity post-infection, leading to organ failure and so increased lethality. To test this hypothesis, we examined lung sections of infected mice for the presence of dying cells using TUNEL and cleaved Caspase-3 staining. As expected, the quantifications revealed the presence of higher numbers of TUNEL- and cleaved Caspase-3-positive cells both in bronchioles and alveoli of *Cflip*^{D377A} mice compared to their *Cflip*^{WT} counterparts (Figure 19N-O). In addition, co-staining with TUNEL and CC10, a marker of club cells in the respiratory bronchioles, revealed a higher number of TUNEL-positive club cells in *Cflip*^{D377A} mice, indicating increased lung tissue damage, than in their *Cflip*^{WT} counterparts (Figure 19P). Collectively, the results obtained from the SARS-CoV 1 infection model together with *in vitro* data from LFs led us to the conclusion that the excessive cell death caused by virus-induced cytokines, including IFNγ and TNF, in *Cflip*^{D377A} mice exacerbates tissue damage and, in turn, leads to increased lethality.

3.2 Immunoprecipitation-based mass spectrometric study of complex II dynamics highlights potential new players in the regulation of TNF-induced cell death.

TNF signalling primarily results in proinflammatory signals rather than in cell death. The cytotoxic potential of TNF is mediated by complex II and it is unleashed only when certain checkpoints that prevent cell death are inactivated. Over the years, a range of checkpoints in TNF signalling were shown to act at different stages to limit the formation and accumulation of complex II in the cytosol.[2,59] The core components of complex II are FADD, Caspase-8, cFLIP, RIPK1 and RIPK3.[63] Over the years, only a few new components with regulatory potential were discovered to interact

directly with complex II, the most recent one being tankyrase-1[134]. It is currently believed that there are still more regulatory molecules associated with complex II that await identification and characterisation. Therefore, we attempted to identify new regulatory proteins associated with complex II that would add another layer to the checkpoints of TNF-induced complex II cytotoxicity. To accomplish this goal, we employed an unbiased, immunoprecipitation-based mass spectrometry-coupled approach.We first generated *Fadd*$^{-/-}$ cells using CRISPR-Cas9 technology (Figure 20A). We functionally validated them by showing that *Fadd* deletion sensitised the cells to TNF alone (Figure 20B). Subsequently, we reconstituted these cells with a C-terminally flag tagged FADD (Figure 20C-D), which rescued the sensitivity to TNF alone (Figure 20E). Next, we confirmed that C-terminally flag-tagged FADD-reconstituted cells could undergo necroptosis following TE- and TBE-treatment. As shown in Figure 20F, we observed higher levels of cell death within 4 h

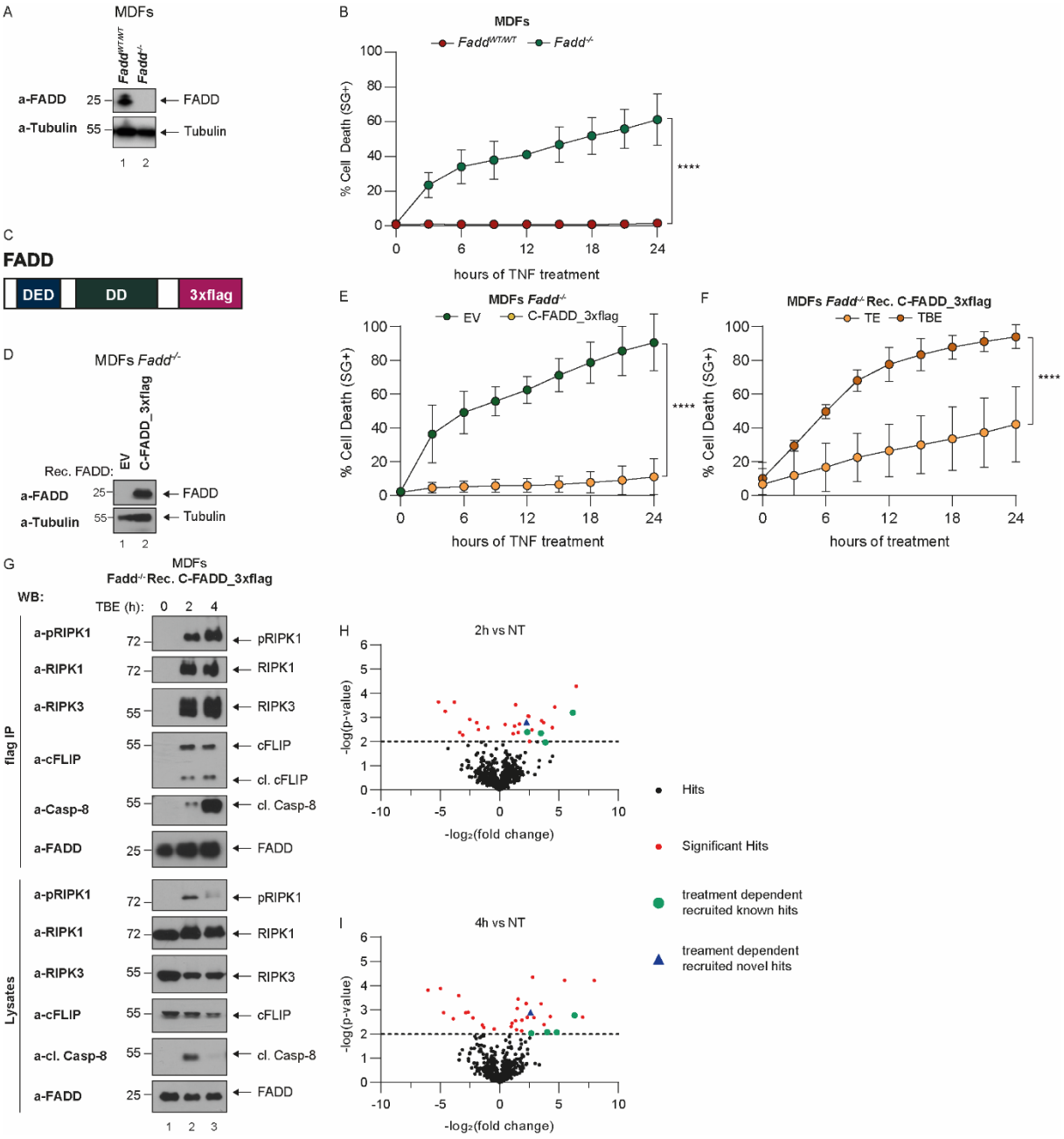

Figure 20. A novel genetic tool to study the composition and dynamics of complex II allowed us to identify potential new regulators of TNF signalling and TNF-induced cell death. A. Deletion of FADD expression in mouse dermal fibroblasts (MDFs) together with respective empty vector (EV) controls were analysed by immunoblotting using the indicated specific antibodies (n=3). **B.** The cell death response of *Fadd*$^{WT/WT}$ and *Fadd*$^{-/-}$ MDFs to TNF (100 ng/ml) was measured over time by calculating the percentage of Sytox Green-positive cells (n=3, mean±SD). **C.** Cartoon depicting FADD domain composition and the C-terminal 3×flag tag. **D.** *Fadd*$^{-/-}$ MDFs were reconstituted with empty vector or C-terminally 3×flag tagged FADD construct. Cell lysates were analysed by immunoblotting using the indicated specific antibodies. (n=2) **E.** *Fadd*$^{-/-}$ MDFs reconstituted as in **(D)** were treated with TNF (100 ng/ml) and cell death response was measured over time by calculating the percentage of Sytox Green-positive cells (n=3, mean±SD). **F.** *Fadd*$^{-/-}$ MDFs were treated with TNF (100 ng/ml), Smac mimetic (250 nM) and Emricasan (1 µM) and the cell death response was measured over time by calculating the percentage of Sytox Green-positive cells. (n=3, mean±SD) **G.** *Fadd*$^{-/-}$ MDFs reconstituted as in (D) were treated with TNF (1 ng/ml) Birinapant (250 nM) and Emricasan (1 µM) for the indicated time points. Cell lysates were subjected to immunoprecipitation using anti-flag antibody conjugated M2 affinity beads. Immunocomplexes and cellular lysates were then analyzed by immunoblotting using the indicated specific antibodies (n=3). **H-I.** Log2 fold change volcano plots of protein enrichment upon TSE treatment in *Fadd*$^{-/-}$ MDFs reconstituted as in **(D)** compared to the untreated or *Fadd*$^{-/-}$ MDFs reconstituted with empty vector controls. Proteins were first filtered by requiring a $p<0.05$ in a pairwise comparison between the treated *Fadd*$^{-/-}$ MDFs reconstituted as in **(D)** with C-terminally 3×flag tagged FADD construct and *Fadd*$^{-/-}$ MDFs reconstituted as in **(D)** with empty vector as negative control in either the untreated or treated samples. Known components of the complex II (RIPK1, RIPK3, FADD, cFLIP and Caspase-8) are labelled and highlighted in green, while potential candidates were highlighted. Statistical analysis of the dataset was conducted in Perseus. Each dot represents a protein hit (n=3). **** P ≤ 0,0001.

post-TSE-treatment compared to TE-treatment. Finally, we confirmed complex II formation by performing anti-flag immunoprecipitation in lysates of cells either treated with TBE for 2 and 4 h or left untreated. As shown in Figure 20G, we observed the recruitment of known complex II components, RIPK1, RIPK3, cFLIP, cleaved Caspase-8, to FADD. After validation of the generated reconstitution system, we analysed the flag-immunoprecipitate from C-terminally flag tagged FADD-reconstituted MDFs treated with TSE for 2 h and 4 h or left untreated using mass spectrometry. Consistent with the immunoprecipitation results, we identified RIPK1, RIPK3, cFLIP and Caspase-8 as significant hits in 2 h and 4 h post-treatment (Figure 20H-I). Following, we sought out other proteins that were significantly enriched in a treatment-dependent manner. Here, we found PPP2R1A, a constant regulatory subunit of protein phosphatase 2 (PP2a). To validate the presence of PPP2R1A in complex II, we performed flag-immunoprecipitation in C-terminally flag tagged FADD reconstitution and *Fadd*$^{-/-}$ MDFs treated with TSE and TNF, respectively. As shown in Figure 21A, we observed the recruitment of RIPK1, cFLIP and most importantly PPP2R1A to FADD 4 h post treatment. This prompted us to generate *Ppp2r1a*$^{-/-}$ MDFs using CRISPR-Cas9 technology to investigate the role of PPP2R1A in the regulation of post-translational modifications in complex II and their impact on complex II cytotoxicity (Figure 21B). Strikingly, *Ppp2r1a*$^{-/-}$ MDFs underwent significantly less TNF-induced necroptosis compared to their *Ppp2r1a*$^{WT/WT}$ counterparts despite having similar levels of proteins related to the respective cell death types (Figure 21B). In contrast, there has been only minor, yet statistically significant, effect on the TNF-induced apoptosis (Figure 21D). These results underline the potential of PPP2R1A and PP2a in the regulation of complex II-mediated cell death outcomes. Altogether, we clearly demonstrated the successful

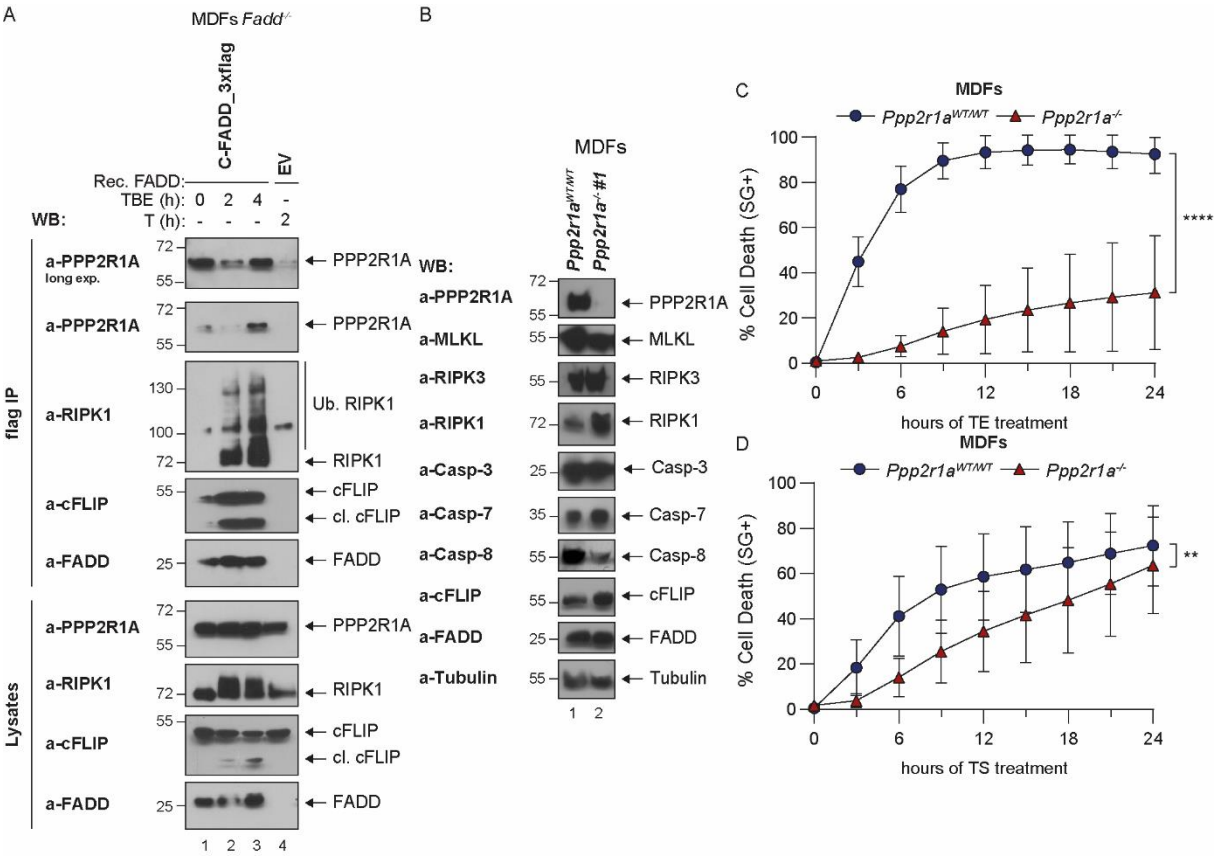

Figure 21. PPP2R1A represents an interesting candidate that potentially has a role in the regulation of TNF-induced cell death. A. *Fadd*$^{-/-}$ mouse dermal fibroblasts (MDFs) were reconstituted with empty vector or C-terminally 3×flag tagged FADD construct were treated with TNF (1 ng/ml) and Emricasan (1 µM) for the indicated time points. Cell lysates were subjected to immunoprecipitation using anti-flag antibody conjugated M2 affinity beads. Immunocomplexes and cellular lysates were then analyzed by immunoblotting using the indicated specific antibodies (n=2). **B.** Deletion of PPP2R1A and expression of cell death-related genes in MDFs together with respective empty vector (EV) controls were analysed by immunoblotting using indicated specific antibodies (n=1). **C.** *Ppp2r1a*$^{WT/WT}$ and *Ppp2r1a*$^{-/-}$ MDFs were treated with TNF (10 ng/ml) and Smac mimetics (250 nM) and cell death was measured over time by calculating the percentage of Sytox Green-positive cells (n=4, mean±SD). **D.** *Ppp2r1a*$^{WT/WT}$ and *Ppp2r1a*$^{-/-}$ MDFs were treated with TNF (1 ng/ml) and Emricasan (1 µM) and cell death was measured over time by calculating the percentage of Sytox Green-positive cells (n=4, mean±SD). ** P ≤ 0,01 and **** P ≤ 0,0001.

establishment of an affinity purification-based mass spectrometry-coupled approach to study the composition of TNF-induced complex II. The shown mass spectrometry results give us a unique opportunity to find novel regulators of TNF-induced complex II-mediated cell death. The identified protein, PPP2R1A, proves to be an interesting candidate and further investigations are now needed to understand its biological relevance on the regulation of complex II formation, its dynamics and ultimately the mitigated cell death outcomes.

4 DISCUSSION

Cell death is an essential part of tissue repair processes following injury and infection. Indeed, cells dying in a programmed manner can instigate inflammatory processes that, in turn, coordinate the healing of the damaged tissue. However, dysregulated cell death can lead to exaggerated inflammation that is detrimental for tissue homeostasis and functioning. Therefore, determining the mechanisms that control stress-induced cell death is fundamental to understand how the organism can cope with and overcome tissue damage. cFLIP is a non-redundant cell death suppressor required to maintain tissue integrity. Its cell death inhibitory functions are due to its heterodimerisation with Caspase-8 and modulation of Caspase-8 activity downstream of immune receptors, including TNF-R1.[74,78,115,123–126] Apart from being a modulator of Caspase-8 activity, cFLIP is also a Caspase-8 substrate, cleaved at position D377. In the present work, we propose that cFLIP cleavage is an essential checkpoint that protects the cells from the cytotoxic potential of TNF and ensures the proper execution of tissue repair programs following damage triggered by different types of stress. Even though the existence of cFLIP cleavage has been known for many years[74,124,131,132], its physiological role has remained poorly understood. This is largely because of the lack of reliable tools that allow functional analysis of cFLIP cleavage under physiological conditions. For this reason, we have generated different genetic *in vitro* and *in vivo* tools, most importantly a novel mouse model bearing non-cleavable cFLIP, and we have studied the molecular dynamics and biological relevance of this cleavage event.

4.1 cFLIP cleavage is a novel prosurvival checkpoint limiting complex II assembly and TNF cytotoxicity.

We showed that the formation of a catalytically active FADD/Caspase-8/cFLIP containing complex was required for cFLIP to be cleaved (Figure 7D-E). In this context, our data strongly support the current cooperative and hierarchical binding model of FADD/Caspase-8/cFLIP in the literature.[74] Moreover, cFLIP cleavage was strictly dependent on the Caspase-8 catalytic activity (Figure 7F). Interestingly, a recent report demonstrated that RIPK3, a potential target of Capsase-8 to supress necroptosis, is rather cleaved by Caspase-3 at D333 residue in mice downstream of executioner caspases (Caspase-8 and -9) under physiological conditions.[167] In the case of cFLIP, however, Caspase-8 appears to be the only caspase targeting cFLIP in mouse cells, possibly since Caspase-8 is the only caspase that comes in close proximity to cFLIP in complex II. In human cells, several reports have shown that Caspase-10, a close homologue of Caspase-8, shares overlapping substrate specificity and is involved in a negative feedback loop for Caspase-8-mediated cell death

under various death-receptor signalling.[168] Hence, it would be interesting to determine whether cFLIP can be cleaved by Caspase-10 and how cFLIP cleavage influence the regulation of Caspase-8 by Caspase-10.

Our data showed that cFLIP cleavage upon TNF-R1 activation occurred only at the D377 residue. (Figure 8D-E).This prompted us to generate the *Cflip*^{D377A} mice with a non-cleavable cFLIP variant. These mice were indistinguishable from their *Cflip*^{WT} littermates (Figure 9) and the cells isolated from *Cflip*^{D377A} mice were not sensitive to TNF alone (Figure 14A). These indicate that cFLIP cleavage is dispensable to supress cell death during embryonic development and under homeostatic conditions. An additional target of Caspase-8 is RIPK1, cleaved at the D325 residue. *Ripk1*$^{D325A/D325A}$ cells, bearing a non-cleavable RIPK1 variant, showed increased sensitivity to TNF-induced necroptosis due to enhanced recruitment and kinase activity of RIPK1 in complex II. It is clear that the cleavage of RIPK1 at the D325 residue is indispensible to suppress TNF cytotoxicity [32,33], as *Ripk1*$^{D325A/D325A}$ mice are embryonically lethal. However, the cleavage of cFLIP at D377 residue regulates TNF-induced cell death under conditions, where the cytotoxic potential of TNF is unleashed. These different outcomes of the Caspase-8-mediated cleavage-dependent checkpoints point out their hierarchical order. There are critical Caspase-8-dependent checkpoints, such as RIPK1, whose perturbation irremediably causes aberrant cell death. However, perturbation of some Caspase-8 dependent checkpoints, such as cFLIP, can be counterbalanced by other mechanisms under normal conditions. Excitingly, future work investigating further potential Caspase-8-mediated cleavage-dependent checkpoints are needed to elucidate their impact on the stability and activity of complex II and the functional and (patho-)physiological consequences of their perturbation.

We found that cFLIP cleavage restrained TNF-induced RIPK1-dependent and -independent cell death. Moreover, abrogation of cFLIP cleavage seemed to exacerbate cell death induced in a TNF-independent manner for example ZBP1-mediated necroptosis (Figure 11). The prosurvival function of this cleavage was related to its ability to limit complex II formation and stability (Figure 12). Therefore, we believe cFLIP cleavage does not directly impact on Caspase-8 activity *per se*, but rather indirectly, by regulating the dynamics of a complex where Caspase-8 is recruited and activated. The assembly of a membrane-bound or cytosolic complex II-like death-inducing platforms containing Caspase-8/cFLIP heterodimer is a common feature among different DR/ligand systems.[56] Therefore, it is tempting to say cFLIP might control cell death downstream of other DR/ligand systems. Thus, studies focusing on the biological significance of cFLIP cleavage in

TRAIL- and FAS-mediated cell death would be beneficial to improve our knowledge of other DR/ligand systems and their respective death-inducing complexes.

Mechanistically, we hypothesise that cFLIP cleavage represents a mechanism that counterbalances complex II formation to keep its killing activity in check. This prosurvival function seemed to be linked to the cleavage-mediated removal of the C-terminal part of the protein, in particular Q469 residue, which was already reported to favour Caspase-8/cFLIP heterodimerisation (Figure 13), in addition to the main Caspase-8/cFLIP heterodimerisation surface being death domain.[74] The enhanced availability of this secondary Caspase-8/cFLIP interaction surface by genetic blockage of cFLIP cleavage seems to enhance Caspase-8 recruitment and thus its enzymatic activity. By promoting Caspase-8/cFLIP heterodimerisation, D377A mutation might also recruit more FADD molecules via death effector domain that in turn can recruit more RIPK1 molecules via death domain. In this context, since complex II was reported to be organized in filamentous structures[74,78,79,145], one might speculate that cleavage of cFLIP negatively regulates the extension of filaments in complex II. A key question arising from these facts is how the D377A mutation modulates filament formation, particularly of Caspase-8, in complex II and affects its stoichiometry. Further structural analysis of the Caspase-8 filaments in the presence of either WT or D377A cFLIP variants would improve our understanding of the impact of cFLIP cleavage on complex II assembly and complex II-mediated Caspase-8 activation.

In the current work, we observed an increase in the ubiquitination of several key cell death components, particularly cFLIP (Figure 12G). Even though cFLIP is predominantly degraded by the ubiquitin-proteasome system[123,126,169], a recent study revealed that there are different ubiquitination events on cFLIP resulting in various outcomes regarding cFLIP dynamics and functions. These are conjugated with various topologies to the different target residues on cFLIP. This study demonstrated that K48- and M1-ubiquitination collectively control the cFLIP levels under normal conditions. It has been shown that LUBAC-mediated M1-ubiquitination of cFLIP at K351/K354 residues is required to protect cFLIP from K48-ubiquitination and subsequent proteasomal degradation.[170,171] Based on our observations of the ubiquitination status and stability of cFLIP (Figure 10 and 12), the ubiquitination event in *Cflip*^{D377A} cells, potentially of M1-topology, may serve as a scaffolding function that is closely linked with increased stability of cFLIP and more importantly complex II. Cleavage of cFLIP at the D377 residue might cause a conformational change that makes the K351/K354 residues inaccessible to LUBAC rendering cFLIP more prone to K48-ubiquination that induces its turnover. If this is the case, under normal conditions, cFLIP cleavage at the D377 residue might block the cell death promoting ubiquitination event on cFLIP.

A key question that remains to be answered is whether enhanced ubiquitination observed in *Cflip*^{D377A} cells is of M1-topology. Despite, it is becoming increasingly clear that cFLIP is ubiquitinated at multiple sites during necroptosis[170–172], only little is known on which E3 ligase is responsible for the ubiquitination events in *Cflip*^{D377A} cells and how these affect its cytotoxic potential. Therefore, it would be worthwhile to investigate the exact mechanisms and individual roles of the different ubiquitination events. This would provide new insights into the ubiquitination-mediated control of cFLIP functions and their impact on complex II-mediated cell death outcomes.

We showed that the rapid activation of NF-κB and MAPK pathways upon activation TNF-R1 remained unaffected by the D377A mutation of cFLIP (Figure 14). In contrast, previous reports have shown that cleaved cFLIP interacts with TRAF2 to activate NF-κB-mediated proinflammatory gene expression in both mouse[173] and human[174,175] malignant immune cells. Besides the direct role of cFLIP, a complex II-like platform containing Caspase-8/cFLIP heterodimer, that promotes cytokine production downstream of TRAIL and FAS signalling, has been identified, reffered to as FADDosome.[160] Similar to TNF-induced complex II formation, cFLIP suppresses cytokine production by inhibiting the assembly of FADDosome.[162] The differing role of cFLIP in NF-κB-mediated gene expression upon activation of diverse DR/ligand systems, more specifically TNF/TNF-R1 compared to TRAIL/TRAIL-R1/2 and FASL/FAS, is still matter of investigation.

4.2 cFLIP cleavage is critical to control cell death extent to ensure tissue repair and homeostasis.

The present work demonstrated that cFLIP cleavage represents a critical checkpoint under pathological conditions. Once cFLIP cleavage abrogated along with the suppression of a primary checkpoint, e.g. Caspase-8-dependent checkpoint, different cell types became dramatically sensitive to TNF-induced cell death (Figure 10, 11 and 19A-B). Consequently, cFLIP cleavage becomes highly relevant in pathological conditions, where cell death checkpoints of TNF signalling are perturbed and the extent of cell death has to be tightly regulated to prevent the detrimental effects of aberrant cell death-driven inflammation.

In this study, we have shown the contribution of cFLIP cleavage in the TNF-dependent, cell death-mediated systemic inflammatory phenotype of *Sharpin*^{cpdm} mice. *Cflip*^{D377A}*Sharpin*^{cpdm} mice exhibited increased cell death in skin, spleen and intestine already in the first weeks after birth and develop dermatitis significantly earlier than *Sharpin*^{cpdm} mice (Figure 15-17). In line with previous reports indicating enhanced formation of complex II upon *Sharpin*-deficiency[164], our data strongly implies that the genetic inhibition of cFLIP cleavage exacarbates the *Sharpin* deficiency-mediated

activation of a FADD/Caspase-8/cFLIP-containing complex. As a result, this accelerates cell death observed in keratinocytes leading to earlier onset of dermatitis. Earlier investigations showed that keratinocyte-specific apoptosis is the main form of cell death in skin inflammation, while necroptosis drives inflammation in internal organs.[100] However, it is unclear whether the increased cell death observed in various organs, most importantly in skin, of *Cflip*^{D377A}*Sharpin*^{cpdm} mice compared to *Sharpin*^{cpdm} mice is apoptosis, necroptosis or both. Indeed, in the skin of 3-weeks-old *Cflip*^{D377A}*Sharpin*^{cpdm} mice, no increase in the cleavage of Caspase-3 was detected, despite the presence of significantly higher amounts of TUNEL-positive cells compared to *Sharpin*^{cpdm} mice (Figure 15D). Therefore, we speculate that either the D377A mutation promotes a switch to necroptosis, which is responsible for the exacerbation of the skin phenotype, or that the peak of Caspase-3 activation occurs earlier than 3 weeks in *Cflip*^{D377A}*Sharpin*^{cpdm} mice. Additionally, the activation of different cell death types in a tissue-specific manner might also affect the disease progression. Thus, further investigations including stainings for phosphorylated MLKL in tissues over an extended time period are required.

In the light of the recent literature, both the abrogation and exacerbation of cell death have detrimental consequences for the wound healing. Indeed, in the absence of cell death, neither tissue repair can be initiated nor the initial inflammatory programs can be resolved. Whereas, excessive cell death can lead to hyperinflammatory responses that are, in turn, detrimental to the tissue.[135,136,138] Consequently, the ability of tissues to overcome stress-induced damage lies in their capacity to tightly control the amplitude of cell death responses by modulating the formation and activity of cell death-inducing complexes. Our findings in *Cflip*^{D377A} mice revealed that the abrogation of cFLIP cleavage impaired wound healing following skin excision (Figure 18). Most likely, this is due to the increased sensitivity of cells in granulation tissue to cell death induced by cytokines in the wound microenvironment. However, it remains an enigma, whether the death of stroma cells causes reduced granulation tissue or the death of macrophages dampens the immune response required to activate the tissue repair processes in *Cflip*^{D377A} mice. Another possibility is that *Cflip*^{D377A} mice fail to resolve the inflammation due to an enhanced release of inflammatory mediators, which leads to exacerbated activation of wound macrophages, in the wound milieu following increased cell death. Thus, a detailed study of wound microenvironment as well as cell type-specific abrogation of cFLIP cleavage in key players of wound healing might be helpful to solve the questions on the precise dynamics and contribution of cell death processes in tissue repair.

We clearly showed that *Cflip*^{D377A} LFs had higher sensitivity to cell death upon IT treatment, which consist of the main cytokines produced during the viral response (Figure 19A-B). Strikingly, these *in vitro* data were accompanied by significantly worse disease progression and severe pathology in *Cflip*^{D377A} mice compared to *Cflip*^{WT} counterparts upon SARS-CoV 1 infection *in vivo* (Figure 19C). We observed augmented levels of cell death in lung epithelial cells (Figure 19N-P), despite similar levels of cytokines and chemokines in the infected *Cflip*^{D377A} mice (Figure 19E-M). Collectively, we envisaged a scenario where the increased cell death observed in the lungs of *Cflip*^{D377A} mice is the result of increased sensitivity of *Cflip*^{D377A} lung epithelial cells to the cytokine storm caused by viral infection[152,176]. This, in turn, leads to a more severe lung pathology and an increased lethality caused by SARS-CoV 1 infection. Mechanistically, we observed that IT-treatment *in vitro* caused apoptosis necroptosis and pyroptosis in *Cflip*^{D377A} LFs (Figure 19B). We speculate that, at least *in vitro*, the activation of MLKL and Caspase-8 is triggered by ZBP1, one of the main IFNγ-induced genes, is known to induce necroptosis via RIPK3 binding and Caspase-8-mediated cell death.[35–37,81,83,177] Hence, it is tempting to say that cFLIP cleavage has a regulatory role in the cytotoxicity of a ZBP1-induced complex II-like cell death platform. *In vivo,* we detected cleaved Caspase-3 staining (Figure 19O) as an indication of apoptosis but, due to the lack of reliable staining for phosphorylated MLKL, it was not possible to determine whether necroptosis also occurs *in vivo.* Further investigations regarding the contribution of different cell death types on SARS-CoV 1-mediated pathology would improve our understanding of the cell death mediated outcomes in viral infection. Altogether, our findings support a model whereby cFLIP cleavage represents a previously unappreciated regulatory mechanism limiting the formation and killing potential of TNF-induced complex II to control the extent of cell death responses following damage for an optimal tissue repair.

4.3 Novel checkpoints add another layer to the complex regulation of TNF cytotoxicity.

The recent findings indicate that different mechanisms repressing the formation of TNF-mediated complex II rely on post-translational modifications, the most significant ones being proteolytic processing, phosphorylation and ubiqutination.[57] Very promisingly, we found PPP2R1A, the constant scaffolding subunit of PP2A, in our immunoprecipitation-based mass spectrometric analysis of complex II (Figure 20H-I). PP2A is a ubiquitously expressed serine-threonine phosphatase and regulates many critical cellular processes, such as proliferation, signal transduction and promisingly apoptosis. This enzyme consists of a structural scaffolding, a regulatory and a catalytic subunit in a heterotrimeric complex. Each subunit has different isoforms,

which are believed to modulate its enzymatic activity, spatial and temporal substrate specificity.[178] Therefore, our highest priority is to validate its presence in complex II biochemically and to identify the composition of the PP2A heterotrimer and its targets in connection with complex II. Since complex II-mediated cell death is mainly regulated and driven by various kinases, we speculate that PP2A, as the first phosphatase identified in the context of complex II, might counteract one or more of these mechanisms. To this end, we observed reduced TNF-induced cell death levels, particularly necroptosis, in *Ppp2r1a*$^{-/-}$ cells, indicating that the dephosphorylation event mediated by PP2A enhances complex II-mediated cell death (Figure 21C-D). This, in turn, might be through the dephosphorylation of an inhibitory phosphorylation event in the regulation of complex II. A recently identified phosphorylation event that prevents the recruitment and thus kinase-dependent cytotoxicity of RIPK1, and consequently complex II, is MK2-mediated phosphorylation at S321 residue. This is an early and transient event in TNF signalling, consistent with the greater differences observed at earlier time points, e.g 3 h and 6 h after TS and TE-treatment, between *Ppp2r1a*$^{WT/WT}$ and *Ppp2r1a*$^{-/-}$ cells than at the end time points (Figure 21C-D). To test this hypothesis, it is crucial to determine the targets of PP2A in complex II using proteomics-based approaches and to evaluate mechanistically its physiological function in the regulation of complex II-mediated cell death. Ultimately, these studies are requisite to clarify the importance of phosphorylation-related mechanisms, their regulation and dynamics in complex II.

4.4 Concluding Remarks

Tightly regulated cell death programmes are indispensable for a well-coordinated response to various insults, such as infection or injury. These stressors are known to activate FADD/Caspase-8/cFLIP-containing complex II and complex II-like death-inducing platforms. Within these complexes, the formation of Caspase-8/cFLIP heterodimer is decisive for cell death outcomes. Here, cFLIP cleavage by Caspase-8 is a novel checkpoint that acts as a protective brake against complex II-mediated cell death. This cleavage counterbalances the extent to which complex II is formed and triggers cytotoxicity. Hence, abrogation of cFLIP cleavage sensitizes cells to TNF-induced complex II-mediated cell death. The mice bearing non-cleavable cFLIP were dramatically more susceptible to various TNF-dependent, cell death-mediated pathological conditions. This was caused by the cell death-driven, inflammation-mediated tissue damage and the impaired tissue repair. Altogether, these data emphasize how important the precise regulation of complex II assembly and cytotoxic activity is to ensure optimal activation of tissue repair programs. It is now becoming clear that the regulation of TNF-induced cell death is intricate. There are many layers of regulation on the complex II-mediated cytotoxicity, beyond the contribution of

known components. We therefore sought out novel regulators of TNF-induced cell death. Our studies evidenced the contribution of PPP2R1A, as potential novel regulator, to the regulation of TNF-induced necroptosis. Further mechanistic studies are key to clarify its regulatory mechanism and physiological role. With these findings and future perspectives in our study, we provide novel insights into the regulation of TNF-induced complex II-mediated cell death at different levels and their (patho-)physiological importance.

5 MATERIAL AND METHODS

5.1 Materials

Table 1. Chemicals, reagents, media and biological materials

Reagent	Provider, Location	Cat No
6× DNA Loading Dye	Thermo Fisher Scientific, USA	R0611
ABC	Kindly provided by CECAD Proteomic Facility, University of Cologne	
CAN	Kindly provided by CECAD Proteomic Facility, University of Cologne	
Acrylamide	Bio-Rad, USA	1610148
Adenine	Sigma-Aldrich, USA	18148
Agarose	Carl Roth, Germany	3810.2
Ampicilin	Carl Roth, Germany	HP62.1
Animal Free Blocker Diluent	Vector Lab, USA	SP-5035-100
Antibiotic/Antimycotic Solution	Thermo Fisher Scientific, USA	15240062
anti-flag M2 beads	Merck Millipore, USA	A2220
AZD5582	MedChem Express, USA	HY-12600
BamHI-High Fidelity	New England BioLabs, USA	R3136L
BD™ CompBeads Anti-Mouse Ig, κ/Negative Control Compensation Particles Set	BD Biosciences, USA	BDB552843
Beta-isodona	ACA Müller/ADAG Pharma AG	9196683
Birinapant	MedChem Express, USA	HY-16591
Blasticidine	InvivoGen, USA	ant-bl-1
Bovine Serum Albumin	Sigma-Aldrich, USA	A8022-100G
CAA	Kindly provided by CECAD Proteomic Facility, University of Cologne	
CAPS	Thermo Fisher Scientific, USA	AAA1703714
CD31 MicroBeads, mouse	Miltenyi Biotec, Germany	130-097-418
Cholera toxin	Enzo Life Sciences, USA	BML-G117-0001
Cisplatin	kind gift from Pascal Meier, UK	
Collagen	Sigma-Aldrich, USA	L7213-100ML
Collagen	Sigma-Aldrich, USA	L7213-100ML
Collagenase Type II	Worthington, USA	44N15307B
cOmplete™ Protease Inhibitor Cocktail	Roche, Swithzerland	11697498001
Cycloheximide	kind gift from Henning Walczak, Germany	
DNA/RNA Shield	Zymo Research, USA	R1100
dNTPs	Promega, USA	U1231;U1211; U1221;U1201
Doxorubicin	kind gift from Pascal Meier, UK	
Doxycycline	kind gift from Pascal Meier, UK	
DTT	Carl Roth, Germany	6908.1
Dulbecco's Balanced Salt Solution (DPBS)	Thermo Fisher Scientific, USA	14190144
Dulbecco's Modified Eagle Medium	Thermo Fisher Scientific, USA	41966052
EcoRI-High Fidelity	New England BioLabs, USA	R3101T
EDTA	Carl Roth, Germany	8043.2
EGF	PeproTech, USA	315-09-500

Emricasan	Absource Diagnostics, Germany	S7775-0005
Endothelial Growth Cell Medium 2	PromoCell, Germany	C-22011
Ethanol	Carl Roth, Germany	5054.1
FBS	Thermo Fisher Scientific, USA	10437028
Formalin	Sigma-Aldrich, USA	HT501128-4L
Formic Acid	Kindly provided by CECAD Proteomic Facility, University of Cologne	
Gelatine	Carl Roth, Germany	0646.1
Gemcitabine	kind gift from Pascal Meier, UK	
GeneRuler Ready to use 1kb Plus DNA Ladder	Thermo Fisher Scientific, USA	SM1333
Glutathatione sepharose beads	GE Healtcare, USA	17-0756-01
GlutaMAX™; Supplement	Thermo Fisher Scientific, USA	35050061
Glutathione	Carl Roth, Germany	6382.3
Glycerol	Carl Roth, Germany	3783.1
Glycine	Carl Roth, Germany	0079.4
GST-TUBE	generated in house by Kalvin Nugraha	
Ham's F12 Nutrient Mix	Thermo Fisher Scientific, USA	2165029
HCl	Carl Roth, Germany	1E2C.1
HEPES	Thermo Fisher Scientific, USA	15630080
Hoechst 33342	Sigma-Aldrich, USA	94403
human TNF	Enzo Life Sciences, USA	ALX-522-087-C010
Hydrocortison	Sigma-Aldrich, USA	H4001-IG
Hygromycin	InvivoGen, USA	ant-hg-1
Imperial Protein Satin (Coomassie Staining solution)	Thermo Fisher Scientific, USA	24615
Insulin	Sigma-Aldrich, USA	I9278-5ML
IPTG	kind gift from Leo Kurian, University of Cologne	
Kanamycin	Carl Roth, Germany	T832.4
KCl	Carl Roth, Germany	HN02.3
Ketamin	WDT, Germany	116810
KHCO3	Carl Roth, Germany	9437.3
LB	Carl Roth, Germany	X964.1
LB Agar	Carl Roth, Germany	X969.2
L-Glutamine	Sigma-Aldrich, USA	
Liquid Nitrogen	Linde, United Kingdom	
LPS	kind gift from Henning Walczak, Germany	
LysC	Kindly provided by CECAD Proteomic Facility, University of Cologne	
Methanol	Carl Roth, Germany	8388.1
Milk (powdered)	Carl Roth, Germany	T145.2
mouse IFNγ	PeproTech, USA	315-05
mouse TNF	Enzo Life Sciences, USA	ALX-522-009-C050
NaCl	Carl Roth, Germany	3957.1
NaOH	Carl Roth, Germany	6771.1
Neomycin	InvivoGen, USA	ant-gn-1
NH4Cl	Carl Roth, Germany	5470.2
Non-essential Aminoacids	Thermo Fisher Scientific, USA	11140050
NP40	Sigma-Aldrich, USA	85124

NuPAGE MOPS SDS Runnig Buffer	Thermo Fisher Scientific, USA	NP000102
Octenisept	SCHÜLKE & MAYR GmbH	121418
Opti-MEM I Reduced Serum Medium	Thermo Fisher Scientific, USA	31985062
ORA™ qPCR Green ROX L Mix	highQu, Germany	QPD1010
Paclitaxel	kind gift from Pascal Meier, UK	
PageRuler Plus Prestained 10 250kDa Protein Ladder	Thermo Fisher Scientific, USA	26620
Paraformaldehyde	PanReac AppliChem, Germany	211511
Penicilin-Streptomycin	Thermo Fisher Scientific, USA	15140122
peqGOLD 100 bp DNA Ladder	VWR, Germany	25-2010
PhosSTOP	Roche, Swithzerland	4906837001
poly I:C	kind gift from Henning Walczak, Germany	
Polybrene	EMD Millipore, USA	TR-1003-G
Polyethylenimine	Polysciences, USA	23966
PR619	LifeSensors, USA	SI9619
ProLong™ Gold Antifade Mountant	Thermo Fisher Scientific, USA	P36930
Protein G beads	Sigma-Aldrich, USA	P3296
Puromycin	InvivoGen, USA	ant-pr-1
Random Hexamers	Thermo Fisher Scientific, USA	SO142
Recombinant Human USP2 Catalytic Domain Protein	R&D Systems, USA	E-504-050
Red Taq DNA polymerase master mix (1,1x)	VWR, Germany	733-2546
RPMI-1640, Glutamax	Thermo Fisher Scientific, USA	61870036
SDS	Carl Roth, Germany	1057.1
Sodium citrate	Sigma-Aldrich, USA	C8532
Sodium deoxycholate	Sigma-Aldrich, USA	D6750
Sodium pyruvate	Thermo Fisher Scientific, USA	35050061
Sucrose	kind gift from Henning Walczak, Germany	
Superose 6 HR 10/30 size exclusion column	Sigma-Aldrich, USA	GE29-0915-96
Sytox Green	Fisher Scientific, USA	S7020
TAE Buffer (50x)	VWR, Germany	K915-1.6L
TEMED	Sigma-Aldrich, USA	S0389
TFA	Kindly provided by CECAD Proteomic Facility, University of Cologne	
Tissue-Tek® O.C.T. Compound	Sakura Finetek, USA	4583
TRIS Base	Carl Roth, Germany	5429.2
Triton-X-100	Carl Roth, Germany	3051.4
Trypsin	Sigma-Aldrich, USA	T4049
Trypsin	Fisher Scientific, USA	25-200-056
Trypsin (Mass Spectrometry)	Kindly provided by CECAD Proteomic Facility, University of Cologne	
UltraPure™ DNase/RNase-Free Distilled Water	Thermo Fisher Scientific, USA	10977049
Xylacin	Serumwerk, Germany	3310
β-mercaptoethanol	Carl Roth, Germany	4227.1

Table 2. Laboratory comsumables

CONSUMABLE	PROVIDER, LOCATION	CAT NO
12-well cell culture plate, flat bottom, poysterene	Sarstedt, Germany	83.3921.005
24-well cell culture plate, flat bottom, poysterene	Sarstedt, Germany	83.3922.005
384-well Hard Shell PCR Plates	BioRad, USA	HSP3805
48-well cell culture plate, flat bottom, poysterene	Sarstedt, Germany	83.3923.005
6-well cell culture plate, flat bottom, poysterene	Sarstedt, Germany	83.3920.005
96-well cell culture plate, flat bottom, polystyrene	Sarstedt, Germany	833924.005
Cell Counting Slides	BioRad, USA	1450011
Cell Scraper M and L	Sarstedt, Germany	833951-2
Cell Strainer, 100 µm	VWR, Germany	732-2759
Cell Strainer, 45 µm	Sigma-Aldrich, USA	CLS431750-50EA
Cell Strainer, 70 µm	Sigma-Aldrich, USA	CLS431751-50EA
Conical centrifuge tubes, sterile (15 ml)	Sarstedt, Germany	62.554.502
Conical centrifuge tubes, sterile (50 ml)	Sarstedt, Germany	62.547.254
CryoPure 2 ml	Sarstedt, Germany	72.379
Glassware	Brand, Germany	
HENKE-JECT® syringes 1 ml TBC	Henke-Sass, Wolf, Germany	5010.200V0
LS Columns	Miltenyi Biotec, Germany	130-042-901)
Microseal	BioRad, USA	MSB1001
Needle, Agani 21Gx11/2 (0,8x38 mm)	Terumo, Japan	AN*2138R1
Needle, Sterican® Gr. 20, 27Gx3/4 (0,40 x 20 mm)	B. Braun, Germany	4657705
NuPAGE™ 4-12% Bis-Tris Mini-Midi Protein Gels, 10-, 15-, 26-well	Thermo Fisher Scientific, USA	NP0335BOX / NP0323BOX / WG1403BOX
Parafilm M	Bemis Company, USA	52858
PCR strip of 8 (200 µl)	Sarstedt, Germany	72.991.002
Petri dish, 92 x 16 mm, transparent, without ventilation cams	Sarstedt, Germany	82.1473.001
Pierce™ PVDF Transfer Membranes (Pore Size=0.45 µm)	Thermo Fisher Scientific, USA	88518
Pipette Tips (10, 200, 1000 µl)	StarLab Group, Germany	S1111
Pipette Tips, filtered (10, 20, 200, 1000 µl)	StarLab Group, Germany	S1120
Protein LoBind® reaction tubes	Eppendorf, Germany	EP0030108116
QuadroMACSTM Separator	Miltenyi Biotec, Germany	130-090-976
SafeSeal Reaction tubes (0,5, 1,5, 2, 5 ml)	Sarstedt, Germany	72.690-699
Scalpel	VWR, Germany	2335526
SDB-RP Stage Tips	Kindly provided by CECAD Proteomic Facility, University of Cologne	
Serological pipette (5, 10, 25, 50 ml)	Sarstedt, Germany	86.1251-1685
Slide-A-Lyzer cassette	Thermo Fisher Scientific, USA	66380
Soft-Ject Syringes 3,5, 10 ml	Air-Tite	89215
Superose 6 HR 10/30 size exclusion column	Sigma-Aldrich, USA	GE29-0915-96
Syringe filters, 45 µM	Carl Roth	P667.1
Tissue culture dish, 150 x 20 mm, transparent, with ventilation cams	Sarstedt, Germany	83.3903

Tissue culture dish, 35 x 10 mm, transparent, with ventilation cams	Sarstedt, Germany	83.3900
Tissue culture dish, 92 x 16 mm, transparent, with ventilation cams	Sarstedt, Germany	83.3902
Tissue culture dish, 92 x 16 mm, transparent, without ventilation cams	Sarstedt, Germany	83.3901
Tissue-Tek® Uni-Cassette®	Sakura Finetech, USA	4117-55
Whatman™ Cellulose chromatography papers	Cytiva, USA	588-3007
X-ray Films	Radiolix, Germany	11820

Table 3. Laboratory equipment

EQUIPMENT	PROVIDER; LOCATION
C1000 Touch Thermal Cycler	BioRad, USA
CFX96 Touch Real-Time PCR Detection System	BioRad, USA
ChemiDoc XRS+ Imaging System	BioRad, USA
ChemiDoc Imaging System	BioRad, USA
PowerPac™ Basic Power Supply	BioRad, USA
OwlTM EasyCastTM B2 Mini Gel Elektrophoresis Chamber	Thermo Fisher Scientific, USA
XCell SureLockTM Mini Cell	Thermo Fisher Scientific, USA
XCell4 SureLockTM Midi Cell	Thermo Fisher Scientific, USA
Ultra-Low Temp Freezer (-80°C)	PHCbi, Japan
Fridge	Liebherr, Germany
Freezer	
Pipettes (3/10/20/200/1000 µl)	Sartorius, Germany
Pipettes (2/10/20/100/200/1000 µl)	Eppendorf, Germany
Fine Scissors and Forceps	Fine Science Tools, Canada
CO2 Laboratory Incubator MCO-170AICUVHL-PA	PHCbi, Japan
Biological Safety Cabinet Class 2 - Mars (Pro)	Labogene, Denmark
Thermomixer, R 1,5 ml	Eppendorf, Germany
Thermomixer, MKR 1,5 ml	Hettich, Germany
Centrifuge, Z383K, Z216MK	Hermle, Germany
Electronic Shaver	
Biopsy Puncher	
GentleMACS Dissociator	Miltenyi BioTec, Germany
Cell Counter	BioRad, USA
Incucyte S3	Sartorius, Germany
TECAN Plate Reader Infinite® 200 PRO M Nano	TECAN, Switzerland
CKX41 Inverted Light Microscope	Olympus Life Sciences, Japan
Multi-channel pipette (300ml)	Eppendorf, Germany
Multi-channel pipette (200ml)	Corning, USA
ÄKTA Purifier Protein Purification System	Cytiva, USA
Medical Film Processor Curix 60	AGFA, Belgium
X-ray Cassettes	Cyvita, USA
Speed Vac vaccum concentrator	Eppendorf, Germany
NanoDrop™ Spectrophotometer	Thermo Fisher Scientific, USA
ChemiDoc™ Touch Imaging System	BioRad, USA
Biophotometer 6131	Eppendorf, Germany
UP200St ultrasonic processor	Hilscher, Germany
J-25 High Speed Centrifuge	Beckman Coulter, USA

Table 4. Kits

PROCESS	KIT	SUPPLIER, LOCATION	CAT NO
Genotyping	Extracta DNA Prep for PCR	QuantaBio, USA	95091-025
Protein Measurement	DC™ Protein Assay Kit I	Bio-Rad, USA	5000111
Immunoblotting	Clarity Western ECL Substrates	Bio-Rad, USA	1705060
Immunoblotting	SuperSignal™ West Femto Maximum Sensitivity Substrates	Thermo Fisher Scientific, USA	34095
Immunoblotting	X-Ray Developer Kit (Developer G153 and Fixer G354)	AGFA, Belgium	
Plasmid Purification	QIAGEN Plasmid Plus Mini/Midi Kit	QIAGEN, Germany	12945
PCR	Q5® High-Fidelity DNA Polymerase Kit	New England BioLabs, USA	M0491L
Gel extraction	QIAquick Gel Extraction Kit	QIAGEN, Germany	28704
RNA Isolation	Quick-RNA Miniprep Plus Kit	Zymo Research, USA	R1058
cDNA Synthesis	MMLV Reverse Transcriptase & Buffer	Promega, USA	M5313
Immunostaining	ApopTag® Red In Situ Apoptosis Detection Kit	Merck, Germany	S7165
Multiplex	Luminex Discovery Assays	R&D Biotechne, USA	
Dephosphorylation	FastAP Phosphatase Kit	Thermo Fisher Scientific, USA	EF0654
Ligation	T4 DNA Ligase Kit	New England BioLabs, USA	R3552S
Flow cytometry	LIVE/DEAD Fixable Far Red stain	Thermo Fisher Scientific, USA	L34973

Table 5. Antibodies

APPLICATION	ANTIBODIES	DILUTION	COMPANY, LOCATION	CAT NO
Flow Cytometry	B220	1:200	BD Biosciences, USA	561881
Flow Cytometry	CD115	1:200	BD Biosciences, USA	135523
Flow Cytometry	CD115	1:200	Biolegend, USA	135517
Flow Cytometry	CD117	1:200	Biolegend, USA	313237
Flow Cytometry	CD11b	1:200	Thermo Fisher Scientific, USA	416-0112-82
Flow Cytometry	CD11b	1:200	Thermo Fisher Scientific, USA	416-0112-82
Flow Cytometry	CD11c	1:200	Biolegend, USA	117333
Flow Cytometry	CD127	1:200	Biolegend, USA	135021
Flow Cytometry	CD135	1:200	Biolegend, USA	135305
Flow Cytometry	CD16/32	1:200	Biolegend, USA	101331
Flow Cytometry	CD172a	1:200	Biolegend, USA	144015
Flow Cytometry	CD172a	1:200	Biolegend, USA	144015
Flow Cytometry	CD19	1:200	BD Biosciences, USA	557791
Flow Cytometry	CD3	1:200	BD Biosciences, USA	100227
Flow Cytometry	CD31	1:100	Miltenyi Bioech	130-123-675
Flow Cytometry	CD34	1:200	Biolegend, USA	119325
Flow Cytometry	CD4	1:200	Biolegend, USA	100547
Flow Cytometry	CD4	1:200	Biolegend, USA	100547
Flow Cytometry	CD45	1:200	Biolegend, USA	147709
Flow Cytometry	CD45	1:200	Biolegend, USA	147709
Flow Cytometry	CD45	1:200	Biolegend, USA	147709
Flow Cytometry	CD8	1:200	Biolegend, USA	100751
Flow Cytometry	F4/80	1:200	Biolegend, USA	111704

Flow Cytometry	Ly6C	1:200	Biolegend, USA	128023
Flow Cytometry	Ly6G	1:200	Biolegend, USA	127607
Flow Cytometry	NK1.1	1:200	BD Biosciences, USA	740663
Flow Cytometry	Sca-1	1:200	Biolegend, USA	108137
Flow Cytometry	Siglec F	1:200	Biolegend, USA	155525
Flow Cytometry	XCR1	1:200	Biolegend, USA	148216
Immunoblotting	Caspase-3	1:1000	Cell Signalling	#9662
Immunoblotting	Caspase-7	1:1000	Cell Signalling	#12827
Immunoblotting	Caspase-8	1:1000	MBL, Japan	#M032-3
Immunoblotting	cFLIP	1:1000	Cell Signalling, USA	#56343
Immunoblotting	cleaved Caspase-3	1:1000	Cell Signalling, USA	#9661
Immunoblotting	cleaved Caspase-8	1:1000	Cell Signalling, USA	#9429S
Immunoblotting	FADD	1:1000	EMD Millipore, USA	#05-486 / 1F7
Immunoblotting	IKBa	1:1000	Cell Signalling, USA	#9242
Immunoblotting	JNK	1:1000	Cell Signalling, USA	#9258
Immunoblotting	MLKL	1:1000	EMD Millipore, USA	#MABC604 / #3204229
Immunoblotting	N4BP1	1:1000	abcam, UK	#ab133610
Immunoblotting	p38	1:1000	Cell Signalling, USA	#9212
Immunoblotting	p65	1:1000	Cell Signalling, USA	#8242
Immunoblotting	pIKBa	1:1000	Cell Signalling, USA	#9246
Immunoblotting	pJNK	1:1000	Cell Signalling, USA	#9255
Immunoblotting	pMLKL	1:1000	abcam, UK	#ab187091
Immunoblotting	pp38	1:1000	Cell Signalling, USA	#9215
Immunoblotting	pp65	1:1000	Cell Signalling, USA	#3033
Immunoblotting	PPP2R1A	1:1000	abcam, UK	#ab24736
Immunoblotting	pRIPK1	1:1000	Cell Signalling, USA	#31122
Immunoblotting	pRIPK3	1:1000	Cell Signalling, USA	#57220
Immunoblotting	RIPK1	1:1000	Cell Signalling, USA	#3493
Immunoblotting	RIPK1	1:2000	BD Biosciences, USA	#610459
Immunoblotting	RIPK3	1:1000	Cell Signalling, USA	#13526
Immunoblotting	Tubulin	1:2000	Thermo Fisher Scientific, USA	T9026 /047M4789V
Immunoblotting	Ubiquitin	1:1000	Santa Cruz Biotechnology, USA	sc-8017
Immunoblotting	ZBP1	1:1000	Adipogene Life Sciences, USA	AG-20B-0010-C100
Immunoblotting	rabbit IgG (heavy and light chain)	1:10000	Jackson ImmuniResearch Lab, USA	112-035-003 7 143578
Immunoblotting	rabbit IgG (light chain)	1:10000	Jackson ImmuniResearch Lab, USA	211-032-171 /142605
Immunoblotting	mouse IgG (light chain)	1:10000	Jackson ImmuniResearch Lab, USA	115-035-174 / 143785
Immunoblotting	mouse IgG (heavy and light chain)	1:10000	Jackson ImmuniResearch Lab, USA	115-035-003 / 143988
Immunoblotting	rat IgG (light chain)	1:10000	Jackson ImmuniResearch Lab, USA	112-035-175 / 141715
Immunoblotting	rat IgG (heavy and light chain)	1:10000	Jackson ImmuniResearch Lab, USA	112-035-003 7 143578
Immunoprecipitation	FADD	1:25	abcam, UK	ab124812

Immunostaining	Alexa Fluor 488	1:200	Thermo Fisher Scientific, USA	A-11008
Immunostaining	CC10	1:50	Santa Cruz Biotechnology, USA	sc365992
Immunostaining	CD31	1:50	BD Biosciences, USA	550274
Immunostaining	α-smooth muscle actin	1:50	Sigma Aldrich, USA	C6198

Table 6. DNA constructs

PLASMIDS	PROVIDER	PURPOSE
pBABE-hygro-FADD_3xflag	generated in house	Reconstitution of C-terminally 3xflag tagged FADD expression
pBABE-neo SV40 LTA	Pascal Meier (The Institute of Cancer Research, London, United Kingdom)	Immortalisation of primary cells (neomycine resistnace)
pBABE-neo-cFLIP D371A	generated in house	Reconsitution of cFLIP expression
pBABE-neo-cFLIP D377A	generated in house	Reconsitution of cFLIP expression
pBABE-neo-cFLIP Q469D	generated in house	Reconsitution of cFLIP expression
pBABE-neo-cFLIP Q469D;D377A	generated in house	Reconsitution of cFLIP expression
pBABE-neo-cFLIP WT	generated in house	Reconsitution of cFLIP expression
pBABE-puro SV40 LTA	Pascal Meier (The Institute of Cancer Research, London, United Kingdom)	Immortalisation of primary cells (puromycin resistance)
pFU-cre hygro	Pascal Meier (The Institute of Cancer Research, London, United Kingdom)	Vector for constitutive cre expression
pGEX-GST TUBE	Pascal Meier (The Institute of Cancer Research, London, United Kingdom)	Vector for bacterial expression of GST-TUBE protein
pMD2.G	Pascal Meier (The Institute of Cancer Research, London, United Kingdom)	Packaging Vector for lentiviral production
pMK-RQ-FADD	designed by GeneArt Gene Synthesis Service	Vector with mouse FADD
psPAX2	Pascal Meier (The Institute of Cancer Research, London, United Kingdom)	Packaging Vector for lentiviral production
pTRIBTZ-cre	Pascal Meier (The Institute of Cancer Research, London, United Kingdom)	Vector for doxycycline inducible cre expression
pTRIBTZ-CrmA	Pascal Meier (The Institute of Cancer Research, London, United Kingdom)	Vector for doxycycline inducible CrmA expression

Table 7. Solutions, Buffer and Media Compositions

BUFFER/SOLUTION/MEDIA	COMPOSITION
1 % Agarose gel	1 % (w/v) Agarose in TAE Buffer
4% (w/v) PFA	40 g Paraformaldehyde up to 1 L PBS pH 7.4
50/50 ABC ACN buffer	50 mM ABC 50 % (v/v) ACN
6× Laemmlie Buffer	3 ml 20 % SDS 3 ml β-mercaptoethanol 4 ml Glycerol
ACK Lysis Buffer	1,55 M NH_4Cl 10 mM $KHCO_3$ 1 mM EDTA
Anesthesia Mixture	100 µg/mg Ketamin 10 µg/mg Xylacin in PBS
Blocking Buffer	5 % (w/v) milk or BSA in TBS-T
BMDM Differentiation Medium	RRMI-1640 10 % (v/v) FBS 1 % (v/v) Penicillin/Streptomycin 20 % (v/v) L292 mouse fibroblast-conditioned medium

Buffer A	0,1 % (v/v) formic acid 80 % (v/v) ACN
Buffer B	0,1 % (v/v) formic acid 80 % (v/v) ACN
D-10	DMEM 10 % (v/v) FBS 1 % (v/v) Penicillin/Streptomycin
Deubiquitinase Buffer	50 mM TRIS-HCl ph 7.5 50 mM NaCl 5 mM DTT
Digestion Solution	90 % (v/v) 10ng/µl Trypsin 10 % (v/v) 50 mM LysC in 50 mM ABC
Elution buffer	5 % (w/v) sucrose 0,1 % (w/v) CHAPS 20 mm HEPES/NaOH 5 mM DTT pH 7,0 50 mM NaCl
Endothelial cell Medium	1:1 (v:v) Endothelial Cell Growth Medium 2:DMEM 10 % (v/v) FBS 1 % (v/v) Penicillin/Streptomycin 1 mM Glutamine 1 mM Sodium pyruvate 20 mM HEPES 1 % (v/v) non-essential amino acids
FACS Buffer	0,5 % BSA 2 mM EDTA in PBS
FastAP Dephosphorylation	30 µl of Restriction digestion mix 1 U FastAP Phosphatase 1× Reaction buffer
Glycerol Stock	60 % (v/v) bacteral culture 20 % (v/v) glycerol
GST-Elution buffer	50 mM Tris-HCl pH 8.5 150 mM NaCl 1 mM DTT 6 mg/ml glutathione
GST-Lysis Buffer	1 % (v/v) Triton-X-100 10 % (v/v) Glycerol 30 mM Tris-HCl pH 7,4 120 mM NaCl 10 mM PR619 supplemented with 50 µg/ml GST-TUBE recombinant protein supplemented with protease and phosphortase inhibitors
Keratinocyte Medium	DMEM 10 % (v/v) FBS, chelated 1 % (v/v) Penicillin/Streptomycin 22 % Ham's F12 Nutrient Mix 2 mM L-Glutamine 0,18 mM Adenine 10 ng/ml EGF 5 µg/ml Insulin 0,5 µg/ml Hydrocortison 0,1 ng/ml cholera toxin
Ligation	3:1 backbone DNA:insert DNA 0,2 U Ligase 1× Liagse Buffer total volume of 10 µl
Lower Buffer	1,5 M Tris-HCl pH 8.8 8 mM EDTA 0,4 % (w/v) SDS
Lysis Buffer (Bacterial Protein Isolation)	300 mM NaCl 1 mM DTT supplemented with protease and phosphortase inhibitors in PBS

Lysis Buffer (Mammalian Protein isolation)	1 % Triton-X-100 10 % Glycerol 30 mM Tris-HCl pH 7,4 120 mM NaCl 10 mM PR619 supplemented with protease and phosphortase inhibitors
PCR Master Mixes (Genotyping)	12,5 µl PCR Master mix 8,5 µl of ddH_2O 1 µM of Forward Primer 1 µM of Reverse Primer
PCR Reaction Mixes (Cloning)	1× Q5 Buffer 400 µM dNTPs 0,5 µM Foward Primer 0,5 µM Reverse Primer 750 ng template DNA 0,02 U/µl Q5 Polymerase 1× GC Enhancer total volume of 25 µl
PCR Reaction Mixes (site directed mutagenesis step 1)	1× Q5 Buffer 200 µM dNTPs 2 µM Foward Primer 2 µM Reverse Primer 500 ng template DNA 0,02 U/µl Q5 Polymerase 1× GC Enhancer total volume of 50 µl
PCR Reaction Mixes (site directed mutagenesis step 2)	1× Q5 Buffer 200 µM dNTPs 2 µM Foward Primer 2 µM Reverse Primer 1:1 PCR1:PCR2 template 0,02 U/µl Q5 Polymerase 1× GC Enhancer total volume of 50 µl
qPCR Reaction Mix	1× ORA™ qPCR Green ROX L Mix 2,5 µM Foward Primer 0,5 µM Reverse Primer 2 µl cDNA
R-10	RPMI-1640 10 % (v/v) FBS 1 % (v/v) Penicillin/Streptomycin
Restriction Digest Reaction Mix	20 U EcoRI 20 U BamHI 1× CutSmart Buffer 1 µg DNA total volume of 30 µl
Reverse Transcription Reaction Mix	1 µg RNA template 1× Random Hexamers 2 mM dNTPs 1× RT Buffer 20 U MMLV Reverse Transcriptase
RIPA Buffer	50 mM Tris-HCl ph 7,4 150 mM NaCl 0,5 % (w/v) Sodium deoxycholate 1 % (w/v) NP40 0,1 % (w/v) SDS supplemented with protease and phosphortase inhibitors
Running Buffer	1× Tris-Glycine Buffer 0,1 % (w/v) SDS
SDS Lysis Buffer	1 % Triton-X-100 10 % Glycerol 30 mM Tris-HCl pH 7,4 120 mM NaCl 2 % (w/v) SDS supplemented with protease and phosphortase inhibitors

SDS-Polyacryamide Resolving gel (10-15 %)	10-15 % (w/v) Acrylamide 0,495 mM TRIS-HCl pH 6.8 0,3 ‰ (w/v) SDS 1 ‰ (v/v) TEMED 0,3 ‰ (w/v) APS
SDS-Polyacryamide stacking gel	6 % (w/v) Acrylamide 0,125 mM TRIS-HCl pH 8.8 0,6 ‰ (w/v) SDS 1,6 ‰ (v/v) TEMED 0,8 ‰ (w/v) APS
TBS 10×	24,2 g Tris 30 g NaCl up to 1L water pH 7,6
TBS Buffer	137 mM NaCl 25 mM Tris-HCl pH 7.4 5 mM KCl
TBS-T	1×TBS Buffer 0,1 % Tween-20
Transfer buffer	1× Tris-Glycine Buffer 20 % (v/v) Methanol
Tris Glycine 10×	30,2 g Tris 144 g Glycine up to 1 L water
Upper Buffer	1,5 M Tris-HCl pH 6.8 8 mM EDTA 0,4 % (w/v) SDS
Washing Buffer Immunoprecipitation	1 % (v/v) Triton-X-100 10 % (v/v) Glycerol 30 mM Tris-HCl pH 7,4 120 mM NaCl

Table 8. Softwares

SOFTWARE	DEVELOPER
Adobe Softwares (Photoshop, Illustrator, Adobe Acrobat)	Adobe, USA
AlphaFold Protein Structure Database	DeepMind, UK; European Molecular Biology Laboratory (EMBL), UK; European Bioinformatics Institute (EBI), UK
BD FACSDiva	BD, USA
Benchling	Benchling, USA
Citavi Reference Management Software	Citavi, Switzerland
FlowJo	BD, USA
GraphPad Prism (Version 9 and 10)	GraphPad, USA
i-control Microplate Reader Software by TECAN	TECAN, Switzerland
ImageJ (Version 1.54g)	National Institutes of Health, USA
ImageLab (Version 6.0.1)	Bio-Rad, USA
Incucyte 202B Software (Basic Analysis and Cell-by-Cell Analysis Modules)	Sartorius, Germany
Maxquant (provided by CECAD Proteomics Facility)	Max Planck Intitute of Biochemistry, Germany
Microsoft Office Products (Word, Excel and PowerPoint)	Microsoft, USA
NDP.view2 Viewing software U12388-01	Hamamatsu Photonics, Japan
Perseus (provided by CECAD Proteomics Facility)	Max Planck Intitute of Biochemistry, Germany
Protein Databank	Research Collaboratory for Structural Bioinformatics, USA
UniProt Database	European Bioinformatics Institute (EBI),UK; Swiss Institute of Bioinformatics (SIB), Switzerland; Protein Information Resource (PIR); US

Table 9. Mouse lines

MOUSE LINES	PROVIDER, LOCATION
Cflip$^{WT/WT}$ C57BL/6	Charles River, USA
Cflip$^{D377A/D377A}$ C57BL/6	generated in-house
Sharpin$^{cpdm/cpdm}$;*Cflip*$^{WT/WT}$ C57BL/6	generated in-house
Sharpin$^{cpdm/cpdm}$;*Cflip*$^{D377A/D377A}$ C57BL/6	generated in-house

Table 10. Cell lines

CELL LINE	PROVIDER, LOCATION
Caspase-3$^{-/-}$;*Caspase-7*$^{-/-}$ MDFs	generated in-house
Caspase-3$^{fl/fl}$;*Caspase-7*$^{fl/fl}$ MDFs	generated in-house
Caspase-8$^{-/-}$ MEFs	Gianmaria Liccardi (University of Cologne, Cologne, Germany)
Caspase-8$^{-/C362S}$ MDFs	Melanie Fritsch, Hamid Kashkar (University of Cologne, Cologne, Germany)
Caspase-8$^{fl/C362S}$ MDFs	Melanie Fritsch, Hamid Kashkar (University of Cologne, Cologne, Germany)
Cflip^{D371A} MDFs	generated in-house
Cflip$^{D371A;D377A}$ MDFs	generated in-house
Cflip^{D377A} MDFs	generated in-house
Cflip$^{D377A;Q469D}$ MDFs	generated in-house
Cflip^{Q469D} MDFs	generated in-house
Cflip^{WT} MDFs	generated in-house
Cflip$^{-/-}$ MDFs	generated in-house
Cflip$^{D377A/D377A}$ BMDMs	generated in-house
Cflip$^{D377A/D377A}$ Keratinocytes	generated in-house
Cflip$^{D377A/D377A}$ LECs	generated in-house
Cflip$^{D377A/D377A}$ LFs	generated in-house
Cflip$^{D377A/D377A}$ MDFs	generated in-house
Cflip$^{fl/fl}$ MDFs	generated in-house
Cflip$^{WT/WT}$ BMDMs	generated in-house
Cflip$^{WT/WT}$ Keratinocytes	generated in-house
Cflip$^{WT/WT}$ LECs	generated in-house
Cflip$^{WT/WT}$ LFs	generated in-house
Cflipwt/wt MDFs	generated in-house
CrmA+ *Cflip*$^{D377A/D377A}$ MDFs	generated in-house
CrmA+ *Cflip*$^{WT/WT}$ MDFs	generated in-house
Fadd$^{-/-}$ MDFs	generated in-house
Fadd$^{C-3xflag}$ MDFs	
Human embryonic kidney 293T cells	Leo Kurian (University of Cologne, Cologne, Germany)
Platinium E cells	Pascal Meier (The Institute of Cancer Research, London, United Kingdom)
Ppp2r1a$^{-/-}$ MDFs	generated in-house

Table 11. Bacterial Strains

BACTERIAL STRAINS	PROVIDER, LOCATION
Escherichia coli Stbl3	Thermo Fisher Scientific, USA
Escherichia coli XL-Blue	kind gift from Leo Kurian (University of Cologne, Cologne, Germany)

5.2 Methods

5.2.1 Animal Experiments

All mouse studies were performed after approval of local government authorities (Landesamt für Natur, Umwelt und Verbraucherschutz Nordrhein-Westfalen, Germany) in accordance with

German animal protection law as well as European, national and institutional guidelines. In order to maintain hygiene standards and avoid contamination, experimental mice were imported and exported according to the instructions of the appropriate animal facility. Animals were housed up to 3-4 female mice and 1 male mouse per cage in the animal facilities of the University of Cologne under standard specific pathogen-free or specific pathogen and opportunist-free conditions. The mice were kept under a 12 h light/dark schedule at 22±2 °C, 55±5 % relative humidity in individually ventilated cages. They were provided with sterilised, commercially available food (Harlan, diet no.2918) and water *ad libitum*. All mice were maintained on a C57BL/6J background. For breeding, male and female mice were placed together at a minimum age of 8 weeks. Litters were weaned and marked with ear tags at the minimum age of 3 weeks and tail biopsies for genotyping were taken at that time. The experimental mouse cohorts were monitored daily and the severity of the genetic mutations were scored according to the criteria defined by local authorities. In case animals required medical attention, they were provided with appropriate care or sacrificed when they developed macroscopically visible skin lesions to minimize suffering. Adult mice were euthanized by cervical dislocation and under the age of 3 weeks by decapitation. Calculations to determine sample size, randomization and blinding were not performed, mice were grouped according to their genotype in mixed sexes.

5.2.1.1 In Vivo Generation of Mouse Models

5.2.1.1.1 Generation of *Cflip*^{D377A} Mice

The *Cflip*^{D377A} mutant mice were generated by the MAGEC laboratory (Walter and Eliza Hall Institute of Medical Research) using CRISPR/Cas9 technology. To generate these mice, 20 ng/µl Cas9 mRNA, 10 ng/µl single guide RNA (sgRNA) (5'-TTGATGGCCCATCTACCTCC-3') and 40 ng/µl oligo donor (5'-GCCAAAGCTCTTTTTTATTAGAACTATGAGTCGT TAGGTAGCCAGTTGGAAGATAGCATCTGGAGGTAGCTGGGCCATCAATAAAAAATGTGGACT CTAAGCCCCTGCAACCCAGACACTGCACAACTCA-3') were microinjected into the cytoplasm of fertilized one-cell stage embryos generated from wild type C57BL/6J breeders. 24 later, two-cell stage embryos were transferred into the uteri of pseudo-pregnant female mice. Viable offspring were genotyped by automated genotyping using next-generation sequencing. (TransnetYX, USA) Targeted animals were backcrossed twice to wild-type (WT) C57BL/6J to eliminate off-target mutations. For all the experiments, *Cflip*^{WT} littermates served as controls.

5.2.1.1.2 Generation of *Sharpin*^{cpdm}*Cflip*^{D377A} Mice

Sharpin^{cpdm} mice were previously described in the literature[97,100,163] and were a generous gift from N. Peltzer and G. Liccardi (University of Cologne, Cologne, Germany). The obtained

Sharpin$^{cpdm/cpdm}$ mice were then crossed with *Cflip*$^{D377A/D377A}$ mice to generate *Sharpin*$^{WTt/cpdm}$*Cflip*$^{WT/D377A}$. To generate and maintain the required genotypes of *Sharpin*$^{WT/WT}$*Cflip*$^{WT/WT}$, *Sharpin*$^{WT/WT}$*Cflip*$^{D377A/D377A}$, *Sharpin*$^{cpdm/cpdm}$*Cflip*$^{WT/WT}$, *Sharpin*$^{cpdm/cpdm}$*Cflip*$^{D377A/D377A}$ in this transgenic strain, the heterozygous mice for both genes were crossed in breeding of further generations and the offspring were genotyped in house. Routine mouse genotyping was performed by polymerase chain reaction (PCR) on genomic DNA isolated from tail/ear biopsies to amplify the genomic region of interest with genotype-specific primer pairs. Genomic DNA was isolated using a DNA extraction kit. In this process, the tissue was lysed by incubating the biopsies with 75 µl extraction buffer at 95 °C for 30 min. Subsequently, the samples were cooled down to room temperature (RT) and mixed with 1:1 (v/v) stabilisation buffer. Point mutations were screened for using WT and mutant allele-specific primers (Table 12) which resulted in the presence or absence of a PCR fragment with a specific fragment size as a readout. PCR master mixes were prepared as indicated in Table 12 and mixed with 1 µl isolated genomic DNA. PCR program consisted of five steps, of which steps 2 to 4 were repeated in cycles to amplify the desired fragment: an initial denaturation (step 1), denaturation (step 2), primer annealing (step 3), extension (step 4) and a final extension (step 5). PCR products were run in 1,5 % agarose gel and visualised using UV light.

Table 12. Genotyping PCR Protocol for *Sharpin* gene

GENE OF INTEREST	PRIMER SEQUENCE	EXPECTED BAND SIZE	PROGRAM	CYCLES
Sharpin^{WT}	WT_Fw:TCGACCAGGTGGC CCGGACATATT WT_Rev:TTAGGCACCGAGC CTGGGG	WT: ~500 bp cpdm: no band	96 °C 4 min 96 °C 30 sec 67 °C 30 sec 72 °C 1 min 30 sec 72 °C 10 min	30
Sharpin^{cpdm}	WT_Fw:TCGACCAGGTGGC CCGGACATATT cpdm_Rev:TTAGGCACCGA GCCTGGGC	WT: no band cpdm: ~500 bp	96 °C 4 min 96 °C 30 sec 67 °C 30 sec 72 °C 1 min 30 sec 72 °C 10 min	30

5.2.1.2 Tissue Preparation

The mice were sacrificed at empirically determined time points. At the beginning of the process, the mice were injected with an anasthesia mixture indicated by for a deep terminal anaesthesia. Following, they were weighed and their back skin was shaved for the collection of skin samples in later steps. Blood samples up to 1 ml were taken via cardiac punctuation. After incubation of 30 min at RT, the blood sample was centrifuged at 4000 rpm for 15 min to gain serum from the supernatant. Serum samples were stored at -80 °C until further processing. The mice were euthanised via excision of the heart. Various organs including skin, spleen, liver, intestines and lungs were prepared for preservation and processing for histopathological assessment. The fat and various

connective tissue around the spleen and liver were removed. The organs were weighted and individually placed into histological cassettes. Lungs were inflated and fixed by inserting a 21 G needle into the trachea and injecting it with a 4 % (w/v) paraformaldehyde (PFA) solution. Once the backflow was blocked, the organ was placed in a histological cassette. The small intestine and colon were cut at the distal end, where it joined the rectum. The intestinal tract was freed from fat and connective tissue and traced back to the stomach. The entire length of the intestines was transferred to a clean petri dish containing phosphate-buffered saline (PBS). The colon, the section between the rectum and caecum, was held from the distal end and cut as close to the caecum as possible. The colon segment was sliced through longitudinally and rinsed with PBS in the petri dish. The cleaned and opened segment of the colon was placed onto the top of a petri dish with the luminal side facing upwards to form a Swiss roll from proximal to distal and placed carefully into a histological cassette. The small intestine was cut into 3 segments: proximal, mid and distal. The proximal segment, the one immediately following the stomach, is equivalent to the duodenum, the mid to the jejunum, and the distal, the one immediately before the colon, to the ileum. Starting from the distal segment, all segments proceed with Swiss rolling as described for the colon and subsequently placed in individual histological cassettes. For the examination of the spleen, liver, intestines and lung samples, the organs were kept in 4 % (w/v) PFA solution at 4 °C overnight and washed and stored with PBS on the following day. Lastly, the back skin was cut into pieces. The subcutaneous fat was removed and small pieces (0,5 cm length) were collected, stretched to paper and fixed with formalin solution in histological cassettes. For histological examination of skin samples, the histological cassettes were transferred into 70 % (v/v) ethanol solution the following day. The organ samples were embedded in paraffin (lung, spleen and skin) or cryopreserved (skin) and cut into 3-5 µm sections in the histology facility. Besides, small pieces of isolated organs were collected and snap-frozen using liquid nitrogen (N_2) separately for extraction of RNA and proteins. These tissue pieces were stored at -80 °C until further processing.

5.2.1.3 Primary Cell Isolation and Cultivation

Upon isolation, primary cells were either immortalised or used for the experiments directly after isolation. All immortalised cells in culture were routinely tested for mycoplasma contamination (Eurofins, Luxembourg) and only mycoplasma-negative cells were used for experimental setup.

5.2.1.3.1 Mouse Dermal Fibroblasts

MDFs were isolated from the tail skin of 8-10-weeks old mice. The tail of the mice was collected and kept on ice until further processing under a sterile hood. Once separated from the tail, the skin was minced with a scalpel and digested in 3 ml trypsin for 1 h at 37 °C. During this process, the

digestion solution was manually shaken several times. 7 ml D-10 were then added and the suspension with digested tail was then filtered through a 100 µm cell strainer. Cells were washed once with PBS and seeded in a 6-cm plate. The following day, the medium was changed with fresh medium to get rid of the dead cells. Two to three days later, they were infected with a simian virus 40 (SV40)-Large T antigen (LTA) expressing retrovirus for immortalization.

5.2.1.3.2 Lung Fibroblasts

LFs were isolated from whole lungs of 8 to 10-weeks-old mice. The lungs were separated from non-lung tissue and were kept in PBS on ice until further processing under a sterile hood. Once cut into small pieces, the lung tissue was transferred into a 2 ml reaction tube and digested with 1,5 ml collagenase type II for 1 h at 37 °C and 500 rpm. One digested lung was seeded on two 15-cm petri dishes containing 20 ml D-10 . After two days or when a substantial amount of cells had been attached, the medium was removed and the cells were washed with PBS, then new medium was added to the plate and cells were grown until confluency before further proceeding with immortalisation. LFs were infected with an SV40-LTA expressing retrovirus for immortalisation.

5.2.1.3.3 Lung Endothelial Cells

LECs were isolated from the lungs of 8 to 12-weeks-old mice. The lungs were washed with PBS, minced and digested in 1 ml collagenase type II for 45 min at 37 °C. The suspension was then filtered through a 70 µm cell strainer and separated with magnetic beads specific to CD31. $CD31^+$ endothelial cells were seeded on gelatine-coated wells and cultured in endothelial cell medium. After the first passage, cells were resorted using the magnetic beads. Isolated primary $CD31^+$ endothelial cells were cultured in endothelial cell medium and the media was refreshed every two to three days. Once the confluency was reached, the cells were used for the planned experiments.

5.2.1.3.4 Bone Marrow-Derived Macrophages

BMDMs were isolated from tibia and femur of 2 months old mice, that were collected and kept in PBS on ice. Under the sterile hood, excess muscle and fibre were removed and bone marrows were flushed out with R-10. The cell suspension was subsequently spun down at 1200 rpm for 5 min. The pellet was resuspended in BMDM differentiation medium and plated on four non-coated 10-cm petri dishes. To differentiate BMDMs, the isolated cells were cultivated for six days in BMDMs differentiation medium. After two to four days of culture, 6 ml BMDMs differentiation medium was added to the cell suspension. Subsequently, the differentiated macrophages were trypsinised and seeded in R-10 on coated dishes according to the experimental setup.

5.2.1.3.5 Mouse Embryonic Fibroblasts

MEFs were isolated from embryos harvested from 12-14 days of pregnant mice. Head and red tissue containing the heart and liver were removed from embryos. Each embryo was placed in a 6-cm dish with trypsin and minced into 1 to 2 cm pieces. After 30 min incubation at 37 °C, the cells were collected in D-10 and the cell suspension was filtered through a 45 µm cell strainer to remove tissue from single cell suspension. After centrifugation, the isolated cells were resuspended in D-10 and plated in a 10-cm dish per embryo. The next day, the medium was changed with fresh medium and the cells were incubated until confluency. MEFs were immortalized via infection with an SV40 Large T antigen expressing retrovirus.

5.2.1.4 Excisional Punch Injury

Mice were anaesthetized by intraperitoneal injection of 100 mg/kg body weight ketamine and 10 mg/kg body weight Rompun. The back skin was shaved using an electric shaver and disinfected with 70 % (v/v) ethanol. Four full-thickness punch biopsies with 6-mm diameter were created on the back using a standard biopsy puncher. For histological analysis, wounds were excised at indicated time points post-injury. The wounds were bisected in the caudocranial direction. The tissue was either fixed overnight in 4 % (v/v) PFA and embedded in parafilm subsequently or embedded in OCT compound and stored at -80 °C. Histological analysis was performed on serial sections from the central portion of the wounds.

5.2.1.5 SARS-CoV 1 Infection

SARS CoV 1 MA15 strain was kindly provided by S. Zúñiga and L. Enjuanes (National Centre for Biotechnology as a part of Spanish National Research Council, Madrid, Spain) and the infection model was performed in collaboration with J. Pardo and D. de Miguel (University of Zaragoza). For the virus titration in the lungs, previously weighed portions were homogenised in 500 µl DMEM with a GentleMACS Dissociator. The homogenates were centrifuged at 1500 rpm for 5 min. Virus titer in the supernatant was determined by $TCID_{50}$/ml assay performing serial dilutions and calculated using the Ramakrishan newly proposed method formula[179].

The animals were kept under standard conditions (as described in Chapter 1.2.1) of temperature, humidity and light at the Research Center on Encephalopathies and Emerging Diseases of the University of Zaragoza. Animal experimentation was approved by the Animal Experimentation Ethics Committee of the University of Zaragoza. The mice were infected intranasally with 10^6 $TCID_{50}$/ml in a total volume of 40 µl PBS after isoflurane anaesthesia. Mice were weighed daily and a clinical score was generated, if needed, following different components: mouse appearance, level of consciousness, activity, response to stimuli, eye appearance, and frequency as well as

quality of respiration. The mice reached the humanitarian endpoint when the clinical score reached 21, the respiratory characteristics were higher than 3 or the weight loss was greater than 25 % of the initial weight. At the indicated time points, lung homogenates and serum samples were obtained for further analysis. For histological analysis, the lung tissue was prepared as described before and embedded in parafilm.

5.2.2 Standard Cell Culture

The cultures of obtained cells were maintained in 10-cm dishes using respective medium under sterile conditions of 37 °C, 95 % relative humidity and 5 % CO_2. Due to hygiene and safety conditions, all the experiments related to cell culture were carried out under sterile conditions using a laminar flow hood. Splitting was performed by trypsinisation. The medium was removed from the dishes, which were subsequently washed with 10 ml PBS. After removing PBS completely, the cells were incubated with 0,25 % trypsin solution for 5 min. at 37 °C. In order to quench the enzymatic activity of trypsin, 10 ml medium was added to the flasks and the cells were transferred to a canonical centrifuge tube. Following, the cell suspension was centrifuged at 1200 rpm for 5 min. The resulting pellet was resuspended in the desired volume of D-10. After determining the cell concentration and viability by cell counter, the cells were plated out into the appropriate petri dishes or plates with the desired seeding density.

5.2.3 Lenti- and Retroviral Production and Infection

Replication incompetent lenti- and retroviral particles were generated in human embryonic kidney (HEK) 293 T and Platinium E cells, respectively. The cells were seeded in a 10-cm petri dish at $2{,}5\times10^6$ cells/dish in 10 ml D-10. The following day, 1 ml Opti-MEM I reduced serum medium containing 10 µg plasmids of interest (Table 13) and 30 µl 1 mg/ml polyethyleneimine were added to the medium and incubated overnight. The medium was changed after 18 h incubation. The supernatant containing viral particles was collected 2 days post-transfection. One day prior to the infection of the target cells, 80.000 cells/well were seeded in 6-well plate. On the day of infection, 3 ml supernatant-containing retroviral particles and 1 µg/ml polybrene were added to the respective wells of 6-well plate and kept for 72 h. To selectively expand the infected cells, 7-days of selection was performed using the respective antibiotics depending on the resistance cassette contained in the retro- or lentiviral plasmid, i.e. Puromycin (4 µg/ml), Hygromycin (200 µg/ml), Blasticidine (6 µg/ml) and Neomycin (1 mg/ml).

Table 13. Composition of transfected plasmid DNA

	HEK CELLS	PLATINIUM CELLS
10 µg DNA	4,85 µg of vector plasmid 3,5 µg of pMD2.G plasmid 1,5 µg of psPAX2 plasmid	10 µg of vector plasmid

5.2.4 *In vitro* Generation of Genetic Tools

5.2.4.1 Genetic Deletion of Different Cell Death Genes

Cflip$^{fl/fl}$ MDFs were isolated from the tail of the respective mice and immortalised. To generate *Cflip*$^{-/-}$ MDFs, these cells were infected with constitutively Cre-expressing lentiviral particles, followed by hygromycin selection.

Caspase-3$^{fl/fl}$*Caspase-7*$^{fl/fl}$ MDFs were isolated from the tail of the respective mice and immortalised. To generate *Caspase-3*$^{-/-}$*Caspase-7*$^{-/-}$MDFs, these cells were infected with doxycycline-inducible Cre-expressing lentiviral particles, followed by blasticidine selection. Subsequently, these cells were clonally selected by serial dilution followed by expansion of single clones until confluency. The selected MDFs were treated with 100 ng/ml doxycycline for 72 h. The genotype was confirmed via immunoblotting.

Caspase-8$^{fl/C362}$ mouse was a generous gift from M. Fritsch and H. Kashkar (University of Cologne, Cologne, Germany). *Caspase-8*$^{fl/C362S}$ MDFs were isolated from the tail of this mouse and immortalised. Subsequently, to generate *Caspase-8*$^{-/C362S}$ MDFs, *Caspase-8*$^{fl/C362S}$ MDFs were infected with doxycycline-inducible Cre-expressing lentiviral particles, followed by blasticidin selection. Subsequently, these cells were clonally selected by serial dilution followed by expansion of single clones. The selected MDFs were treated with 100 ng/ml doxycycline for 72 h. The genotype was confirmed via immunoblotting.

To generate *Fadd*$^{-/-}$ MDFs, *Fadd*$^{WT/WT}$ MDFs were infected with lentiviral particles expressing guide RNA targeting *Fadd* gene and Cas9 together with green fluorescence protein (GFP). Subsequently, GFP-expressing cells were sorted by fluorescence-activated cell sorting with fluorescence channel 489/511 nm and expanded clonally until confluency. The genotype of selected clones was confirmed via immunoblotting.

To generate cells with *phosphatase 2 scaffold subunit A alpha (PPP2R1A)* deletion, *Ppp2r1a*$^{WT/WT}$ MDFs were electroporated to deliver 2 µM Cas9 protein and 10 µM guide RNA targeting *Ppp2r1a* gene (5'-CATAGACGAACTCCGCAATG-3') together with 10 µM tracRNA incorporated with fluorescent dye ATTO554 and 4 µM electroporation enhancer using SG Cell line 4D X Kit according to the manufacturer's instructions. The next day, the ATTO554-positive cells were sorted by fluorescence-activated cell sorting with fluorescence channel 554/576 and expanded clonally until confluency. The genotype of selected clones was confirmed via immunoblotting.

5.2.4.2 cFLIP Reconstitution System

Generation of reconstitution systems for WT and mutant cFLIP variants (D371A, D377A, D371A/D377A, Q469D, D377A/Q469D) was conducted in *Cflip*$^{-/-}$ background originating from *Cflip*$^{fl/fl}$ MDFs infected with Cre-expressing lentiviral particles, followed by antibody selection with hygromycin. The coding sequences of different cFLIP variants were cloned in the pBABE retroviral vectors carrying Neomycin resistance. These constructs were used to produce retroviral particles for subsequent infection of *Cflip*$^{-/-}$ MDFs to express the different cFLIP variants, followed by antibiotic selection with neomycin.

5.2.4.3 FADD Reconstitution System

Reconstitution system for C-terminally tagged FADD was conducted in *Fadd*$^{-/-}$ cells generated using CRISPR-Cas9 technology in-house. The C-terminal flag tag was incorporated into the coding sequence by PCR and cloned in the pBABE retroviral vectors containing hygromycin resistance. These constructs were used to produce retroviral particles for subsequent infection of *Fadd*$^{-/-}$ cells to express the C-terminally flag-tagged FADD, followed by antibiotic selection with hygromycin.

5.2.4.4 Generation of CrmA-expressing cells

For a controlled expression of CrmA, *Cflip*^{WT} and *Cflip*^{D377A} MDFs were infected with doxycycline-inducible CrmA expressing lentiviral particles. To selectively expand the infected cells, 7-days of selection was performed using blasticidin. To express sublethal doses of CrmA, the cells were treated with 100 ng/ml doxycycline for 72 h prior to further treatments as indicated in figure legends. The expression of CrmA was confirmed via immunoblotting.

5.2.5 Cell Death Assay

To monitor the cell death process, cells were seeded at densities according to their growth rate (8.000 cells/well for MDFs and LFs, 10.000 cells/well for LECs and 50.000 cells/well for BMDMs) the day before the stimulation. The following day, the cells were treated as indicated in figure legends in triplicates in the presence of 5 µM Sytox Green. Live uptake of Sytox Green by dead cells was monitored every hour with 10× magnification over the indicated time period using Incucyte S3. Two to four images per well were captured, analysed and averaged. The dead cell content was measured in the metric “green-positive object count per well normalized to confluency” using the Basic Analyzer of Incucyte 2020B software. The positive control, values from cells treated with TSE, was taken as 100 % death and with this, the percentage of cell death over time was calculated.

5.2.6 Influenza A Viral Infection

Viral infection of LFs with IAV was performed in collaboration with M. Pasparakis (University of Cologne, Cologne, Germany). IAV strain A/PR/8/34 (H1N1, Puerto Rico 8) was obtained from American Type Culture Collection (USA). The virus was propagated in the allantoic cavity of 9-11-day-old embryonated SPF chicken eggs and viral titres were enumerated by standard plaque assays. LFs were infected with PR8 virus (multiplicity of infection [MOI] 2) in a serum-free medium for 2 h. The complete DMEM medium was replaced after 2 h. Cell death was measured by the incorporation of Draq7 monitored every hour with 10× magnification over the indicated time period using Incucyte S3. Two to four images per well were captured, analysed and averaged. The dead cell content was measured in the metric “red-positive object count per well normalized to confluency” using the Basic Analyzer of Incucyte 2020B software.

5.2.7 Protein Extraction *in vitro*

Cells were seeded prior to the treatment until confluency and treated as indicated in the figure legends. Cells were lysed in lysis buffer on ice. The volume of the lysis buffer was adjusted to the cell number and application. (Table 14) The lysates were incubated for 10 min on ice, then centrifuged at 14.000 rpm for 15 to 20 min. Subsequently, the supernatant was transferred into a new 1,5 ml reaction tube. The protein content was determined using absorbance measurement with DC™ reagents and TECAN absorbance reader according to manufacturer’s instructions. Normalised to the lowest protein concentration, the lysates were aliquoted and 6× laemmli buffer was added to the lysates. The samples were boiled for 5 min at 95 °C and kept subsequently at -20 °C until further processing.

Table 14. Lysis buffer volume for different applications

Cells Seeded in	Lysis Buffer Volume (µL)	Application
10 cm dish	200	Protein lysate
10 cm disch	1000	Immunoprecipitation
15 cm disch	1000	Immunoprecipitation
6 cm dish	120	Protein lysate
6-well plate	100	Protein lysate

5.2.8 Protein Precipitation

Cells were seeded prior to the treatment until confluency and treated as indicated in figure legends. Following the treatment, the supernatant of the cells was collected and spun down at 5.000 rpm for 5 min at 4 °C to get rid of cell debris. The supernatant was transferred into a new 1,5 ml reaction tube and mixed with methanol and chloroform in 1:1:0,3 (v/v) ratio, respectively. The mixture was inverted several times and spun down at maximum speed for 15 min at 4 °C to separate the

aqueous phase, interphase and organic phase. The aqueous phase, the top level, was discarded and the left phases were mixed with 800 µl methanol. After mixing through inversion, the sample spun down at maximum speed for 15 min at 4 °C. Following, the supernatant was discarded and the pellet with protein precipitate was dried under a fume hood for 15 min. The cells were lysed in SDS lysis buffer. To fragment the released DNA, the samples were resuspended several times using a syringe. A repeated cycle of freezing at -80 °C and thawing to RT was utilized to increase the efficiency of DNA fragmentation. Lastly, the dried protein precipitated was resuspended in appropriate lysates and the samples were boiled with 6× laemmli buffer for 5 min at 95 °C. The samples were stored subsequently at -20 °C until further processing.

5.2.9 Protein Extraction *ex vivo*

The collected tissue samples were mixed with liquid nitrogen in a mortar and minced until pulverised. Subsequently, these were divided for protein and RNA isolation and stored at -80 °C until further processing. For protein isolation, the pulverised samples were resuspended with 500 µl of RIPA Buffer. Following, the samples were sonicated on ice for 3×10 sec at 95 % amplitude with 3 sec rest in between to avoid high heat-induced protein aggregation. The samples were rotated for 20 min at 4 °C. and then centrifuged at 13.500 rpm for 20 min at 4 °C. The proteins solved in the aqueous phase are collected gently and proceeded with protein quantification as described in chapter 1.2.6 using serial dilutions of samples. The samples were boiled with 6× laemmli buffer for 5 min at 95 °C and kept at -20 °C until further processing.

5.2.10 Immunoprecipitation

5.2.10.1 FADD Immunoprecipitation

Cells were seeded prior to the treatment until confluency and treated as indicated in the figure legends. Following the treatment, they were lysed in 1 ml lysis buffer/sample. The protein content was quantified and normalised as indicated in the chapter 1.2.6. 60 µl lysate was aliquoted as the input sample and boiled with 12 µl 6× laemmli buffer at 95 °C for 5 min. Parallelly, 25 µl protein G Sepharose beads were blocked for 1 h at 4 °C with lysis buffer containing 1 % bovine serum albumin (BSA) and were bound with 1,5 µg antibody/sample FADD specific antibody for 2 h at 4 °C. Subsequently, the previously prepared beads and the respective cleared lysates were mixed and rotated for 4 h at 4 °C. Thereafter, the beads were collected by centrifugation at 5.000 rpm for 30 sec and washed three times with washing buffer. Immunocomplexes were eluted by boiling 60 µl 1× laemmli buffer. The samples were kept at -20 °C until further processing.

5.2.10.2 Flag Immunoprecipitation

Cells were seeded prior to the treatment until confluency and treated as indicated in the figure legends. Following to the treatment, they were lysed in 1 ml lysis buffer/sample. The protein content was quantified and normalised as indicated in the chapter 1.2.6. 60 µl lysate was aliquoted as the input sample and boiled with 12 µl 6× laemmli buffer at 95 °C for 5 min. 40 µl anti-flag M2 beads were added to the respective lysate volume and the mixture was rotated for 4 h at 4 °C. Subsequently, the beads were collected by centrifugation at 5.000 rpm for 30 sec and washed three times with washing buffer. Immunocomplexes were eluted by boiling 40 µl 1× laemmli buffer. The samples were kept at -20 °C until further processing.

5.2.10.3 TUBE Assay

Cells were seeded prior to the treatment until confluency and treated as indicated in the figure legends. Following to the treatment, they were lysed in 1 ml GST-lysis buffer/sample. Lysates were rotated for 20 min at 4 °C, then clarified at 14.000 rpm for 20 min at 4 °C. The protein content was quantified and normalised as indicated in the chapter 1.2.6. 60 µl lysate was aliquoted as the input sample and boiled with 12 µl 6× laemmli buffer at 95 °C for 5 min. Normalised to the lowest protein content, the respective volume of lysates and 30 µl glutathione sepharose beads/samples were rotated at 4 °C overnight. The following day, the beads were collected by centrifugation at 5.000 rpm for 30 sec and washed three times with washing buffer. For the digestion with deubiquitinase USP2, samples were washed with deubiquitinase buffer. Each sample was then equally divided into two 1,5 ml reaction tubes. One of these samples was incubated with 2 µM USP2 in 30 µl deubiquitinase buffer for 1 h at 37 °C, while the other one was incubated under the same conditions without USP2 addition. Pulldown samples were eluted by adding 6 µl 6× laemmli buffer into the sample followed by boiling at 95 °C for 5 min. The samples were kept at -20 °C until further processing.

5.2.11 Size Exclusion Chromatography

Size exclusion chromatography was performed in collaboration with M. MacFarlane (University of Cambridge, Cambridge, UK). Cells were seeded prior to the treatment until confluency and treated as indicated in the figure legends. Following the treatment, cells were lysed and separated on a Superose 6 HR 10/30 size exclusion column and an ÄKTA Purifier protein purification system, essentially as described previously.[180] The Superose 6 column was eluted with the elution buffer at 0,4 ml/min and 0,5 or 1,0 ml fractions were collected. Aliquots from each fraction were retained for immunoblotting and fractions 12-16, 17-21, 22-26, 27-31, 32-36, 37-41, 42-46 and 47-51 were pooled and used for immunoprecipitation experiments.

5.2.12 Immunoblotting

Cell lysates and/or immunoprecipitates were prepared as described previously and preserved in laemmli buffer at -20 °C. Normalized to the lowest protein content, the appropriate loading volume of the sample was separated by sodium dodecyl sulphate polyacrylamide gel electrophoresis (SDS-PAGE) in 10 to 15 % gels at 110 V for 2,5 h. The proteins were then transferred to a polyvinylidene difluoride (PVDF) membrane that was activated in 100 % methanol prior to the transfer. The transfer was performed at 100 V for 1 h at 4 °C. Following, the membrane was blocked with 5 % milk in TBS-T solution for 1 h at RT. The proteins were stained with the primary antibodies as indicated in the figures overnight at 4 °C. The following day, the membrane was washed three times with TBS-T before incubating with respective secondary horseradish peroxidase-coupled antibodies for 1 h at RT. Subsequently, the membrane was washed three times with TBS-T and developed using enhanced chemiluminescence substrates. Signals from the protein bands were then acquired by X-ray films and a medical film processor with various exposure times.

5.2.13 Mass Spectrometry

Mass spectrometric analysis of the immunoprecipitates was performed in collaboration with CECAD Proteomics Facility (University of Cologne, Cologne, Germany). The immunoprecipitates were prepared as described previously and preserved in laemmli buffer at -20°C. For processing, the samples were reduced in 1,4-dithiothreitol (DTT) to a final concentration of 5 mM for 30 min at 56 °C. Additionally, the cysteine residues were alkylated in 40 mM chloroacetamide (CAA) for 30 mins at RT in the dark. Subsequently, 40 µl immunoprecipitate was separated by SDS-PAGE in precast 4 % -12 % gradient gels at 110 V for 30 min. The gel was stained with Coomassie staining solution for 1 h at RT. The stained gel bands for each sample were excised, chopped into smaller pieces and each sample lane was transferred into a new 1,5 ml Protein LoBind reaction tube. Gel pieces were washed in 100 µl 50/50 ABC/ACN buffer for 20 min at RT twice and in 100 µl acetonitrile (ACN) for 10 min at RT once. Afterwards, the excessive solution was discarded and the gels were dried for 15 min at RT. Gel pieces were destained and dehydrated by repetitive steps of incubation with 100 ml 50 mM ammonium bicarbonate (ABC) and 100 ml ACN each for 15 min at RT. Then, the gel pieces were dried for 15 min at RT. The proteins were digested in gel with 150 µl digestion solution containing proteases lysyl endopeptidase (LysC) and trypsin for 30 min at 4 °C. The excessive digestion solution was removed and 150 µl 50 mM ABC were added to cover the gel pieces completely for the overnight incubation. The following day, the excessive solution was transferred into a new 1,5 ml Protein LoBind reaction tube. The gel pieces were covered with 100 µl solution containing 30 % (v/v) ACN and 3 % (v/v) trifluoroacetic acid (TFA) for 20 min at RT. The extract was combined with the previously collected digested fraction. Next, the gel pieces were

covered with 100 µl ACN for 20 min at RT. The extract was combined with previously collected digestion fractions. The collected fractions were dried up to 50 µl to remove the organic buffer using a SpeedVac vacuum concentrator. The samples were acidified by addition of formic acid to a final concentration of 1 % (v/v) and centrifuged at 13.000×rcf for 5 min. The supernatant with eluted peptides was loaded onto styrene-divinylbenzene reverse phase sulfonate stage tips containing two layers of discs. Prior to this, the stage tips were equilibrated with 20 µl methanol, 20 µl buffer B and two times 20 µl buffer A by centrifugation at 2.600 rpm up to 2 min. The loaded stage tips were washed with 30 µl buffer A and B by centrifugation at 2.600 rpm for 3 min. The loaded stage tips were kept at 4 °C until further processing.

Samples were acquired and analysed by the CECAD Proteomics Facility (University of Cologne, Cologne, Germany) on an Orbitrap Exploris 480 (granted by the German Research Foundation under INST 216/1163-1 FUGG) mass spectrometer equipped with a FAIMSpro differential ion mobility device that was coupled to a Vanquish neo in trap-and-elute setup. The samples were loaded onto a pre-column (Acclaim 5 µm PepMap 300 µ Cartridge) with a flow of 60 µl/min before reverse-flushed onto an in-house packed analytical column (30 cm length, 75 µm inner diameter, filled with 2,7 µm Poroshell EC120 C18, Agilent). Peptides were chromatographically separated with an initial flow rate of 400 nl/min and the following gradient: initial 2 % buffer B, up to 6 % in 3 min. Then, the flow was reduced to 300 nl/min and increased to 20 % buffer B in 26 min, up to 35 % buffer B within 15 min and up to 98 % buffer B within 1 min while again increasing the flow to 400 nl/min, followed by column wash with 95 % buffer B and reequilibration to the initial condition. The FAIMSpro was operated at -40 V compensation voltage and electrode temperatures of 99,5 °C for the inner and 85 °C for the outer electrode. The mass spectrometer was operated in data-dependent acquisition top 24 mode with MS1 scans acquired from 350 *m/z* to 1400 *m/z* at 60.000 resolution and an AGC target of 300 %. MS2 scans were acquired at 15.000 resolution with a maximum injection time of 22 ms and an AGC target of 300 % in a 1,4 Th window and a fixed first mass of 110 m/z. All MS1 scans were stored as profile, all MS2 scans as centroid.

All mass spectrometric raw data was processed essentially as described previously[181] with Maxquant (version 2.2) using default parameters against a chimeric database consisting of the murine canonical Uniprot database (downloaded 04.01.2023) merged with the sequence of the C-terminally flag tagged FADD construct with the match-between-runs option enabled between replicates. The follow-up analysis was done in Perseus 1.6.15 essentially as described previously.[182] The protein groups were filtered for potential contaminants and insecure identifications. The remaining IDs were filtered for data completeness in at least one group and

missing values were imputed by sigma downshift (0.3 σ width, 1.8 σ downshift). Afterwards, FDR-controlled two-sided t-tests were performed.

5.2.14 Generation of DNA constructs

Mouse WT and D377A mutant cFLIP templates were amplified from mouse complementary DNA (cDNA) using the primers and PCR program as in Table 15. The D371A cFLIP variant was generated by site-directed mutagenesis via two-step PCR as indicated in Table 16, whereas Q469D and D377A;Q469D cFLIP variants were amplified from cFLIP WT and D377A templates respectively using an elongated reverse primer and PCR program as in Table 15. FADD WT template was purchased as a synthetic DNA construct and utilized to amplify C-terminally 3×flag tagged FADD using the primers and PCR program listed in Table 15. These PCR products were then cloned into pBABE retroviral vectors through a sequential double digest with BamHI and EcoRI restriction enzymes, each 1 h at 37 °C. Then, these were dephosphorylated with FastAP for 10 min at 37 °C and heat inactivated for 15 min at 75 °C. The products were run in 1 % agarose gel and extracted using gel extraction kit according to the manufacturer's instructions. The PCR products and the plasmid backbone were ligated overnight at 16 °C. The next day, the reaction was heat-inactivated for 20 min at 65 °C. To amplify the generated plasmids, they were transformed into *Escherichia coli Stbl3* strain. The correct assembly of generated plasmids was confirmed via sequencing. The bacterial colonies expressing these plasmids were cultured in 50 ml Lysogeny broth (LB) medium with respective antibiotics overnight and the plasmids were isolated using a commercially available plasmid purification kit. In this process, the bacterial suspension was centrifuged at 5.000 rpm for 20 min at 4 °C. The pellet was lysed according to the manufacturer's instructions. Thereafter, DNA was bound to spin columns, which was eluted subsequently in DNase/Rnase-free water. The DNA concentrations were quantified using a NanoDrop™ Spectrophotometer.

Table 15. Standard PCR protocol to amplify the indicated gene of interest

GENE OF INTEREST	PRIMER SEQUENCE	EXPECTED BAND SIZE	PROGRAM	CYCLES
FADD	C-3×flag_Fw: GGTGGTGGTGGTGGTGG GATCCGCCACCATGGACCCA TTCCTGGTG C-3×flag_Rev: GGTGGTGGTGGTGGTGGTGA ATTCTCATCACTTGTCGTCGT CGTCCTTGTAGTCGATGTCGT GGTCCTTGTAGTCACCGTCG TGGTCCTTGTAGTCTGATCCA CCGCCG	C-FADD_3xflag: ~750 bp	1. 98 °C 1 min 2. 98 °C 30 s 3. 55 °C 45 s 4. 72 °C 1 min 5. 72 °C 2 min	32 (step 2-4)
cFLIP WT and D377A variants	Fw: GGTGGTGGATCCGCCACCAT GGCCCAGAGCCCTGTGTCT Rev: GGTGGTGAATTCTCACGTAG GAGCCAGGATGAG	WT: ~1500 bp band D377A: ~1500 bp band	1. 98 °C 1 min 2. 98 °C 30 s 3. 58 °C 45 s 4. 72 °C 1 min 30 s 5. 72 °C 2 min	32 (step 2-4)
cFLIP Q469D variant	Fw: GGTGGTGGATCCGCCACCAT GGCCCAGAGCCCTGTGTCT Rev: GGTGGTGAATTCTCACGTAG GAGCCAGGATGAGTTTCTTC CTCAGAGTGTGGTCCAGGCT GAGGCTGTA	Q469D: ~1500 bp band D377A:Q469D: ~1500 bp band	1. 98 °C 1 min 2. 98 °C 30 s 3. 58 °C 45 s 4. 72 °C 1 min 30 s 5. 72 °C 2 min	32 (step 2-4)

Table 16. Site-directed mutagenesis via two-step PCR protocol to amplify the indicated genes of interest

GENE OF INTEREST	PRIMER SEQUENCE	EXPECTED BAND SIZE	PROGRAM	CYCLES
D371A (step 1)	D371A_1: GGTGGTGGATCCGCCACCAT GGCCCAGAGCCCTGTGTCT D371A_2: TACCTCCAGGCTG CTAGCTTCCAA D371A_3: AGCCAGTTGGAAGCTAGCAG CCTG D371A_4: GGTGGTGAATTCTCACGTAG GAGCCAGGATGAG	D371A PCR 1/2: ~1200 bp D371A PCR 3/4: ~300 bp	1. 95 °C 5 min 2. 95 °C 30 s 3. 54 °C 30 s 4. 72 °C 1 min 5. 72 °C 5 min	25 (steps 2-4)
D371A (step 2)	D371A_1: GGTGGTGGATCCGCCACCAT GGCCCAGAGCCCTGTGTCT D371A_4: GGTGGTGAATTCTCACGTAG GAGCCAGGATGAG	D371A: ~1500 bp	1. 95 °C 5 min 2. 50 °C 30 s 3. 72 °C 1 min 30 s 4. 95 °C 30 s 5. 54 °C 30 s 6. 72 °C 1 min 30 s 7. 72 °C 5 min	15 (step 4-6)

5.2.15 Quantitative Reverse Transcription PCR (RT-qPCR)

Cells were seeded prior to the treatment until confluency and treated as indicated in the figure legends. The samples were preserved in 400 µl DNA/RNA Shield at 4 °C until further processing. RNA was isolated using the commercially available RNA isolation kit according to the manufacturer's instructions. In this process, RNA in lysates were bound to spin columns. For the removal of genomic DNA, the columns were treated with DNase I. After washing, RNA was eluted

in DNase/RNase free water. The RNA concentrations were quantified using a NanoDrop™ Spectrophotometer. cDNA from 1 µg RNA was synthesized using the MMLV reverse transcriptase according to the manufacturer's instructions. Then, qPCR was performed using the ORA™ qPCR Green ROX L Mix according to the manufacturer's instructions using gene-specific primer pairs in a real-time PCR thermocycler. The amount of target gene mRNA detected was normalized to Actin mRNA values.

Table 17.Standard qPCR protocol for the indicated gene of interest

GENE OF INTEREST	PRIMER SEQUENCE	PROGRAM	CYCLES
TNF	TNF_Fw: CATCTTCTCAAAATTCGAGTGACAA	1. 95 °C 2 min 2. 95 °C 5 s 3. 60 °C 30 s 4. 65 °C 30 s	32 (step 2-3)
	TNF_Rev: TGGGAGTAGACAAGGTACAACCC		
CCL2	CCL2_Fw: CCACTCACCTGCTGCTACTCAT		
	CCL2_Rev: TGGTGATCCTCTTGTAGCTCTCC		
Actin	Actin_Fw: ATGGTGGGAATGGGTCAGAAGGAC		
	Actin_Rev: CATTGTAGAAGGTGTGGTGC		

5.2.16 Flow cytometry

Flow cytometric analysis of immune compartments of *Cflip*^{WT} and *Cflip*^{D377A} mice was performed and analysed using the gating strategy as previously described[183] in collaboration with N. Peltzer (University of Cologne, Cologne, Germany). The spleen and bone marrow were isolated and mashed through a cell strainer to gain single-cell suspension. The isolated cells were washed once with FACS buffer by centrifugation. Following, they are resuspended in 1 ml ACK lysis buffer and incubated for 10 min in the dark at RT. The samples were washed with 14 ml FACS buffer by centrifugation. Before starting with the staining process, the compensation for each panel was done using compensation beads and single stained samples. Each sample was distributed into up to respective panels (Table 18) and was first stained with live and dead staining for 10 min in the dark. After washing the cells with FACS buffer, the extracellular staining was performed using three staining master mixes for 30 min at dark. The samples were washed with FACS buffer twice and resuspended with FACS buffer for acquisition. The samples were acquired in BD FACSCanto II flow cytometer using BD FACSDiva Software and analysed in FlowJo. Unstained samples and single-stained samples were used for appropriate voltage settings that have clear positive and negative populations

.

Table 18. Panel composition for flow cyotmetric analysis of immune cell populations

PANEL	FLUOROPHORE	MARKER	PROVIDER, LOCATION	CAT NO	FINAL DILUTION
Panel 1	BV711	NK1.1	BD Biosciences, USA	740663	1:200
	PE-Dazzle	CD172a	Biolegend, USA	144015	1:200
	PerCP-Cy5.5	Siglec F	Biolegend, USA	155525	1:200
	BV421	CD3	BD Biosciences, USA	100227	1:200
	APC-Cy7	CD19	BD Biosciences, USA	557791	1:200
	BV605	CD4	Biolegend, USA	100547	1:200
	BV510	CD8	Biolegend, USA	100751	1:200
	PE-Cy7	CD115	BD Biosciences, USA	135523	1:200
	BV650	CD11b	Thermo Fisher Scientific, USA	416-0112-82	1:200
	PE	Ly6G	Biolegend, USA	127607	1:200
	Aleax Fluor 700	Ly6C	Biolegend, USA	128023	1:200
	FITC	CD45	Biolegend, USA	147709	1:200
Panel 2	PE-Cy7	B220	BD Biosciences, USA	561881	1:200
	BV421	XCR1	Biolegend, USA	148216	1:200
	BV650	CD11b	Thermo Fisher Scientific, USA	416-0112-82	1:200
	BV785	CD11c	Biolegend, USA	117333	1:200
	FITC	CD45	Biolegend, USA	147709	1:200
	BV605	CD4	Biolegend, USA	100547	1:200
	PE	F4/80	Biolegend, USA	111704	1:200
	PE-Dazzle	CD172a	Biolegend, USA	144015	1:200
Panel 3	BV421	CD16/32	Biolegend, USA	101331	1:200
	BV605	CD115	Biolegend, USA	135517	1:200
	BV785	CD117	Biolegend, USA	313237	1:200
	FITC	CD45	Biolegend, USA	147709	1:200
	BB700	CD127	Biolegend, USA	135021	1:200
	PE	CD135	Biolegend, USA	135305	1:200
	PE-Dazzle	Sca-1	Biolegend, USA	108137	1:200
	PE-Cy7	CD34	Biolegend, USA	119325	1:200

5.2.17 Immunostainings

In the sections of samples obtained from the histology facility (University of Cologne, Cologne, Germany), standard rehydration and a short antigen retrieval with 1× sodium citrate pH 6,0 was performed in a microwave for 5 min at 80 % power, except for CD31-stained cryosections. Tissue sections were then permeabilised with 0,2 % (v/v) Triton X-100 in Animal-Free Blocker and Diluent at RT for 10 min. Next, the sections were stained with primary antibodies as indicated in figure legends overnight at 4°C. Primary antibodies were then visualized by secondary antibodies conjugated to Alexa Fluor 488 diluted in 0,2 % (v/v) Triton X-100 in Animal-Free Blocker and diluent containing Hoechst 33342 for nuclei staining at RT for 1 h. For the detection of dead cells, the ApopTag® Red In Situ Apoptosis Detection Kit was used. Briefly, sample sections were washed twice with PBS and treated with equilibration buffer for 10 s, incubated with the working strength TdT enzyme for 1 h at 37 °C, followed by 10 min of stop buffer and subsequent 30 min of Rhodamine antibody solution at RT. Slides were washed with PBS and mounted with ProLong™ Gold Antifade Mountant. Finally, images were acquired with a confocal fluorescence microscope and analysed using ImageJ.

5.2.18 Immunohistochemistry

The fixed and paraffin-embedded organs were sectioned (3 µm). Hematoxylin and eosin (H&E) stainings of the sections were performed in the histology facility (University of Cologne, Cologne, Germany). The stained sections were scanned with Slidescanner and analysed using NDP.view2 viewing software and ImageJ. Histological evaluation of PFA-fixed and paraffin-embedded intestinal Swiss rolls was performed using the scoring system as previously described.[30] In brief, histopathology scores were composed of four parameters: epithelial hyperplasia, epithelial injury, tissue inflammation and epithelial cell death.[184] Histological sub-scores for each parameter: 0 absent, 1 mild, 2 moderate, 3 severe. An "area factor" for the fraction of affected tissue was assigned (1 = 0-25%; 2 = 25-50%; 3 = 50-75%; 4 = 75-100%). Each area was scored individually and multiplied with the corresponding area factor. The total histology score was calculated as a sum of all parameter scores multiplied by their area factors. The maximum score was 48. The evaluation was performed in a blinded fashion.

5.2.19 Chemokine and Cytokine Multiplex Analysis

Cytokine and chemokine analyses of sera from *Cflip*^{WT} and *Cflip*^{D377A} mice infected with SARS CoV-1 were performed by Luminex Discovery Assays with the indicated analytes as indicated in figure legend according to the manufacturer's instructions. Briefly, the samples were mixed 1:1 (v/v) with a microparticle cocktail provided by the manufacturer and incubated for 2 h at RT. After the washing steps, the beads were incubated with a biotinylated antibody cocktail and streptavidin-coupled Phycoerythrin conjugate for 1 h individually. The signal of colour-coded microparticles was detected using Luminex 200 xMAP system and was used to calculate the cytokine concentration with the help of standards provided by the manufacturer.

5.2.20 Statistical Analysis

The number of independent experiments for each dataset is indicated in the respective figure legends. The raw data of each experiment was first exported to Excel, sorted, normalised and transferred to GraphPad Prism 7.04 for further statistical and graphical analysis. Multiple comparisons were performed with a student's t-test, repeated measure ANOVA and log rank Mantel-Cox test, whose values are represented in the figures as * $P \leq 0,05$, ** $P \leq 0,01$, *** $P \leq 0,001$and **** $P \leq 0,0001$ using Prism.

6 REFERENCES

1. Peltzer, N. & Walczak, H. Cell Death and Inflammation - A Vital but Dangerous Liaison. *Trends in immunology* **40,** 387–402 (2019).
2. Annibaldi, A. & Meier, P. Checkpoints in TNF-Induced Cell Death: Implications in Inflammation and Cancer. *Trends in molecular medicine* **24,** 49–65 (2018).
3. Vanden Berghe, T., Kaiser, W.J., Bertrand, M.J. & Vandenabeele, P. Molecular crosstalk between apoptosis, necroptosis, and survival signaling. *Molecular & cellular oncology* **2,** e975093 (2015).
4. Wallach, D., Kang, T.-B. & Kovalenko, A. Concepts of tissue injury and cell death in inflammation: a historical perspective. *Nature reviews. Immunology* **14,** 51–59 (2014).
5. Galluzzi, L. *et al.* Molecular mechanisms of cell death: recommendations of the Nomenclature Committee on Cell Death 2018. *Cell death and differentiation* **25,** 486–541 (2018).
6. Vitale, I. *et al.* Apoptotic cell death in disease-Current understanding of the NCCD 2023. *Cell death and differentiation* **30,** 1097–1154 (2023).
7. Pasparakis, M. & Vandenabeele, P. Necroptosis and its role in inflammation. *Nature* **517,** 311–320 (2015).
8. Riera Romo, M. Cell death as part of innate immunity: Cause or consequence? *Immunology* **163,** 399–415 (2021).
9. Kerr, J.F., Wyllie, A.H. & Currie, A.R. Apoptosis: a basic biological phenomenon with wide-ranging implications in tissue kinetics. *British journal of cancer* **26,** 239–257 (1972).
10. Nakanishi, K., Maruyama, M., Shibata, T. & Morishima, N. Identification of a caspase-9 substrate and detection of its cleavage in programmed cell death during mouse development. *The Journal of biological chemistry* **276,** 41237–41244 (2001).
11. Muzio, M. *et al.* FLICE, a novel FADD-homologous ICE/CED-3-like protease, is recruited to the CD95 (Fas/APO-1) death--inducing signaling complex. *Cell* **85,** 817–827 (1996).
12. Lakhani, S.A. *et al.* Caspases 3 and 7: key mediators of mitochondrial events of apoptosis. *Science (New York, N.Y.)* **311,** 847–851 (2006).
13. Julien, O. & Wells, J.A. Caspases and their substrates. *Cell death and differentiation* **24,** 1380–1389 (2017).
14. Sakahira, H., Enari, M. & Nagata, S. Cleavage of CAD inhibitor in CAD activation and DNA degradation during apoptosis. *Nature* **391,** 96–99 (1998).
15. Nagata, S. Apoptotic DNA fragmentation. *Experimental cell research* **256,** 12–18 (2000).

16. Chaitanya, G.V., Steven, A.J. & Babu, P.P. PARP-1 cleavage fragments: signatures of cell-death proteases in neurodegeneration. *Cell communication and signaling : CCS* **8,** 31 (2010).
17. Lazebnik, Y.A., Kaufmann, S.H., Desnoyers, S., Poirier, G.G. & Earnshaw, W.C. Cleavage of poly(ADP-ribose) polymerase by a proteinase with properties like ICE. *Nature* **371,** 346–347 (1994).
18. Geng, Y.J. *et al.* Caspase-3-induced gelsolin fragmentation contributes to actin cytoskeletal collapse, nucleolysis, and apoptosis of vascular smooth muscle cells exposed to proinflammatory cytokines. *European journal of cell biology* **77,** 294–302 (1998).
19. Kothakota, S. *et al.* Caspase-3-generated fragment of gelsolin: effector of morphological change in apoptosis. *Science (New York, N.Y.)* **278,** 294–298 (1997).
20. Green, D.R. The Coming Decade of Cell Death Research: Five Riddles. *Cell* **177,** 1094–1107 (2019).
21. Cai, Z. *et al.* Plasma membrane translocation of trimerized MLKL protein is required for TNF-induced necroptosis. *Nature cell biology* **16,** 55–65 (2014).
22. Dondelinger, Y. *et al.* MLKL compromises plasma membrane integrity by binding to phosphatidylinositol phosphates. *Cell reports* **7,** 971–981 (2014).
23. Garcia, L.R. *et al.* Ubiquitylation of MLKL at lysine 219 positively regulates necroptosis-induced tissue injury and pathogen clearance. *Nature communications* **12,** 3364 (2021).
24. Liu, Z. *et al.* Oligomerization-driven MLKL ubiquitylation antagonizes necroptosis. *The EMBO journal* **40,** e103718 (2021).
25. Kaiser, W.J. *et al.* Toll-like receptor 3-mediated necrosis via TRIF, RIP3, and MLKL. *The Journal of biological chemistry* **288,** 31268–31279 (2013).
26. Günther, C. *et al.* Caspase-8 controls the gut response to microbial challenges by Tnf-α-dependent and independent pathways. *Gut* **64,** 601–610 (2015).
27. Günther, C. *et al.* Caspase-8 regulates TNF-α-induced epithelial necroptosis and terminal ileitis. *Nature* **477,** 335–339 (2011).
28. Kovalenko, A. *et al.* Caspase-8 deficiency in epidermal keratinocytes triggers an inflammatory skin disease. *The Journal of experimental medicine* **206,** 2161–2177 (2009).
29. Oberst, A. *et al.* Catalytic activity of the caspase-8-FLIP(L) complex inhibits RIPK3-dependent necrosis. *Nature* **471,** 363–367 (2011).
30. Schwarzer, R., Jiao, H., Wachsmuth, L., Tresch, A. & Pasparakis, M. FADD and Caspase-8 Regulate Gut Homeostasis and Inflammation by Controlling MLKL- and GSDMD-Mediated Death of Intestinal Epithelial Cells. *Immunity* **52,** 978-993.e6 (2020).

31. Varfolomeev, E.E. *et al.* Targeted disruption of the mouse Caspase 8 gene ablates cell death induction by the TNF receptors, Fas/Apo1, and DR3 and is lethal prenatally. *Immunity* **9,** 267–276 (1998).
32. Lalaoui, N. *et al.* Mutations that prevent caspase cleavage of RIPK1 cause autoinflammatory disease. *Nature* **577,** 103–108 (2020).
33. Newton, K. *et al.* Cleavage of RIPK1 by caspase-8 is crucial for limiting apoptosis and necroptosis. *Nature* **574,** 428–431 (2019).
34. Fu, Y. *et al.* Cloning of DLM-1, a novel gene that is up-regulated in activated macrophages, using RNA differential display. *Gene* **240,** 157–163 (1999).
35. Jiao, H. *et al.* Z-nucleic-acid sensing triggers ZBP1-dependent necroptosis and inflammation. *Nature* **580,** 391–395 (2020).
36. Rodriguez, D.A. *et al.* Caspase-8 and FADD prevent spontaneous ZBP1 expression and necroptosis. *Proceedings of the National Academy of Sciences of the United States of America* **119,** e2207240119 (2022).
37. Peng, R. *et al.* Human ZBP1 induces cell death-independent inflammatory signaling via RIPK3 and RIPK1. *EMBO reports* **23,** e55839 (2022).
38. Brennan, M.A. & Cookson, B.T. Salmonella induces macrophage death by caspase-1-dependent necrosis. *Molecular microbiology* **38,** 31–40 (2000).
39. Davis, B.K., Wen, H. & Ting, J.P.-Y. The inflammasome NLRs in immunity, inflammation, and associated diseases. *Annual review of immunology* **29,** 707–735 (2011).
40. Kumari, P., Russo, A.J., Shivcharan, S. & Rathinam, V.A. AIM2 in health and disease: Inflammasome and beyond. *Immunological reviews* **297,** 83–95 (2020).
41. Latz, E., Xiao, T.S. & Stutz, A. Activation and regulation of the inflammasomes. *Nature reviews. Immunology* **13,** 397–411 (2013).
42. Faustin, B. *et al.* Reconstituted NALP1 inflammasome reveals two-step mechanism of caspase-1 activation. *Molecular cell* **25,** 713–724 (2007).
43. Shi, J. *et al.* Cleavage of GSDMD by inflammatory caspases determines pyroptotic cell death. *Nature* **526,** 660–665 (2015).
44. Martinon, F., Burns, K. & Tschopp, J. The inflammasome: a molecular platform triggering activation of inflammatory caspases and processing of proIL-beta. *Molecular cell* **10,** 417–426 (2002).
45. Heilig, R. *et al.* The Gasdermin-D pore acts as a conduit for IL-1β secretion in mice. *European journal of immunology* **48,** 584–592 (2018).

46. Evavold, C.L. *et al.* The Pore-Forming Protein Gasdermin D Regulates Interleukin-1 Secretion from Living Macrophages. *Immunity* **48,** 35-44.e6 (2018).
47. Kayagaki, N. *et al.* NINJ1 mediates plasma membrane rupture during lytic cell death. *Nature* **591,** 131–136 (2021).
48. Degen, M. *et al.* Structural basis of NINJ1-mediated plasma membrane rupture in cell death. *Nature* **618,** 1065–1071 (2023).
49. Kayagaki, N. *et al.* Non-canonical inflammasome activation targets caspase-11. *Nature* **479,** 117–121 (2011).
50. Kayagaki, N. *et al.* Caspase-11 cleaves gasdermin D for non-canonical inflammasome signalling. *Nature* **526,** 666–671 (2015).
51. Chen, K.W. *et al.* Extrinsic and intrinsic apoptosis activate pannexin-1 to drive NLRP3 inflammasome assembly. *The EMBO journal* **38** (2019).
52. Demarco, B. *et al.* Caspase-8-dependent gasdermin D cleavage promotes antimicrobial defense but confers susceptibility to TNF-induced lethality. *Science advances* **6** (2020).
53. Orning, P. *et al.* Pathogen blockade of TAK1 triggers caspase-8-dependent cleavage of gasdermin D and cell death. *Science (New York, N.Y.)* **362,** 1064–1069 (2018).
54. Sarhan, J. *et al.* Caspase-8 induces cleavage of gasdermin D to elicit pyroptosis during Yersinia infection. *Proceedings of the National Academy of Sciences of the United States of America* **115,** E10888-E10897 (2018).
55. Walczak, H. Death receptor-ligand systems in cancer, cell death, and inflammation. *Cold Spring Harbor perspectives in biology* **5,** a008698 (2013).
56. Annibaldi, A. & Walczak, H. Death Receptors and Their Ligands in Inflammatory Disease and Cancer. *Cold Spring Harbor perspectives in biology* **12** (2020).
57. Varfolomeev, E. & Vucic, D. Intracellular regulation of TNF activity in health and disease. *Cytokine* **101,** 26–32 (2018).
58. van Loo, G. & Bertrand, M.J.M. Death by TNF: a road to inflammation. *Nature reviews. Immunology* **23,** 289–303 (2023).
59. Huyghe, J., Priem, D. & Bertrand, M.J.M. Cell death checkpoints in the TNF pathway. *Trends in immunology* **44,** 628–643 (2023).
60. Griewahn, L., Köser, A. & Maurer, U. Keeping Cell Death in Check: Ubiquitylation-Dependent Control of TNFR1 and TLR Signaling. *Frontiers in cell and developmental biology* **7,** 117 (2019).
61. Liccardi, G. & Annibaldi, A. MLKL post-translational modifications: road signs to infection, inflammation and unknown destinations. *Cell death and differentiation* **30,** 269–278 (2023).

62. Peltzer, N., Darding, M. & Walczak, H. Holding RIPK1 on the Ubiquitin Leash in TNFR1 Signaling. *Trends in cell biology* **26,** 445–461 (2016).

63. Micheau, O. & Tschopp, J. Induction of TNF receptor I-mediated apoptosis via two sequential signaling complexes. *Cell* **114,** 181–190 (2003).

64. Kucka, K. & Wajant, H. Receptor Oligomerization and Its Relevance for Signaling by Receptors of the Tumor Necrosis Factor Receptor Superfamily. *Frontiers in cell and developmental biology* **8,** 615141 (2020).

65. Hsu, H., Huang, J., Shu, H.B., Baichwal, V. & Goeddel, D.V. TNF-dependent recruitment of the protein kinase RIP to the TNF receptor-1 signaling complex. *Immunity* **4,** 387–396 (1996).

66. Rothe, M., Pan, M.G., Henzel, W.J., Ayres, T.M. & Goeddel, D.V. The TNFR2-TRAF signaling complex contains two novel proteins related to baculoviral inhibitor of apoptosis proteins. *Cell* **83,** 1243–1252 (1995).

67. Haas, T.L. *et al.* Recruitment of the linear ubiquitin chain assembly complex stabilizes the TNF-R1 signaling complex and is required for TNF-mediated gene induction. *Molecular cell* **36,** 831–844 (2009).

68. Lork, M., Verhelst, K. & Beyaert, R. CYLD, A20 and OTULIN deubiquitinases in NF-κB signaling and cell death: so similar, yet so different. *Cell death and differentiation* **24,** 1172–1183 (2017).

69. Webster, J.D. & Vucic, D. The Balance of TNF Mediated Pathways Regulates Inflammatory Cell Death Signaling in Healthy and Diseased Tissues. *Frontiers in cell and developmental biology* **8,** 365 (2020).

70. Wang, C. *et al.* TAK1 is a ubiquitin-dependent kinase of MKK and IKK. *Nature* **412,** 346–351 (2001).

71. Oeckinghaus, A., Hayden, M.S. & Ghosh, S. Crosstalk in NF-κB signaling pathways. *Nature immunology* **12,** 695–708 (2011).

72. Sabio, G. & Davis, R.J. TNF and MAP kinase signalling pathways. *Seminars in immunology* **26,** 237–245 (2014).

73. Jaco, I. *et al.* MK2 Phosphorylates RIPK1 to Prevent TNF-Induced Cell Death. *Molecular cell* **66,** 698-710.e5 (2017).

74. Hughes, M.A. *et al.* Co-operative and Hierarchical Binding of c-FLIP and Caspase-8: A Unified Model Defines How c-FLIP Isoforms Differentially Control Cell Fate. *Molecular cell* **61,** 834–849 (2016).

75. Newton, K. *et al.* Activity of protein kinase RIPK3 determines whether cells die by necroptosis or apoptosis. *Science (New York, N.Y.)* **343,** 1357–1360 (2014).

76. Newton, K. *et al.* Activity of caspase-8 determines plasticity between cell death pathways. *Nature* **575,** 679–682 (2019).
77. Fritsch, M. *et al.* Caspase-8 is the molecular switch for apoptosis, necroptosis and pyroptosis. *Nature* **575,** 683–687 (2019).
78. Fox, J.L. *et al.* Cryo-EM structural analysis of FADD:Caspase-8 complexes defines the catalytic dimer architecture for co-ordinated control of cell fate. *Nature communications* **12,** 819 (2021).
79. Humphreys, L.M. *et al.* A revised model of TRAIL-R2 DISC assembly explains how FLIP(L) can inhibit or promote apoptosis. *EMBO reports* **21,** e49254 (2020).
80. Muendlein, H.I. *et al.* cFLIPL protects macrophages from LPS-induced pyroptosis via inhibition of complex II formation. *Science (New York, N.Y.)* **367,** 1379–1384 (2020).
81. Muendlein, H.I. *et al.* ZBP1 promotes LPS-induced cell death and IL-1β release via RHIM-mediated interactions with RIPK1. *Nature communications* **12,** 86 (2021).
82. Yang, D. *et al.* ZBP1 mediates interferon-induced necroptosis. *Cellular & molecular immunology* **17,** 356–368 (2020).
83. Jeffries, A.M., Suptela, A.J. & Marriott, I. Z-DNA binding protein 1 mediates necroptotic and apoptotic cell death pathways in murine astrocytes following herpes simplex virus-1 infection. *Journal of neuroinflammation* **19,** 109 (2022).
84. Muendlein, H.I. *et al.* ZBP1 promotes inflammatory responses downstream of TLR3/TLR4 via timely delivery of RIPK1 to TRIF. *Proceedings of the National Academy of Sciences of the United States of America* **119,** e2113872119 (2022).
85. Zhang, J. *et al.* Ubiquitin Ligases cIAP1 and cIAP2 Limit Cell Death to Prevent Inflammation. *Cell reports* **27,** 2679-2689.e3 (2019).
86. Tenev, T. *et al.* The Ripoptosome, a signaling platform that assembles in response to genotoxic stress and loss of IAPs. *Molecular cell* **43,** 432–448 (2011).
87. Dixit, V.M. *et al.* Tumor necrosis factor-alpha induction of novel gene products in human endothelial cells including a macrophage-specific chemotaxin. *The Journal of biological chemistry* **265,** 2973–2978 (1990).
88. Wang, C.Y., Mayo, M.W., Korneluk, R.G., Goeddel, D.V. & Baldwin, A.S. NF-kappaB antiapoptosis: induction of TRAF1 and TRAF2 and c-IAP1 and c-IAP2 to suppress caspase-8 activation. *Science (New York, N.Y.)* **281,** 1680–1683 (1998).
89. Micheau, O., Lens, S., Gaide, O., Alevizopoulos, K. & Tschopp, J. NF-kappaB signals induce the expression of c-FLIP. *Molecular and cellular biology* **21,** 5299–5305 (2001).

90. Zhang, R. *et al.* Bclaf1 regulates c-FLIP expression and protects cells from TNF-induced apoptosis and tissue injury. *EMBO reports* **23,** e52702 (2022).
91. Peltzer, N. & Annibaldi, A. Cell Death-Related Ubiquitin Modifications in Inflammatory Syndromes: From Mice to Men. *Biomedicines* **10** (2022).
92. Zinngrebe, J., Montinaro, A., Peltzer, N. & Walczak, H. Ubiquitin in the immune system. *EMBO reports* **15,** 28–45 (2014).
93. Allensworth, J.L., Sauer, S.J., Lyerly, H.K., Morse, M.A. & Devi, G.R. Smac mimetic Birinapant induces apoptosis and enhances TRAIL potency in inflammatory breast cancer cells in an IAP-dependent and TNF-α-independent mechanism. *Breast cancer research and treatment* **137,** 359–371 (2013).
94. Hennessy, E.J. *et al.* Discovery of a novel class of dimeric Smac mimetics as potent IAP antagonists resulting in a clinical candidate for the treatment of cancer (AZD5582). *Journal of medicinal chemistry* **56,** 9897–9919 (2013).
95. Miles, M.A., Caruso, S., Baxter, A.A., Poon, I.K.H. & Hawkins, C.J. Smac mimetics can provoke lytic cell death that is neither apoptotic nor necroptotic. *Apoptosis : an international journal on programmed cell death* **25,** 500–518 (2020).
96. Kirisako, T. *et al.* A ubiquitin ligase complex assembles linear polyubiquitin chains. *The EMBO journal* **25,** 4877–4887 (2006).
97. Gerlach, B. *et al.* Linear ubiquitination prevents inflammation and regulates immune signalling. *Nature* **471,** 591–596 (2011).
98. Ikeda, F. *et al.* SHARPIN forms a linear ubiquitin ligase complex regulating NF-κB activity and apoptosis. *Nature* **471,** 637–641 (2011).
99. Berger, S.B. *et al.* Cutting Edge: RIP1 kinase activity is dispensable for normal development but is a key regulator of inflammation in SHARPIN-deficient mice. *Journal of immunology (Baltimore, Md. : 1950)* **192,** 5476–5480 (2014).
100. Kumari, S. *et al.* Sharpin prevents skin inflammation by inhibiting TNFR1-induced keratinocyte apoptosis. *eLife* **3** (2014).
101. Dondelinger, Y., Darding, M., Bertrand, M.J.M. & Walczak, H. Poly-ubiquitination in TNFR1-mediated necroptosis. *Cellular and molecular life sciences : CMLS* **73,** 2165–2176 (2016).
102. Annibaldi, A. *et al.* Ubiquitin-Mediated Regulation of RIPK1 Kinase Activity Independent of IKK and MK2. *Molecular cell* **69,** 566-580.e5 (2018).
103. Dynek, J.N. *et al.* c-IAP1 and UbcH5 promote K11-linked polyubiquitination of RIP1 in TNF signalling. *The EMBO journal* **29,** 4198–4209 (2010).

104. Tang, Y. *et al.* K63-linked ubiquitination regulates RIPK1 kinase activity to prevent cell death during embryogenesis and inflammation. *Nature communications* **10,** 4157 (2019).
105. Draber, P. *et al.* LUBAC-Recruited CYLD and A20 Regulate Gene Activation and Cell Death by Exerting Opposing Effects on Linear Ubiquitin in Signaling Complexes. *Cell reports* **13,** 2258–2272 (2015).
106. Wertz, I.E. *et al.* De-ubiquitination and ubiquitin ligase domains of A20 downregulate NF-kappaB signalling. *Nature* **430,** 694–699 (2004).
107. Dondelinger, Y., Vandenabeele, P. & Bertrand, M.J.M. Regulation of RIPK1's cell death function by phosphorylation. *Cell cycle (Georgetown, Tex.)* **15,** 5–6 (2016).
108. Dondelinger, Y. *et al.* NF-κB-Independent Role of IKKα/IKKβ in Preventing RIPK1 Kinase-Dependent Apoptotic and Necroptotic Cell Death during TNF Signaling. *Molecular cell* **60,** 63–76 (2015).
109. Lafont, E. *et al.* TBK1 and IKKε prevent TNF-induced cell death by RIPK1 phosphorylation. *Nature cell biology* **20,** 1389–1399 (2018).
110. Gareus, R. *et al.* Normal epidermal differentiation but impaired skin-barrier formation upon keratinocyte-restricted IKK1 ablation. *Nature cell biology* **9,** 461–469 (2007).
111. Li, Z.W. *et al.* The IKKbeta subunit of IkappaB kinase (IKK) is essential for nuclear factor kappaB activation and prevention of apoptosis. *The Journal of experimental medicine* **189,** 1839–1845 (1999).
112. Pasparakis, M. *et al.* TNF-mediated inflammatory skin disease in mice with epidermis-specific deletion of IKK2. *Nature* **417,** 861–866 (2002).
113. Taft, J. *et al.* Human TBK1 deficiency leads to autoinflammation driven by TNF-induced cell death. *Cell* **184,** 4447-4463.e20 (2021).
114. Dondelinger, Y. *et al.* MK2 phosphorylation of RIPK1 regulates TNF-mediated cell death. *Nature cell biology* **19,** 1237–1247 (2017).
115. Tummers, B. & Green, D.R. Caspase-8: regulating life and death. *Immunological reviews* **277,** 76–89 (2017).
116. Kaiser, W.J. *et al.* RIP3 mediates the embryonic lethality of caspase-8-deficient mice. *Nature* **471,** 368–372 (2011).
117. Weinlich, R. *et al.* Protective roles for caspase-8 and cFLIP in adult homeostasis. *Cell reports* **5,** 340–348 (2013).
118. Tummers, B. *et al.* Caspase-8-Dependent Inflammatory Responses Are Controlled by Its Adaptor, FADD, and Necroptosis. *Immunity* **52,** 994-1006.e8 (2020).

119. Zhang, J., Cado, D., Chen, A., Kabra, N.H. & Winoto, A. Fas-mediated apoptosis and activation-induced T-cell proliferation are defective in mice lacking FADD/Mort1. *Nature* **392,** 296–300 (1998).
120. Dillon, C.P. *et al.* Survival function of the FADD-CASPASE-8-cFLIP(L) complex. *Cell reports* **1,** 401–407 (2012).
121. Welz, P.-S. *et al.* FADD prevents RIP3-mediated epithelial cell necrosis and chronic intestinal inflammation. *Nature* **477,** 330–334 (2011).
122. Bonnet, M.C. *et al.* The adaptor protein FADD protects epidermal keratinocytes from necroptosis in vivo and prevents skin inflammation. *Immunity* **35,** 572–582 (2011).
123. Safa, A.R. Roles of c-FLIP in Apoptosis, Necroptosis, and Autophagy. *Journal of carcinogenesis & mutagenesis* **Suppl 6** (2013).
124. Micheau, O. *et al.* The long form of FLIP is an activator of caspase-8 at the Fas death-inducing signaling complex. *The Journal of biological chemistry* **277,** 45162–45171 (2002).
125. Pop, C. *et al.* FLIP(L) induces caspase 8 activity in the absence of interdomain caspase 8 cleavage and alters substrate specificity. *The Biochemical journal* **433,** 447–457 (2011).
126. Ram, D.R. *et al.* Balance between short and long isoforms of cFLIP regulates Fas-mediated apoptosis in vivo. *Proceedings of the National Academy of Sciences of the United States of America* **113,** 1606–1611 (2016).
127. Yeh, W.C. *et al.* Requirement for Casper (c-FLIP) in regulation of death receptor-induced apoptosis and embryonic development. *Immunity* **12,** 633–642 (2000).
128. Wittkopf, N. *et al.* Cellular FLICE-like inhibitory protein secures intestinal epithelial cell survival and immune homeostasis by regulating caspase-8. *Gastroenterology* **145,** 1369–1379 (2013).
129. Panayotova-Dimitrova, D. *et al.* cFLIP regulates skin homeostasis and protects against TNF-induced keratinocyte apoptosis. *Cell reports* **5,** 397–408 (2013).
130. Piao, X. *et al.* c-FLIP maintains tissue homeostasis by preventing apoptosis and programmed necrosis. *Science signaling* **5,** ra93 (2012).
131. Shu, H.B., Halpin, D.R. & Goeddel, D.V. Casper is a FADD- and caspase-related inducer of apoptosis. *Immunity* **6,** 751–763 (1997).
132. Krueger, A., Schmitz, I., Baumann, S., Krammer, P.H. & Kirchhoff, S. Cellular FLICE-inhibitory protein splice variants inhibit different steps of caspase-8 activation at the CD95 death-inducing signaling complex. *The Journal of biological chemistry* **276,** 20633–20640 (2001).

133. Huyghe, J. *et al.* ATG9A prevents TNF cytotoxicity by an unconventional lysosomal targeting pathway. *Science (New York, N.Y.)* **378,** 1201–1207 (2022).
134. Liu, L. *et al.* Tankyrase-mediated ADP-ribosylation is a regulator of TNF-induced death. *Science advances* **8,** eabh2332 (2022).
135. Eming, S.A., Martin, P. & Tomic-Canic, M. Wound repair and regeneration: mechanisms, signaling, and translation. *Science translational medicine* **6,** 265sr6 (2014).
136. Lucas, T. *et al.* Differential roles of macrophages in diverse phases of skin repair. *Journal of immunology (Baltimore, Md. : 1950)* **184,** 3964–3977 (2010).
137. Eming, S.A., Murray, P.J. & Pearce, E.J. Metabolic orchestration of the wound healing response. *Cell metabolism* **33,** 1726–1743 (2021).
138. Injarabian, L. *et al.* FADD- and RIPK3-mediated cell death ensures clearance of Ly6Chigh wound macrophages from damaged tissue. *The Journal of investigative dermatology* (2023).
139. Willenborg, S. *et al.* Mitochondrial metabolism coordinates stage-specific repair processes in macrophages during wound healing. *Cell metabolism* **33,** 2398-2414.e9 (2021).
140. Barrientos, S., Stojadinovic, O., Golinko, M.S., Brem, H. & Tomic-Canic, M. Growth factors and cytokines in wound healing. *Wound repair and regeneration : official publication of the Wound Healing Society [and] the European Tissue Repair Society* **16,** 585–601 (2008).
141. Vince, J.E. When Beauty Is Skin Deep: Regulation of the Wound Response by Caspase-8, RIPK3, and the Inflammasome. *The Journal of investigative dermatology* **135,** 1936–1939 (2015).
142. Best, S.M. Viral subversion of apoptotic enzymes: escape from death row. *Annual review of microbiology* **62,** 171–192 (2008).
143. Callus, B.A. & Vaux, D.L. Caspase inhibitors: viral, cellular and chemical. *Cell death and differentiation* **14,** 73–78 (2007).
144. Thome, M. *et al.* Viral FLICE-inhibitory proteins (FLIPs) prevent apoptosis induced by death receptors. *Nature* **386,** 517–521 (1997).
145. Fu, T.-M. *et al.* Cryo-EM Structure of Caspase-8 Tandem DED Filament Reveals Assembly and Regulation Mechanisms of the Death-Inducing Signaling Complex. *Molecular cell* **64,** 236–250 (2016).
146. Hillert, L.K. *et al.* Long and short isoforms of c-FLIP act as control checkpoints of DED filament assembly. *Oncogene* **39,** 1756–1772 (2020).
147. Li, F.-Y., Jeffrey, P.D., Yu, J.W. & Shi, Y. Crystal structure of a viral FLIP: insights into FLIP-mediated inhibition of death receptor signaling. *The Journal of biological chemistry* **281,** 2960–2968 (2006).

148. Zhou, Q. *et al.* Target protease specificity of the viral serpin CrmA. Analysis of five caspases. *The Journal of biological chemistry* **272,** 7797–7800 (1997).
149. Ray, C.A. *et al.* Viral inhibition of inflammation: cowpox virus encodes an inhibitor of the interleukin-1 beta converting enzyme. *Cell* **69,** 597–604 (1992).
150. Oltean, T. *et al.* Viral dosing of influenza A infection reveals involvement of RIPK3 and FADD, but not MLKL. *Cell death & disease* **12,** 471 (2021).
151. Karki, R. *et al.* ZBP1-dependent inflammatory cell death, PANoptosis, and cytokine storm disrupt IFN therapeutic efficacy during coronavirus infection. *Science immunology* **7,** eabo6294 (2022).
152. Karki, R. & Kanneganti, T.-D. Innate immunity, cytokine storm, and inflammatory cell death in COVID-19. *Journal of translational medicine* **20,** 542 (2022).
153. Karki, R. *et al.* Synergism of TNF-α and IFN-γ Triggers Inflammatory Cell Death, Tissue Damage, and Mortality in SARS-CoV-2 Infection and Cytokine Shock Syndromes. *Cell* **184,** 149-168.e17 (2021).
154. Dillon, C.P. *et al.* RIPK1 blocks early postnatal lethality mediated by caspase-8 and RIPK3. *Cell* **157,** 1189–1202 (2014).
155. Bolze, A. *et al.* Whole-exome-sequencing-based discovery of human FADD deficiency. *American journal of human genetics* **87,** 873–881 (2010).
156. Chun, H.J. *et al.* Pleiotropic defects in lymphocyte activation caused by caspase-8 mutations lead to human immunodeficiency. *Nature* **419,** 395–399 (2002).
157. Alvarez-Diaz, S. *et al.* The Pseudokinase MLKL and the Kinase RIPK3 Have Distinct Roles in Autoimmune Disease Caused by Loss of Death-Receptor-Induced Apoptosis. *Immunity* **45,** 513–526 (2016).
158. Onizawa, M. *et al.* The ubiquitin-modifying enzyme A20 restricts ubiquitination of the kinase RIPK3 and protects cells from necroptosis. *Nature immunology* **16,** 618–627 (2015).
159. Gitlin, A.D. *et al.* Integration of innate immune signalling by caspase-8 cleavage of N4BP1. *Nature* **587,** 275–280 (2020).
160. Henry, C.M. & Martin, S.J. Caspase-8 Acts in a Non-enzymatic Role as a Scaffold for Assembly of a Pro-inflammatory "FADDosome" Complex upon TRAIL Stimulation. *Molecular cell* **65,** 715-729.e5 (2017).
161. Koenig, A. *et al.* The c-FLIPL cleavage product p43FLIP promotes activation of extracellular signal-regulated kinase (ERK), nuclear factor κB (NF-κB), and caspase-8 and T cell survival. *The Journal of biological chemistry* **289,** 1183–1191 (2014).

162. Davidovich, P., Higgins, C.A., Najda, Z., Longley, D.B. & Martin, S.J. cFLIPL acts as a suppressor of TRAIL- and Fas-initiated inflammation by inhibiting assembly of caspase-8/FADD/RIPK1 NF-κB-activating complexes. *Cell reports* **42,** 113476 (2023).
163. Rickard, J.A. *et al.* TNFR1-dependent cell death drives inflammation in Sharpin-deficient mice. *eLife* **3** (2014).
164. Ang, R.L. *et al.* Immune dysregulation in SHARPIN-deficient mice is dependent on CYLD-mediated cell death. *Proceedings of the National Academy of Sciences of the United States of America* **118** (2021).
165. Wang, Y., Grunewald, M. & Perlman, S. Coronaviruses: An Updated Overview of Their Replication and Pathogenesis. *Methods in molecular biology (Clifton, N.J.)* **2203,** 1–29 (2020).
166. Yuan, C. *et al.* The role of cell death in SARS-CoV-2 infection. *Signal transduction and targeted therapy* **8,** 357 (2023).
167. Newton, K. *et al.* Caspase cleavage of RIPK3 after Asp333 is dispensable for mouse embryogenesis. *Cell death and differentiation* (2024).
168. Boatright, K.M., Deis, C., Denault, J.-B., Sutherlin, D.P. & Salvesen, G.S. Activation of caspases-8 and -10 by FLIP(L). *The Biochemical journal* **382,** 651–657 (2004).
169. Safa, A.R. c-FLIP, a master anti-apoptotic regulator. *Experimental oncology* **34,** 176–184 (2012).
170. Tang, Y. *et al.* Linear ubiquitination of cFLIP induced by LUBAC contributes to TNFα-induced apoptosis. *The Journal of biological chemistry* **293,** 20062–20072 (2018).
171. Nakabayashi, O. *et al.* MIND bomb 2 prevents RIPK1 kinase activity-dependent and -independent apoptosis through ubiquitylation of cFLIPL. *Communications biology* **4,** 80 (2021).
172. Roberts, J.Z. *et al.* The SCFSkp2 ubiquitin ligase complex modulates TRAIL-R2-induced apoptosis by regulating FLIP(L). *Cell death and differentiation* **27,** 2726–2741 (2020).
173. Kataoka, T. & Tschopp, J. N-terminal fragment of c-FLIP(L) processed by caspase 8 specifically interacts with TRAF2 and induces activation of the NF-kappaB signaling pathway. *Molecular and cellular biology* **24,** 2627–2636 (2004).
174. Golks, A., Brenner, D., Krammer, P.H. & Lavrik, I.N. The c-FLIP-NH2 terminus (p22-FLIP) induces NF-kappaB activation. *The Journal of experimental medicine* **203,** 1295–1305 (2006).
175. Park, Y.K. *et al.* Cleaved c-FLIP mediates the antiviral effect of TNF-α against hepatitis B virus by dysregulating hepatocyte nuclear factors. *Journal of hepatology* **64,** 268–277 (2016).

176. Karki, R. & Kanneganti, T.-D. The 'cytokine storm': molecular mechanisms and therapeutic prospects. *Trends in immunology* **42,** 681–705 (2021).
177. Lei, X., Chen, Y., Lien, E. & Fitzgerald, K.A. MLKL-Driven Inflammasome Activation and Caspase-8 Mediate Inflammatory Cell Death in Influenza A Virus Infection. *mBio,* e0011023 (2023).
178. Seshacharyulu, P., Pandey, P., Datta, K. & Batra, S.K. Phosphatase: PP2A structural importance, regulation and its aberrant expression in cancer. *Cancer letters* **335,** 9–18 (2013).
179. Ramakrishnan, M.A. Determination of 50% endpoint titer using a simple formula. *World journal of virology* **5,** 85–86 (2016).
180. Tenev, T. *et al.* The Ripoptosome, a signaling platform that assembles in response to genotoxic stress and loss of IAPs. *Molecular cell* **43,** 432–448 (2011).
181. Tyanova, S., Temu, T. & Cox, J. The MaxQuant computational platform for mass spectrometry-based shotgun proteomics. *Nature protocols* **11,** 2301–2319 (2016).
182. Tyanova, S. *et al.* The Perseus computational platform for comprehensive analysis of (prote)omics data. *Nature methods* **13,** 731–740 (2016).
183. Liu, Z., Gu, Y., Shin, A., Zhang, S. & Ginhoux, F. Analysis of Myeloid Cells in Mouse Tissues with Flow Cytometry. *STAR protocols* **1,** 100029 (2020).
184. Laurien, L. *et al.* Autophosphorylation at serine 166 regulates RIP kinase 1-mediated cell death and inflammation. *Nature communications* **11,** 1747 (2020).

7 SUPPLEMENTARY DATA

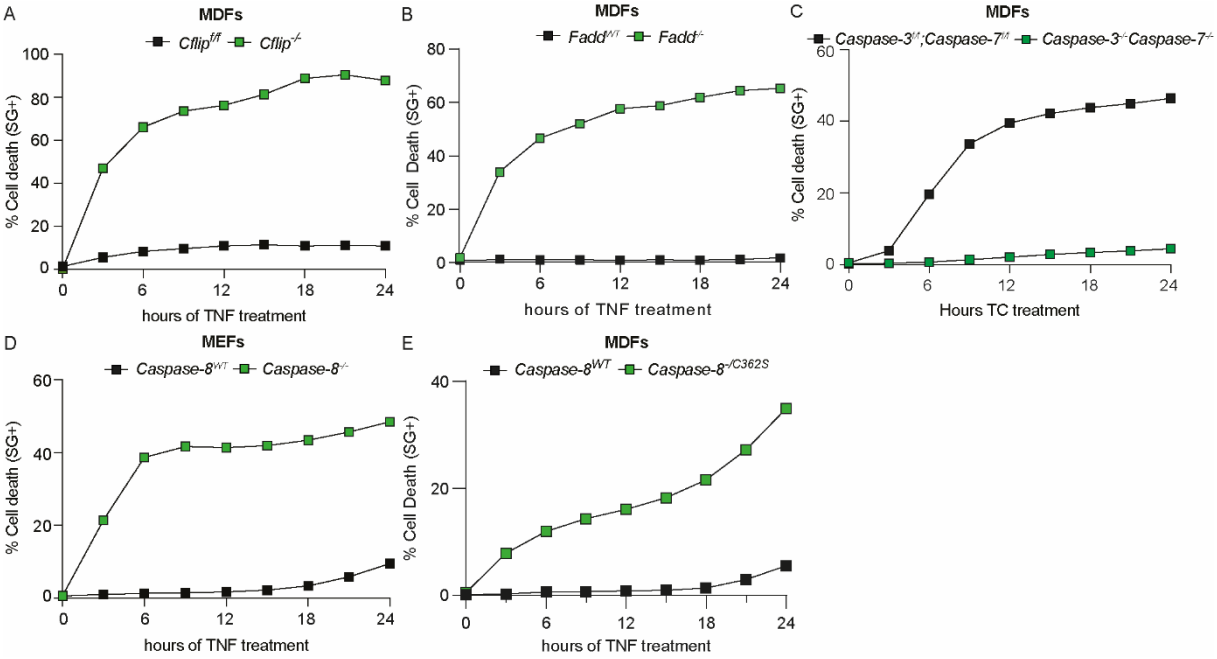

Supplementary Figure 1. cFLIP cleavage requires FADD and catalytically active Caspase-8. A-F. *Cflip*$^{fl/fl}$ and *Cflip*$^{-/-}$ (A) and FADD$^{WT/WT}$ and FADD$^{-/-}$ **(B)** mouse dermal fibroblasts (MDFs) were treated with TNF (100 ng/ml). Caspase-3$^{fl/fl}$Caspase-7$^{fl/fl}$ and Caspase-3$^{-/-}$Caspase-7$^{-/-}$ **(C)** MDFs were treated with TNF (100 ng/ml) and Cycloheximide (1 µg/ml). Caspase-8$^{WT/WT}$ and Caspase-8$^{-/-}$ **(D)** mouse embryonic fibroblasts (MEFs) and Caspase-8$^{WT/WT}$ and Caspase-8$^{-/C362S}$ **(E)** MDFs were treated with TNF (100 ng/ml). Cell death was measured over time by calculating the percentage of Sytox Green-positive cells (n=1).

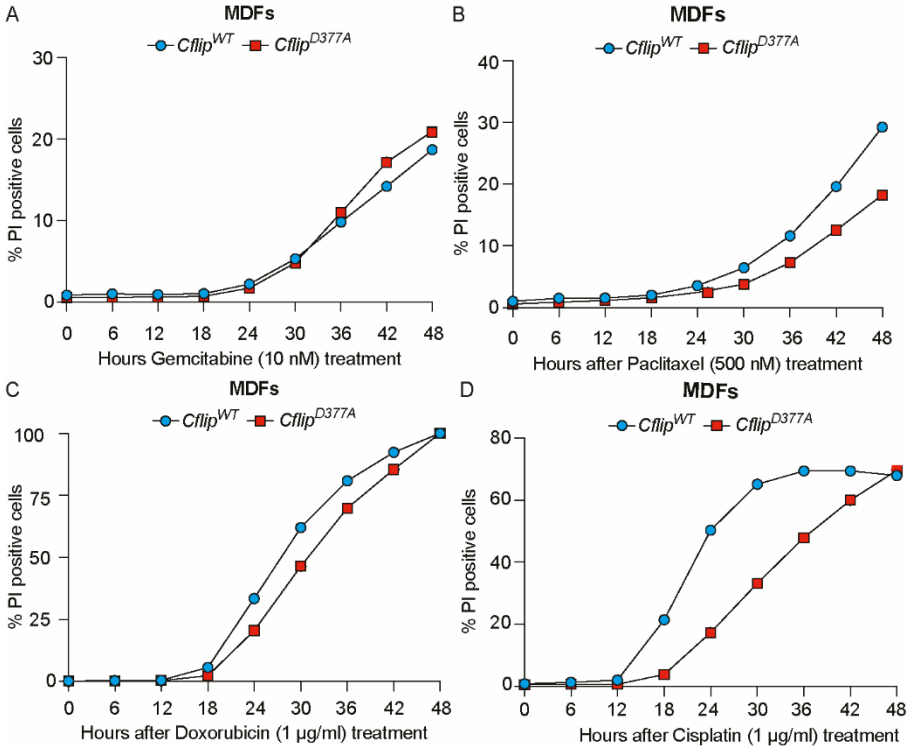

Supplementary Figure 2. cFLIP cleavage does not impact cell death responses induced by genotoxins. A-D. *Cflip*^{WT} and *Cflip*^{D377A} mouse dermal fibroblast (MDFs) were treated with Gemcitabine (10 nM, **A**), Paclitaxel (500 nM, **B**), Doxorubicin (1 µg/ml, **C**) and Cisplatin (1 µg/ml, **D**) and cell death was measured over time by calculating the percentage of Sytox Green-positive cells (n=1).

8 ACKNOWLEDGEMENT

To date, I have received a great deal of support and assistance. It was a pleasure to work with all the people, who helped me make this thesis possible with such dedication.

First of all, I would like to express my sincere appreciation to my supervisor and first examiner, Dr. Alessandro Annibaldi, for giving me the opportunity to work on this fascinating project and for always having an open door for any kind of problem or frustrating situation. His guidance and constructive discussions have taught me many invaluable lessons both inside and outside of science. I highly appreciate his significant contributions in deepening my scientific understanding, his help in developing my abilities in critical thinking and his mentorship.

I would like to thank Prof. Dr. Kay Hofmann for being a member of my thesis advisor committee and second examiner. Your support with scientific input and mentoring over the years is greatly valued. I am also deeply grateful to Prof. Dr. Hamid Kashkar for taking the time out of his busy schedule to discuss about the project during the annual meetings. I would like to express my gratitude to Prof. Dr. Andrea Morandi for his willingness to be the external examiner and Prof. Dr. Stephanie Kath Schorr for being a member of the thesis defence committee.

I would like to express my gratitude to all our collaborators in this project. In particular, I would like to thank Prof. Dr. Marion Macfarlane and her team for their experimental expertise and helpful discussions, Prof. Dr. Sabine Eming and her team for their expertise in skin, Prof. Dr. Julian Pardo and Dr. Diego de Miguel along with Dr. Henning Walczak and Dr. Marie Christine Albert for their work with the SARS-CoV infection model, Dr. Melanie Fritsch for providing experimental mice, and lastly Dr. Jan-Wilm Lackmann, Dr. Stefan Müller and their team for their amazing scientific support in proteomics and the data analysis.

My special thanks and appreciation go to the current and former members of our research group: Dr. Kristel Martinez Lagunas for sharing the project and spending countless hours in the lab with me, Carlos Carvajal Fraile, for his technical, organisational and emotional support, Matea Zrilic for all the time, help and interests shared both in and out of the lab, Ina Lisewski for the music sessions and deep cell culture conversations, Kristie Bariboloka for all the videos we made in the lab and the films we watched together. Your contributions have been very special in this journey. Furthermore, I would like to acknowledge the help at different stages of this project from our students: Kalvin Nughara, Erika Janakova, Natalia Igual, Guila Gangatossa, Donna Sperber and Michael Venturini for the great working atmosphere. Thank you for all the special moments and birthdays we celebrated together.

I would like to expand my appreciation to our PAL family, Dr. Nieves Peltzer, foremost for accepting taking my defence minutes and her expertise in *Sharpin*^{cpdm} model, and Dr. Gianmaria Liccardi for engaging in insightful discussions, as well as the members of Peltzer and Liccardi Labs, Julia Saggau, particularly for proof reading, Ximena Hildebrandt and Mohammed Ibrahim for their expertise in flow cytometry, together with many others, who joined the family on this journey, for their great support and provision of reagents. I would like to also thank Prof. Dr. Leo Kurian and our neighbours in the Kurian lab, Kaustubh Kalamkar and Dr. Deniz Bartsch, for many reagents and philosophical conversations over the years.

Furthermore, I'm heartily thankful to my friends for their patience, wise counsel, sympathetic ear, even at the most difficult times, and proof reading. You made me feel supported at every stage.

Finally, and most importantly, I owe my deepest acknowledgement to my beloved family for their unwavering support. Thank you for your unconditional and endless love and guidance, especially during the most challenging times. Your belief in me has been a constant source of motivation. I cannot express how much this means to me. None of these would have not been possible to reach without you.

This chapter of my life has been an unforgettable adventure. This is not the end, life is just beginning. I am excited to see what the future holds.

Deniz Pinar Savcigil

9 ERKLÄRUNG ZUR DISSERTATION

„Hiermit versichere ich an Eides statt, dass ich die vorliegende Dissertation selbstständig und ohne die Benutzung anderer als der angegebenen Hilfsmittel und Literatur angefertigt habe. Alle Stellen, die wörtlich oder sinngemäß aus veröffentlichten und nicht veröffentlichten Werken dem Wortlaut oder dem Sinn nach entnommen wurden, sind als solche kenntlich gemacht. Ich versichere an Eides statt, dass diese Dissertation noch keiner anderen Fakultät oder Universität zur Prüfung vorgelegen hat; dass sie - abgesehen von unten angegebenen Teilpublikationen und eingebundenen Artikeln und Manuskripten - noch nicht veröffentlicht worden ist sowie, dass ich eine Veröffentlichung der Dissertation vor Abschluss der Promotion nicht ohne Genehmigung des Promotionsausschusses vornehmen werde. Die Bestimmungen dieser Ordnung sind mir bekannt. Darüber hinaus erkläre ich hiermit, dass ich die Ordnung zur Sicherung guter wissenschaftlicher Praxis und zum Umgang mit wissenschaftlichem Fehlverhalten der Universität zu Köln gelesen und sie bei der Durchführung der Dissertation zugrundeliegenden Arbeiten und der schriftlich verfassten Dissertation beachtet habe und verpflichte mich hiermit, die dort genannten Vorgaben bei allen wissenschaftlichen Tätigkeiten zu beachten und umzusetzen. Ich versichere, dass die eingereichte elektronische Fassung der eingereichten Druckfassung vollständig entspricht."

Teilpublikationen:

Martinez Lagunas K*, **Savcigil DP*,** Zrilic M, et al. Cleavage of cFLIP restrains cell death during viral infection and tissue injury and favors tissue repair. Sci Adv. 2023;9(30):eadg2829. 2023 Jul 26. doi:10.1126/sciadv.adg2829 *contributed equally

05.02.2024 Deniz Pinar Savcigil D.P. Savcigil

Datum, Name und Unterschrift

SCIENCE ADVANCES | RESEARCH ARTICLE

IMMUNOLOGY

Cleavage of cFLIP restrains cell death during viral infection and tissue injury and favors tissue repair

Kristel Martinez Lagunas[1]†, Deniz Pinar Savcigil[1]†, Matea Zrilic[1], Carlos Carvajal Fraile[1], Andrew Craxton[2], Emily Self[2], Iratxe Uranga-Murillo[3], Diego de Miguel[3], Maykel Arias[3,4,5], Sebastian Willenborg[6], Michael Piekarek[6], Marie Christine Albert[7,8], Kalvin Nugraha[1], Ina Lisewski[1], Erika Janakova[1], Natalia Igual[1], Wulf Tonnus[9,10], Ximena Hildebrandt[1,7,11], Mohammed Ibrahim[1,7,11], Marlies Ballegeer[12,13], Xavier Saelens[12,13], Andrew Kueh[14,15], Pascal Meier[16], Andreas Linkermann[9,10,17], Julian Pardo[3,4,5], Sabine Eming[1,6,7,18], Henning Walczak[7,8,19], Marion MacFarlane[2], Nieves Peltzer[1,7,11], Alessandro Annibaldi[1]*

Cell death coordinates repair programs following pathogen attack and tissue injury. However, aberrant cell death can interfere with such programs and cause organ failure. Cellular FLICE-like inhibitory protein (cFLIP) is a crucial regulator of cell death and a substrate of Caspase-8. However, the physiological role of cFLIP cleavage by Caspase-8 remains elusive. Here, we found an essential role for cFLIP cleavage in restraining cell death in different pathophysiological scenarios. Mice expressing a cleavage-resistant cFLIP mutant, *Cflip*^{D377A}, exhibited increased sensitivity to severe acute respiratory syndrome coronavirus (SARS-CoV)–induced lethality, impaired skin wound healing, and increased tissue damage caused by *Sharpin* deficiency. In vitro, abrogation of cFLIP cleavage sensitizes cells to tumor necrosis factor(TNF)–induced necroptosis and apoptosis by favoring complex-II formation. Mechanistically, the cell death–sensitizing effect of the D377A mutation depends on glutamine-469. These results reveal a crucial role for cFLIP cleavage in controlling the amplitude of cell death responses occurring upon tissue stress to ensure the execution of repair programs.

INTRODUCTION

Cell death is a fundamental biological process that ensures tissue homeostasis and orchestrates tissue remodeling following injury or infection. However, if on the one hand abrogation of cell death responses can prevent the activation of repair programs, on the other hand exacerbated cell death can lead to tissue failure (*1*–*3*). Therefore, the ability of tissues to control the extent of cell death under stress conditions is of fundamental importance for the activation of optimal repair programs. Tumor necrosis factor (TNF) is a proinflammatory cytokine that is produced in response to a large variety of stressors, including viral infection and injury, and it can initiate repair processes by inducing the expression of proinflammatory genes or by triggering cell death (*1*, *4*, *5*). The mechanisms regulating the decision between these two outcomes are of fundamental importance for the maintenance of tissue homeostasis and for the capacity of tissues to overcome damage (*6*, *7*).

Binding of TNF to TNF receptor 1 (TNFR1) results in the formation of two spatially and temporally distinct complexes (*8*). A membrane-bound complex, called complex-I, is assembled on the intracellular death domain (DD)–containing portion of TNFR1. It is composed of adaptor proteins, such as TNFR1-associated death domain protein (TRADD) and TRAF2 (TNFR-associated factor 2); kinases, such as RIPK1 (receptor-interacting protein kinase 1), IKKα and IKKβ [inhibitor of nuclear factor κB (NF-κB) kinase subunits α and β], TAK1 (transforming growth factor β–activated kinase 1), TANK-binding kinase 1 (TBK1), and IKKε; and E3 ligases, such as cellular inhibitor of apoptosis protein 1 and 2 (cIAP1/2) and linear ubiquitin chain assembly complex (LUBAC) (*9*–*14*). The concerted action of phosphorylation and ubiquitination events ensures the correct assembly and stability of the complex, leading to the activation of genes required to mount an inflammatory response (*1*, *15*, *16*). Any perturbation of phosphorylation or ubiquitination processes leads to the formation of a secondary, cytoplasmic complex, referred to as complex-II (*1*, *14*, *16*–*21*). This complex consists of Fas associated via death domain (FADD), RIPK1, cellular FLICE-like inhibitory protein (cFLIP$_L$), Caspase-8 and, depending on the cell types, RIPK3 (*18*, *22*). Complex-II has cytotoxic activity and can trigger Caspase-8–mediated apoptosis and RIPK1/RIPK3/mixed lineage kinase domain like

[1]Center for Molecular Medicine Cologne, University of Cologne, Robert-Koch Strasse 21, 50931, Cologne, Germany. [2]MRC Toxicology Unit, University of Cambridge, Tennis Court Road, Cambridge, CB2 1QR, UK. [3]Aragón Health Research Institute (IIS Aragón), Biomedical Research Centre of Aragón (CIBA), Zaragoza, Spain. [4]Department of Microbiology, Radiology, Pediatry and Public Health, University of Zaragoza, Zaragoza, Spain. [5]CIBER de Enfermedades Infecciosas, Instituto de Salud Carlos III, Madrid, Spain. [6]Department of Dermatology, University of Cologne, 50937 Cologne, Germany. [7]Cologne Excellence Cluster on Cellular Stress Responses in Aging-Associated Diseases (CECAD), University of Cologne, 50931 Cologne, Germany. [8]Institute of Biochemistry I, Medical Faculty, University of Cologne, 50931 Cologne, Germany. [9]Division of Nephrology, Department of Internal Medicine 3, University Hospital Carl Gustav Carus at the Technische Universität Dresden, Dresden, Germany. [10]Biotechnology Center, Technische Universität Dresden, Dresden, Germany. [11]Department of Translational Genomics, University of Cologne, Weyertal 115b, 50931 Köln, Germany. [12]VIB-UGent Center for Medical Biotechnology, VIB, B-9052 Ghent, Belgium. [13]Department of Biochemistry and Microbiology, Ghent University, B-9000 Ghent, Belgium. [14]Walter and Eliza Hall Institute of Medical Research, Parkville, VIC, Australia. [15]Department of Medical Biology, The University of Melbourne, Parkville, VIC 3010, Australia. [16]The Breast Cancer Now Toby Robins Research Centre, The Institute of Cancer Research, London, UK. [17]Division of Nephrology, Department of Medicine, Albert Einstein College of Medicine, Bronx, NY, USA. [18]Institute of Zoology, Developmental Biology Unit, University of Cologne, 50674 Cologne, Germany. [19]Centre for Cell Death, Cancer, and Inflammation (CCCI), UCL Cancer Institute, University College, London WC1E 6BT, UK.
*Corresponding author. Email: a.annibaldi@uni-koeln.de
†These authors contributed equally to this work.